UNIVERSITY OF CALIFORNIA,
IRVINE

Measuring Uptake and Reaction of Atmospherically Relevant Systems

DISSERTATION

submitted in partial satisfaction of the requirements
for the degree of

DOCTOR OF PHILOSOPHY

in Chemistry

by

Michelle Christine Fairhurst

Dissertation Committee:
Professor Barbara J. Finlayson-Pitts, Chair
Professor Sergey A. Nizkorodov
Professor Craig Murray

2017

DEDICATION

To Justin and my family: grandma, grandpa,
mom, sisters, all my aunts, uncles and cousins:
you are my pillars of support and I thank you
all for supporting me and never saying “more school?”

I hope I’ve made you all proud.

“Nevertheless, she persisted”
– Said to a female senator on the floor
who was perceived to “overstep”.
Now, a motivational mantra to keep going
in the face of adversity.

Contents

LIST OF FIGURES vi

LIST OF TABLES xiv

ACKNOWLEDGMENTS xv

CURRICULUM VITAE xvii

ABSTRACT OF THE DISSERTATION xxii

CHAPTER 1: INTRODUCTION 1

I. The Importance of Atmospheric Particles 1

II. Primary vs. Secondary Organic Aerosol 2

III. Mechanisms of Particle Formation and Growth 2

IV. Acid–Base Reactions in the Atmosphere 5

V. The Importance of Model Systems 6

VI. Project Goals 7

CHAPTER 2: EXPERIMENTAL METHODS 9

I. Uptake of Gas Phase Species with Single Compounds as Models for SOA 9

II. Generation and Uptake of Gas Phase Species onto SOA 13

III. The Use of Self-Assembled Monolayers to Avoid Uptake onto Clean Crystal Surfaces 15

IV. Reaction of Gas Phase Amines with Soild Dicarboxylic Acids Using a Custom–Built Flow System 16

VI. Knudsen Cell Studies of Amines/Ammonia on Diacids 24

VII. Formation of Aminium Salts and Viscosity Measurements 30

VIII. Reaction of Amines and Diacids Using a Flow Reactor and Direct Analysis in Real Time Mass Spectrometry (DART-MS) 31

CHAPTER 3: RESULTS – REACTIONS OF GAS PHASE SPECIES ON SOA MODELS 34

I. Characterization of Squalane Coatings 34

II. Uptake of Non–Polar Gases on SOA and SOA Models 36

III. Uptake of Polar Gases on SOA Models 51

IV. Conclusions 57

CHAPTER 4: RESULTS – REACTION OF AMINES ON DIACIDS USING A FLOW REACTOR 59

I. Uptake of BA on Solid Diacids 59

II. Uptake of sBA on Solid Diacids 68

III. Conclusions for Flow Reactor Experiments using Solid Diacids 76

IV. Uptake of BA on Diacid Slurry 76

V. Conclusions 92

CHAPTER 5: RESULTS – UPTAKE OF AMINES/AMMONIA ON DIACIDS USING KNUDSEN CELL 94

I. Uptake of BA onto C3 – C8 Diacids 94

II. Conclusions for BA on Diacids 112

III. Uptake of Other Amines and Ammonia onto C3 – C7 Diacids 113

IV. Conclusions 135

CONCLUSIONS AND ATMOSPHERIC IMPLICATIONS 137

REFERENCES 140

LIST OF FIGURES

Figure 2-1. Structures of squalane and Fomblin ®. 10

Figure 2-2. Structures of gas phase species used in ATR uptake studies. 11

Figure 2-3. Schematic of two different types of squalane coatings on the Ge ATR crystal. 12

Figure 2-4. Schematic of impactor used in SOA ATR studies. Figure adapted from Kidd et al.[56] 14

Figure 2-5. Plot of the $–CH_3$ stretch peak areas for SOA as a function of impaction time. 15

Figure 2-6. Structure of octadecyltrichlorosilane (C18 alkyl SAM). 15

Figure 2-7. Schematic of the flow reactor coupled to the QMS. IG = ion gauge. P_{FT} = total pressre in the flow reactor (Torr). MFC = mass flow controller. 17

Figure 2-8. Structures of diacids used in flow reactor studies. 18

Figure 2-9. Structures of gas phase amines used in flow reactor studies. 18

Figure 2-10. Calibration curve for 610A flow meter using Helium. 19

Figure 2-11. Schematic of the Knudsen cell interfaced to the QMS. IG = ion gauge. 25

Figure 2-12. Structures of diacids used in Knudsen cell studies. 26

Figure 2-13. Gas phase amines and ammonia used in Knudsen cell studies. 27

Figure 2-14. Schematic of the flow reactor used to measure reactions of amines with diacids. Inset is the DART interface. Adapted from Zhao et al.[186] 32

Figure 3-1. IR spectrum of squalane droplets. 35

Figure 3-2. Peak height of the asymmetric $–CH_3$ stretch for nebulized squalane droplets as a function of coats on the ATR crystal. 36

Figure 3-3. IR spectrum of neat IBN using a transmission cell with CaF_2 windows. 37

Figure 3-4. Spectra showing uptake of 20 ppm IBN on a) a thick film and b) squalane droplets. Baselines adjusted for clarity. 38

Figure 3-5. Typical plots of the number of IBN molecules in a) a thick film and b) squalane droplets as a function of time. 40

Figure 3-6. Plot of the rate of IBN molecules on squalane droplets per area vs. $t^{-1/2}$ of for the linear uptake region. 43

Figure 3-7. Schematic representation of IBN coming to equilibrium with squalane droplets. 44

Figure 3-8. IR spectrum of a thick film of Fomblin ®. 45

Figure 3-9. a) Uptake of 100 ppm IBN on a thick film of Fomblin ®. Baselines are adjusted for clarity. b) Absorbance of the asymmetric $–ONO_2$ peak as a function of time. 46

Figure 3-10. Calibration curve of moles of IBN in 1 mL Fomblin ®. 47

Figure 3-11. Equal volumes of IBN and Fomblin ® after mixing. 48

Figure 3-12. IR spectrum of α-pinene/O_3 SOA impacted for 10 minutes (blue) and 180 minutes (red). 49

Figure 3-13. a) IR spectrum of 100 ppm IBN in 10 min. impacted SOA. b) Peak area of the nitrate stretch at 1280 cm^{-1} as a function of time. 50

Figure 3-14. IR difference spectrum of IBN on SOA impacted for 180 minutes under flow conditions. B) Peak area of the nitrate stretch as a function of time on 180 min. impacted SOA (purple) and 10 min. impacted SOA (green). 51

Figure 3-15. IR spectrum of pure liquid hydroxyacetone (HA) using a transmission cell with CaF_2 windows. 52

Figure 3-16. a) Peak at 1704 cm^{-1} due to HA uptake into a thick film of squalane. b) Trend of C=O peak height as a function of gas flow. 53

Figure 3-17. IR spectrum of neat acetone using a transmission cell with CaF_2 windows. 53

Figure 3-18. Gas phase IR spectrum of 200 ppm (4.9×10^{15} molecules cm^{-3}) acetic acid in ultra zero air. Pathlength of cell = 9 cm. T = 295 K. P_{tot} = 1 atm. 55

Figure 3-19. Peak area of C=O stretch for 100 ppm acetic acid in a thick film (400 μm) of Fomblin ® (red) and on a clean Ge ATR crystal (green). Line indicates the swtich of gas phase acetic acid flow to only air flow. Open symbols represent evaporation. 56

Figure 3-20. Peak areas of C=O stretch for acetic acid onto Fomblin ® (red) on a Ge crystal, a clean Ge ATR crystal (green), and the C18 SAM on the Si ATR crystal (purple). Line indicates the swtich of gas phase acetic acid flow to only air flow. Open symbols represent evaporation. 57

Figure 4-1. Uptake of $(5 – 9) \times 10^{13}$ molecules cm^{-3} BA on solid C2 – C5 diacids in a flow reactor. Total pressure (P_{FT}) in the reactor = 0.8 – 1.0 Torr. 60

Figure 4-2. Typical first-order kinetics plot for $(5 – 9) \times 10^{13}$ molecules cm^{-3} BA on solid C2 – C5 diacids..... 61

Figure 4-3. Photos of oxalic acid (C2) coated flow reactor A) before and B) after amine exposure. The flow reactor shows a frosted outline of the spokes at the end of the flow reacotr (red box) as well as frosting on the perforated spokes..... 62

Figure 4-4. Uptake of 1×10^{14} molecules cm^{-3} BA on solid oxalic acid (C2) using a flow reactor. P_{FT} = 0.9 Torr. 65

Figure 4-5. Uptake profiles of C3 – C5 solid diacids with a) 1×10^{14} molecules cm^{-3} and b) 2×10^{14} molecules cm^{-3} BA using a flow reactor. P_{FT} = 0.9 Torr. 67

Figure 4-6. Uptake profiles for $(7 – 9) \times 10^{13}$ molecules cm^{-3} sBA on solid C2 – C5 diacids using a flow reactor. P_{FT} = 0.8 – 0.9 Torr. 69

Figure 4-7. First order rate plots for (7 – 9) × 10^{13} molecules cm^{-3} sBA on C2, C3, and C5 solid diacids. 70

Figure 4-8. Uptake profiles for C2, C3, and C5 diacids at sBA concentrations of a) 1 × 10^{14} molecules cm^{-3} and b) 2 × 10^{14} molecules cm^{-3} in the flow reactor. P_{FT} = 0.8 – 0.9 Torr. 73

Figure 4-9. Uptake of 1 × 10^{14} molecules cm^{-3} sBA on solid succinic acid (C4) in the flow reactor. P_{FT} = 0.9 Torr. 74

Figure 4-10. First-order rate plots for a) 1 × 10^{14} molecules cm^{-3} and b) 2 × 10^{14} molecules cm^{-3} sBA on succinic acid (C4). 75

Figure 4-11. Photos of C2 – C5 diacid slurry coatings before and after exposure to BA. 77

Figure 4-12. Uptake profiles for a) (3 – 4) × 10^{13} molecules cm^{-3}, b) (7 – 8) × 10^{13} molecules cm^{-3}, c) 2 × 10^{14} molecules cm^{-3}, and d) 3 × 10^{14} molecules cm^{-3} BA on malonic acid (C3) in the flow reactor. P_{FT} = 0.9 Torr. 78

Figure 4-13. First–order rate plots for a) (3 – 4) × 10^{13} molecules cm^{-3}, b) (7 – 8) × 10^{13} molecules cm^{-3}, c) 2 × 10^{14} molecules cm^{-3}, and d) 3 × 10^{14} molecules cm^{-3} BA on malonic acid (C3) using the flow reactor. Each symbol represents a different trial. 79

Figure 4-14. Uptake profiles for a) (3 – 4) × 10^{13} molecules cm^{-3}, b) (7 – 8) × 10^{13} molecules cm^{-3}, c) 2 × 10^{14} molecules cm^{-3}, and d) 3 × 10^{14} molecules cm^{-3} BA on glutaric acid (C5) using a flow reactor. P_{FT} = 0.9 Torr 81

Figure 4-15. First–order rate plots for a) (3 – 4) × 10^{13} molecules cm^{-3}, b) (7 – 8) × 10^{13} molecules cm^{-3}, c) 2 × 10^{14} molecules cm^{-3}, and d) 3 × 10^{14} molecules cm^{-3} BA on glutaric acid (C5) using the flow reactor. Each symbol represents a different trial. 82

Figure 4-16. Uptake profiles for a) (3 – 4) × 10^{13} molecules cm^{-3}, b) (7 – 8) × 10^{13} molecules cm^{-3}, c) 2 × 10^{14} molecules cm^{-3}, and d) 3 × 10^{14} molecules cm^{-3} BA on succinic acid (C4) using the flow reactor. P_{FT} = 0.9 Torr. 83

Figure 4-17. First–order rate plots for a) (3 – 4) × 10^{13} molecules cm^{-3}, b) (7 – 8) × 10^{13} molecules cm^{-3}, c) 2 × 10^{14} molecules cm^{-3}, and d) 3 × 10^{14} molecules cm^{-3} BA on succinic acid (C4) using the flow reactor. 84

Figure 4-18. Uptake profiles for a) 2 × 10^{14} molecules cm^{-3}, and b) 3 × 10^{14} molecules cm^{-3} BA on oxalic acid (C2) using the flow reactor. P_{FT} = 0.8 – 0.9 Torr. 85

Figure 4-19. First–order rate plots for a) 2 × 10^{14} molecules cm^{-3}, and b) 3 × 10^{14} molecules cm^{-3} BA on oxalic acid (C2). 85

Figure 4-20. Zoomed in view of the initial drop in amine signal once the inlet is pulled back, followed by the exponential increase in amine signal, which is indicative of surface saturation. 87

Figure 4-21. a) Uptake profile for (3 – 4) × 10^{13} molecules cm^{-3} BA on malonic acid (C3). b) Zoomed in view of intensity of the amine while the inlet is held at 1 cm with fit of Equation 4.12. 91

Figure 5-1. a) Uptake profiles for odd carbon diacids: malonic acid (C3), glutaric acid (C5), and pimelic acid (C7). b) Uptake profiles for even carbon diacids: succinic acid (C4), adipic acid (C6), and suberic acid (C8). $[BA]_0$ = (3 – 5) × 10^{11} molecules cm^{-3} for all experiments. Sensivitiy on the lock–in amplifier for experiments with malonic (C3) and glutaric (C5) acids was 100 mV. For experiments with succinic (C4), adipic (C6), pimelic (C7), and suberic (C8) acids, sensitivity was increased to 10 mV. 95

Figure 5-2. Summary of initial uptake coefficients, γ, for BA on C3–C8 diacids. Dashed lines are for BA concentrations of 10^{11} molecules cm^{-3} and solid lines are for 10^{12} molecules cm^{-3}.

Error bars represent a propagation of errors (2σ). *Uptake coefficients for C8 represent an upper limit. 101

Figure 5-3. Arrangement of diacid lattice as reported by Thalladi et al.[138] for a) pimelic acid (C7) and b) suberic acid (C8). Chains are linked end–to–end via hydrogen bonding between –COOH groups and intramolecular chains are held together via dispersion forces between methylene groups. The odd carbon diacids have a twisted conformation and more torsional strain than the even carbon diacids. 102

Figure 5-4. Formation of liquid and solid salts from aqueous mixtures of n-butylamine and diacids. 2:1 Butylaminium salts for a) odd carbon diacids and b) even carbon diacids. 1:1 Butylaminium salts for c) odd carbon diacids and d) even carbon diacids. 104

Figure 5-5. Malonic acid (C3) a) before and b) after exposure to 41 Torr pure BA and suberic acid (C8) d) before and d) after exposure to 29 Torr pure BA via vacuum manifold. 106

Figure 5-6. Uptake of 5×10^{12} molecules cm^{-3} BA on succinic acid (C4) (A_{surf} ~21 cm^2)..... 108

Figure 5-7. a) Uptake profile for 4×10^{12} molecules cm^{-3} BA on glutaric acid (C5) (A_{surf} ~ 2 cm^2). Glutaric acid (C5) b) before and c) after reaction in the Knudsen cell with a total exposure time of 60 minutes. 108

Figure 5-8. Uptake coefficients as a function of time for a) 3×10^{11} molecules cm^{-3}, b) 3.9×10^{12} molecules cm^{-3}, and c) 8.8×10^{12} molecules cm^{-3} BA on glutaric acid (C5) symbols represent experimental values, solid line is the KM–SUB predicted uptake coefficients. The different colors of the symbols represent repeats of the experiments. Model calculations performed by Dr. Pascale Lakey and Professor Manabu Shiraiwa. Adapted from Fairhurst et al.[210] 110

Figure 5-9. Evolution of concentrations of a) glutaric acid (C5) and b) product concentrations after exposure to 8.8×10^{12} molecules cm^{-3} BA (units of contour lines are cm^{-3}). Evolution of concentrations of c) adipic acid (C6) and d) reactant product concentrations after exposure to 4.7×10^{12} molecules cm^{-3} BA (scales of contour lines are 10^{21} cm^{-3}). Model calculations performed by Dr. Pascale Lakey and Professor Manabu Shiraiwa. Figure adapted from Fairhurst et al.[210] 112

Figure 5-10. Uptake of ammonia (NH_3) and amines at concentrations of $(3 – 5) \times 10^{11}$ molec cm^{-3} on malonic acid (C3), succinic acid (C4) and glutaric acid (C5). The succinic acid surface area was 20 cm^2. For all of the malonic acid runs except NH_3, A_{surf} = 2 cm^2 ; for NH_3, A_{surf} = 9 cm^2. For glutaric acid, A_{surf} = 2 cm^2 for MA, EA and DMA, 14 cm^2 for NH_3 and 16 cm^2 for TMA. Note the expanded scales used to show the succinic acid (C4) data. No uptake was observed on adipic (C6) or pimelic (C7) acids. For all primary and secondary amines on malonic (C3) and glutaric (C5) acids, sensitivity on the lock–in amplifier was 100 mV. For all amines (except for EA) and ammonia on succinic acid (C4) and TMA on glutaric acid (C5) sensitivity on the lock–in amplifier was increased to 3 mV. For EA on succinic acid (C4), the sensitivity was 10 mV. 115

Figure 5-11. Schematic of uptake coefficients derived for a) amines on malonic acid (C3), and b) derivation of steady-state uptake coefficients for all other diacids. 122

Figure 5-12. Summary of uptake coefficients (γ_{ss}) ($\pm 2\sigma$) for amines and ammonia on C3 – C7 solid diacids. Dashed lines are data at 10^{11} molecules cm^{-3} and solid lines are data at 10^{12} molecules cm^{-3}. Uptake coefficients for MA, EA and DMA on malonic acid (C3) are extrapolated uptake coefficients ($\gamma_{0,ss}$) as reported in Table 1. Values for glutaric acid (C5) at

10^{12} molecules cm^{-3} are γ_0 as reported in Table 5-5. Arrows and parentheses indicate an upper limit. 124

Figure 5-13. Products formed from the evaporation of aqueous 2:1 or 1:1 mixtures of MA, EA, DMA, TMA or NH_3 with odd carbon diacids. Green stars indicate a MSIL that converted to a slushy material. 131

Figure 5-14. Products formed from the evaporation of aqueous 2:1 or 1:1 mixtures of MA, EA, DMA or TMA with even carbon diacids. 132

LIST OF TABLES

Table 2-1. Physical and chemical properties of squalane and Fomblin ®..... 10

Table 2-2. Diacid edge lengths measured using dial calipers. Averages are of 20 crystals. 22

Table 2-3. Sieve sizes and corresponding average lengths of each diacid crystal. Average lengths were derived from a sample size of 20 crystals..... 26

Table 3-1. Measured Henry's law constants[a] 41

Table 4-1. Summary of experimental conditions and uptake coefficients for BA on solid diacids. 63

Table 4-2. Summary of experimental conditions for sBA on solid C2 – C5 diacids. 72

Table 5-1. Uptake coefficients (γ) for different concentrations of n-butylamine on different surface areas of diacids. 96

Table 5-2. Measured viscosities (μ) and densities (ρ_f) for 2:1 and 1:1 amine:diacid mixtures. 105

Table 5-3. Uptake coefficients (γ) for ammonia and amines on malonic acid (C3). 116

Table 5-4. Uptake coefficients (γ) for ammonia and amines on succinic acid (C4). 117

Table 5-5. Uptake coefficients (γ) for ammonia and amines on glutaric acid (C5). 118

Table 5-6. Uptake coefficients (γ) for ammonia and amines on adipic acid (C6). 119

Table 5-7. Uptake coefficients for ammonia and amines on pimelic acid (C7). 120

Table 5-8. Measured viscosities (μ) and densities (ρ_f) for 2:1 and 1:1 ammonia or amines–diacid mixtures..... 129

ACKNOWLEDGMENTS

Thank you to Justin Fairhurst for supporting me when I threw the PhD program into our plans midway through my Master's program. Although it has been a journey, you have always been right there by my side and for that I thank you.

To my family, which includes my mom, sisters, my grandma and grandpa, and all my aunts, uncles, and cousins. To me, this is my core family. You all have been there from the beginning and although you may not have understood what graduate school entails, you have all been there cheering me on. I love you all!

Professor Finlayson–Pitts, thank you for being such an excellent mentor! Thank you for all your advice and guidance not only with research, but with my career. You've taught me what it means to be a great researcher. You are a role model and I am very honored to have come through your research laboratory.

To the Finlayson–Pitts' lab, both past and present members. What a fantastic group to be a part of! You all have been my community where I felt safe asking you for guidance on a myriad of subjects. Thank you for genuinely being interesting in my academic career with the group. I will forever cherish our lunch time memories! Thank you to Dr. Carla Kidd for showing me the ropes during my first and second years. Thank you to Michael Ezell for working with me on the amine–diacid project. Thank you, Mike for your muscle power, both with taking apart the QMS and for awesome discussions. Kristine Arquero and Allison Vander Wall: thank you both for our office conversations and for being awesome women in chemistry!

Professors Nizkorodov and Murray for being great committee members. Thank you for being candid with your answers on any questions I have had throughout the years.

To my academic pillars who have helped me succeed, even with the hurdles of being a first–generation student. The Student Support Services at California Lutheran University helped me navigate being an undergraduate and made sure I was on track to graduate. Thank you to the Minority Opportunities in Research Program at California State University, Los Angeles for giving me my first real experience in research, as well as creating a diverse academic environment. Thank you to Dr. Krishna Foster for being an amazing mentor at CSU Los Angeles. Thank you for always being ready and willing to provide excellent advice.

Lastly, none of this research would be possible without funding from the National Science Foundation. Thank you to the Chemistry at the Space Time Limit (CaSTL) at UC Irvine for the fellowship I received my first year.

Fairhurst, M.C., Ezell, M.J., Kidd, C., Lakey, P. S. J., Shiraiwa, M., Finlayson-Pitts, B.J. "Kinetics, mechanisms and ionic liquids in the uptake of *n*-butylamine onto low molecular weight dicarboxylic acids." Phys. Chem. Chem. Phys., 2017, 19, 4827-4839. Reproduced by permission of the PCCP Owner Societies.
http://pubs.rsc.org//content/articlehtml/2017/cp/c6cp08663b

CURRICULUM VITAE

Michelle Fairhurst
9527 Stephens St., Pico Rivera, CA 90660 | 805-890-5078 | ROAM@UCI.EDU

EDUCATION

University of California, Irvine — September 2012 – August 2017
Ph.D. in Chemistry, GPA: 3.87
Dissertation: Measuring Uptake and Reaction of Atmospherically Relevant Systems
Advanced to Candidacy: 2014

California State University, Los Angeles — June 2010 – June 2012
M.S. in Chemistry, GPA: 3.68
Thesis title: "Optimization of Analytical Techniques for Characterization of Oxygenated Benzo[a]Pyrene on Environmental Surfaces"

California Lutheran University — August 2006 –May 2010
B.S. in Biology, B.A. in Chemistry, GPA: 3.07

RESEARCH EXPERIENCE

University of California, Irvine — February 2013 – August 2017
Graduate Research Assistant
Principal Investigator: Dr. Barbara Finlayson-Pitts
Measuring uptake coefficients to understand the mechanisms of reactions between atmospherically relevant reaction systems. The overall goal is to determine if there exists a structure-reactivity relationship between the two species to better understand the chemistry behind particle growth and formation.

Utilized attenuated total reflectance–infrared spectroscopy to measure uptake of polar and non–polar gases on different liquid substrates, and SOA from the oxidation of α–pinene.

Performed extensive studies on the reaction between amines and dicarboxylic acids. Initial experiments were conducted on a small, glass flow reactor coupled to a quadrupole mass spectrometer. Uncertainties in the surface area of the solid dicarboxylic acids and limitations on the time resolution of the experiments led to the use of a Knudsen cell to measure the kinetics of this reaction system.

California State University, Los Angeles June 2010 – June 2012
Graduate Research Assistant
Principal Investigator: Dr. Krishna Foster
Developed a Master's thesis that optimized current extraction and detection techniques to successfully analyze carcinogenic polycyclic aromatic compounds, specifically quinone derivatives, adsorbed onto environmental surfaces using gas chromatography/mass spectrometry.

Ventura County Sheriff's Forensic Laboratory May 2009 – August 2009
Student Intern
Supervisors: Paul Crowley and Dea Boheme
Assisted in method validation for the use of solid-phase extraction columns to determine the concentration of cocaine and its metabolite present in ante-mortem and post-mortem urine for use in the county's Toxicology section of the Forensic Science Laboratory.

PUBLICATIONS

Fairhurst, M.C., Ezell, M.J., Finlayson-Pitts, B.J. "Knudsen Cell Studies of the Uptake of Gaseous Ammonia and Amines onto C3 – C7 Solid Dicarboxylic Acids" **2017,** *Phys. Chem. Chem. Phys.* Submitted.

Zhao, Y., Fairhurst, M.C., Wingen, L.M., Perraud, V., Ezell, M.J., Finlayson-Pitts, B.J. "New insights into atmospherically relevant reaction systems using direct analysis in real time-mass spectrometry (DART-MS)." *Atmos. Meas. Tech.*., **2017,** 10, 1373-1386.

Fairhurst, M.C., Ezell, M.J., Kidd, C., Lakey, P. S. J., Shiraiwa, M., Finlayson-Pitts, B.J. "Kinetics, mechanisms and ionic liquids in the uptake of *n*-butylamine onto low molecular weight dicarboxylic acids." *Phys. Chem. Chem. Phys.*, **2017,** 19, 4827-4839.

PRESENTATIONS

Fairhurst, M.C., Lakey, P.S.J. "What Appears on the Surface is Not What it Seems: Isn't it I(r)onic?" AirUCI Air Quality and Climate Symposium, University of California, Irvine, April 19, 2017 (Oral presentation).

Fairhurst, M.C., Ezell, M.J., Kidd, C., Finlayson-Pitts, B.J. "Measuring Uptake Coefficients for Amines on Dicarboxylic Acids as Models for Secondary Organic Aerosol Growth" 33rd Informal Symposium on Kinetics and Photochemical Processes in the Atmosphere, Irvine, CA. March 24, 2016.

Fairhurst, M.C., Ezell, M.J., Kidd, C., Finlayson-Pitts, B.J. "Measuring Uptake Coefficients for Amines on Dicarboxylic Acids as Models for Secondary Organic Aerosol Growth" 251st American Chemical Society National Meeting, San Diego, CA. March 16, 2016.

Fairhurst, M.C., Ezell, M.J., Kidd, C., Finlayson-Pitts, B.J. Measuring Uptake Coefficients for Amines on Dicarboxylic Acids as Models for Secondary Organic Aerosol Growth" 32nd Informal Symposium on Kinetics and Photochemical Processes in the Atmosphere, Northridge, CA. April 3, 2015.

Fairhurst, M.C., Kidd, C., Ezell, M.J., Finlayson-Pitts, B.J. "Measuring Uptake Coefficients and Henry's Law Constants of Gas-Phase Species with Models for Secondary Organic Aerosol" American Geophysical Union Fall Meeting, San Francisco, CA. December 16, 2014. (Oral presentation).

Fairhurst, M.C., Kidd, C., Ezell, M.J., Finlayson-Pitts, B.J. "Investigating the Fundamental Chemistry Behind Particle Growth in the Atmosphere" California State University, Los Angeles Minority Opportunities in Research (MORE) Programs Science Research Retreat, Lake Arrowhead, CA. September 5, 2014. (Oral presentation).

Fairhurst, M.C., Kidd, C., Ezell, M.J., Finlayson-Pitts, B.J. "Investigating the Fundamental Chemistry Behind Particle Growth in the Atmosphere" AirUCI Seminar, Irvine, CA. September 2, 2014. (Oral presentation).

Fairhurst, M.C., Kidd, C., Finlayson-Pitts, B.J. "Measuring Henry's Law Constants and Uptake Coefficients for Gas-Phase Species on Model Secondary Organic Aerosol" 31st Informal Symposium on Kinetics and Photochemical Processes in the Atmosphere, Riverside, CA. March 12, 2014.

Fairhurst, M.C., Kidd, C., Finlayson-Pitts, B.J. "Measuring Uptake Coefficients for Gas-Phase Species on Model Secondary Organic Aerosol" AirUCI International Science Workshop, Laguna Beach, CA. January 22-23, 2014.

Roa, M.C., Foster, K.L. "Method Development for the Separation and Characterization of Oxygenated Benzo[a]Pyrene using Gas Chromatography-Mass Spectrometry" American Chemical Society National Meeting, San Diego, CA. March 25, 2012.

Roa, M.C., Foster, K.L. "Method Development for the Separation and Characterization of Oxygenated Benzo[a]Pyrene using Gas Chromatography-Mass Spectrometry" Poster presented at the 2012 MORE Programs Poster Session, Los Angeles, CA. February 3, 2012.

Roa, M.C., Cabrera, E., Foster, K.L. "Optimization of Analytical Techniques for the Detection of Oxygenated Polycyclic Aromatic Hydrocarbons on Environmental Surfaces" Poster presented at the 2011 MORE Programs Poster Session, Los Angeles, CA. January 2011.

TEACHING EXPERIENCE

University of California, Irvine — September 2012 – June 2016

General Chemistry Lecture Teaching Assistant

- Led student discussion sections which consisted of working out practice problems that were separate from classwork.
- Composed and consulted on homework, discussion worksheets, and exams.
- Team-taught a full general chemistry lecture.
- Conducted office hours to engage with students about coursework.
- Organized review sessions prior to exams

University of California, Irvine — September 2012 – June 2016

General Chemistry and Honor's/Major's General Chemistry Laboratory Teaching Assistant

- Taught two lab sections per quarter with a focus on the experiment of the week as well as safety messages.
- Graded lab reports and returned in a timely manner. In the Honor's and Major's course, lab reports consisted of typed out reports.
- Conducted office hours to engage with students regarding lab reports.

AWARDS

- Chemistry at the Space-Time Limit (CaSTL) Fellow – University of California, Irvine — September 2012 – June 2013
- National Institutes of Health (NIH) Minority Biomedical Research Support Program – Research Initiative for Scientific Enhancement (MBRS-RISE) Graduate Fellowship – California State University, Los Angeles — June 2010 – July 2012
- California Lutheran University Dean's List — May 2010

OUTREACH

Irvine Unified School District - Ask-A-Scientist Night — October 2016

- Provided guidance for middle school students on their proposed science fair projects. The students explain their projects and ask questions about possible directions or ideas regarding the projects.

American Chemical Society's National Chemistry Week at the Santa Ana Zoo — October 2016

- Along with Iota Sigma Pi, developed a science demonstration where zoo visitors could reveal secret messages using acid/base chemistry.

AirUCI Guided Lab Tours February 2013 – July 2017

- AirUCI is a collaborative, multidisciplinary unit at UC Irvine where the common research goal is to understand processes involved in climate change. As a whole, research labs conduct demonstrations in labs and discuss ongoing research.

Girls Inc., Costa Mesa, CA June 2013 – May 2014

- As part of Iota Sigma Pi, we visited Girls Inc., an after-school program for young girls, to show the girls chemistry demonstrations and also serve as representatives for women in chemistry.

X-treme Careers, Moorpark, CA April 2010

- Presented to middle school students on what it takes to work in a forensic science laboratory as part of their afterschool program to learn about possible future career choices.

PROFESSIONAL AFFILIATIONS

American Geophysical Union
Iota Sigma Pi
American Chemical Society

ABSTRACT OF THE DISSERTATION

Measuring Uptake and Reaction of Atmospherically Relevant Systems

By

Michelle Christine Fairhurst

Doctor of Philosophy in Chemistry

University of California, Irvine, 2017

Professor Barbara J. Finlayson-Pitts, Chair

Atmospheric particles adversely affect climate, visibility, and health and thus the need to understand their formation and growth mechanisms is essential. However, the lack of complete understanding of these mechanisms may be a result of the complexity of the interactions between gas and particle phase species. Model systems of atmospherically relevant species are often utilized to better understand the chemistry of these reactions in the atmosphere.

This dissertation work explores uptake and reaction of various atmospherically relevant reaction systems to determine if the chemical properties of the gas and condensed phases affect the mechanism of uptake. In the first approach, attenuated total reflectance–Fourier transform infrared (ATR–FTIR) spectroscopy was used to measure the uptake of various gas phase species on different low viscosity liquids and on secondary organic aerosol (SOA) generated from the ozonolysis of α–pinene. Uptake of gas phase isobutyl nitrate (IBN) into squalane and Fomblin ® was rapid, with equilibrium established quickly. A higher concentration of gas phase IBN was

needed to see uptake into Fomblin ®, which may be due to the increased number of polar groups compared to squalane. Uptake of IBN onto laboratory generated SOA was much slower than squalane, which may be indicative of the much higher viscosity of SOA. Polar compounds were readily taken up onto the clean ATR crystal, even with a self–assembled monolayer fixed to the crystal surface.

The second system of interest was the reaction between gas phase amines and solid dicarboxylic acids (diacids), which was carried out using two different techniques. The first technique utilized a flow reactor coupled to a quadrupole mass spectrometer. The second method involved a Knudsen cell interfaced to the mass spectrometer. Uptake coefficients for *n*–butylamine on solid C2 – C5 diacids were on the order of $10^{-3} – 10^{-2}$ using the flow reactor. Experiments conducted using the Knudsen cell had measured uptake coefficients from 10^{-1} to $\leq 10^{-6}$, depending on the number of carbon atoms in the diacid chain. Those experiments performed using the flow reactor were operated at time constants that may have been too slow to capture the initial uptake of the amine onto the diacid. This manifest itself into a lack of difference in uptake coefficients between diacids, as well as signs of surface saturation. Further exploration of this reaction using the Knudsen cell concluded that uptake coefficients for odd carbon number diacids are orders of magnitude larger than the even carbon number diacids. This difference is due to the dissimilarities in packing of the crystal structures, as well as the formation of an ionic liquid layer on the surface that is able to provide replenishment of the diacid. Subsequent studies of different primary amines, as well as dimethylamine, trimethylamine, and ammonia show that structure of the amine also affects the kinetics and formation of the ionic liquid layer.

These reaction systems show that the nature of the gas and condensed phase species both play a large role in uptake and reaction of the gas phase. Results from these experiments show that overall assumptions in the interactions between the gas and condensed phases may not be accurate in predicting concentrations of atmospheric particles. Experiments carried out on these reaction systems highlight the benefits of studying model systems in order to gain a better understanding of one component of atmospheric interactions between two species. Ultimately, these and other model systems will help build a better understanding on a molecular level of the chemistry behind particle growth in the atmosphere.

CHAPTER 1: INTRODUCTION

I. The Importance of Atmospheric Particles

The need to understand the chemistry behind atmospheric particles is essential due to their adverse effects on health and climate. Particles are classified by their size with those < 10 μm in diameter categorized as coarse, and those < 2.5 μm as fine.[1-3] The fine particles can easily deposit into the lungs and can often lead to serious respiratory illnesses[1, 2, 4-12] and increased mortality.[6, 13-15] On a molecular level, pollutants can increase the concentration of reactive oxygen species in the lung lining fluid.[11] Additionally, lung lining fluid contains surface–active antioxidants to protect the lungs from pollutants such as ozone. However, studies have shown that the ozonolysis of these surfactants can occur,[16-18] which have implications for potential chemistry occurring in the lung lining fluid.

Particles can also affect climate via their ability to scatter and/or absorb incoming solar radiation. At sizes ~ 100 nm and above, particles can become efficient in scattering incoming radiation. Radiative forcing is used to describe the balance of incoming solar radiation based on a particular forcing agent, such as particles.[19] The net radiative forcing for aerosol particles is negative, indicating these particles have an overall cooling effect.[19] However, other types of particles, such as black carbon, have an overall positive radiative forcing, signifying it has a warming effect.[19] Once at diameters of 100 nm or larger, particles can also act as cloud condensation nuclei (CCN).[20-25] These CCN serve as nucleation points for the formation of cloud droplets which in turn scatter incoming radiation.[20-22, 24, 25]

II. Primary vs. Secondary Organic Aerosol

There are two main types of atmospheric particles as classified by source: primary and secondary. Particles can also be categorized as either organic or inorganic, with 20 – 90% grouped as organic in composition.[26] Primary organic aerosol (POA) particles are emitted directly from their sources, which include anthropogenic (biomass burning, and combustion)[4, 27-29] and biogenic sources (volcanic eruptions, and sea salt).[4, 27] Oxidation of anthropogenic and biogenic volatile organic compounds (VOCs) via common atmospheric oxidants such as O_3, NO_x, and OH,[12, 27, 28, 30] lead to the formation of lower volatility, highly oxidized products known as secondary organic aerosol (SOA).[3, 28-30] Common classes of these oxygenated products include carboxylic acids (–COOH), alcohols, aldehydes, ketones, and nitrates.[27-30] However, in cases where oxidation leads to fragmentation of the carbon chains to form lower molecular weight oxygenated products, these products tend to be more volatile.[27, 28, 30] Ultimately, oxidation of VOCs lead to the production of CO_2,[27, 28] which in turn has a warming effect on the atmosphere due to the positive radiative forcing value.[19]

III. Mechanisms of Particle Formation and Growth

The formation of new particles in the atmosphere takes place via a stepwise process. First, through molecular collisions, the formation of a cluster is achieved.[3, 31-34] This cluster then grows to a critical size in which further growth of this nucleus dominates.[3, 31-35] The rate of nucleation of this critical cluster is dependent its chemical composition as well as the concentrations of the gas molecules that subsequently grow this cluster.[3, 31] In the atmosphere, nucleation commonly occurs via interactions of multiple types of gas phase molecules, such as organics, inorganic acids, bases, and/or water.[3, 31-35]

Subsequent growth of atmospheric particles can occur via condensation of gas phase species onto the existing particles.[3, 4, 32-34, 36] Products from VOC oxidation with sufficiently low vapor pressure can condense onto pre–existing particles.[26, 29-31] The size of the particle also governs condensation of gases via the Kelvin effect. This theory states that the vapor pressure at a particle surface is increased over the curved surface and with increasing particle radius, this vapor pressure over the droplet decreases.[3, 31, 33] Therefore, in order for condensational growth to occur, the particle must have a sufficiently large radius so that the vapor pressure of the particle is small enough to prevent evaporation of the particle.[3, 31]

Partitioning of the gas phase species is dependent on the properties of the gas and particle. For example, particle phase is known to affect the rate at which gas phase molecules partition into the particle.[37-39] It had been assumed for decades that atmospheric particles are liquid–like, and thus grow via a thermodynamic quasi–equilibrium with gas phase species.[27, 36, 38-45] Pankow derived a set of equations that take into account the activities and pressures of the gas and particle phases to describe the equilibrium partitioning between the two species.[43, 44] An expression for the fractional mass yield of SOA is given by using the SOA mass concentration produced for a given amount of gas phase species reacted.[40, 46-50] Using this relationship, several studies of SOA yields from a variety of gas phase precursors have shown that SOA yield is a function of the SOA mass concentration.[40, 47, 48, 51, 52]

The equilibrium partitioning theory assumes that the particle is a well–mixed low viscosity material in which the particle's equilibrium mixing times will be sufficiently fast.[37-39]

However, recent experiments have shown that the behavior of SOA did not match a well–mixed, low viscosity, easily diffusible particle. Abramson et al.[53] showed that tracer compounds in the presence of generating SOA become trapped in the SOA particles with little evaporation of the tracer occurring over 24 hours. Estimated diffusion coefficients for these tracers in SOA led to the conclusion that the SOA material is more tar–like.[53] Perraud et al.[46] found that when plotting the ratio of the mass concentration of organic nitrates in the particle phase over mass concentration of the particulate matter as a function of concentration of organic nitrates in the gas phase, the plot was non–linear which indicated that equilibrium gas–particle partitioning was not occurring. Cappa and Wilson[54] compared the volatility of compounds associated with lubricating oil and SOA components from the ozonolysis of α–pinene. Mass spectrometry studies showed that high vapor pressure compounds associated with the lubricating oil evaporated as expected at high temperatures, while the mass spectrum of SOA remained unchanged, indicating no evaporation of SOA components.[54]

These studies, and numerous others, have shown that under certain conditions, SOA particles can adopt a more viscous or tar–like phase,[46, 53-64] in which case gas phase species irreversibly condense on particles by a diffusion–limited process.[3, 38, 65] Using the Stokes–Einstein equation, the diffusion coefficient of a substance is inversely related to the viscosity.[37, 38] Thus, compounds in these high viscosity SOA particles are expected to have very low diffusion coefficients, therefore creating diffusion limitations under some conditions which may depend on particle size, volatility, and mass loading of SOA.[37, 38]

IV. Acid–Base Reactions in the Atmosphere

Particle growth can also occur via heterogeneous reactions in the atmosphere. The most common example of heterogeneous reactions is acid–base reactions that can form their respective salts. Extensive studies on the reaction of NH_3 with sulfuric acid have been conducted, with the conclusion that these reactions are important in new particle formation.[31, 66-72] In addition to NH_3, studies of the reaction of amines with sulfuric acid have also been carried out.[66, 71-76] Recent studies on methanesulfonic acid and amines have been performed to assess their importance in new particle formation and growth.[77-83]

The acid–base reactions involving amines and ammonia are important and relevant to the atmosphere. Amines and ammonia are ubiquitous in the atmosphere, with concentrations of ammonia generally surpassing those of amines.[84-90] Concentrations of amines are around ppb levels near agricultural sources, while in other regions, levels reach ppt amounts and are typicall 1 – 3 orders of magnitude lower than concentrations of ammonia.[84, 91] However, ammonia has been shown to be less effective at forming particles with sulfuric acid[66, 71, 72, 74, 76, 92] and methanesulfonic acid[77, 78] when compared to amines. The oxidation of gas phase amines can also lead to SOA formation.[93-107] Ammonia has also been observed to affect properties of SOA, including yield,[108, 109] morphology,[109-112] composition,[108, 110, 112-115] optical properties[108, 111, 116, 117] and evaporation kinetics.[110]

In addition to inorganic acids, organic acids are also present in organic particulate matter.[118-122] Laboratory studies on the reaction of amines with some organic acids, such as citric and humic acids have been studied with results showing a difference in uptake between the

two acids.[123] Larger uptake was observed for amines on citric acid which was correlated with the higher acidity of citric acid compared to humic acid.[123] Steric effects were also shown to control the difference in reactivity of the amines for a given acid.[123] Another class of organic acids are dicarboxylic acids (diacids), which are found in particles from different regions around the world.[124-131] Relevant to the acid–base chemistry mentioned above, ammonium and aminium ions often coexist with diacid anions in atmospheric particles.[132-134] Thus, a molecular level understanding of amine–diacid reactions can contribute to an accurate predication for particle formation and growth in the atmosphere. However, it is also of significant intrinsic chemical interest because of the dependence of the various properties of diacids on the carbon chain length and structure.[135-140]

V. The Importance of Model Systems

Atmospheric models tend to under–predict ambient particle concentrations, with this discrepancy possibly stemming from the inability to account for the complex heterogeneous chemistry occurring in the atmosphere.[141-144] Therefore, laboratory studies of model systems are often utilized to understand one component of the reactions occurring in the atmosphere.

Squalane, a C30 saturated hydrocarbon, has been used as a proxy for hydrocarbons released from anthropogenic sources. The oxidation of squalane using OH radicals has shown that the resulting products contain oxygenated functional groups.[145] Another property that changes upon oxidation of squalane is that the hygroscopicity increases as squalane is exposed to OH for long periods of time.[146]

The fraction of collisions of gas molecules with the particle surface leading to reaction is known as the uptake coefficient, γ, and $\gamma = 1$ would indicate that all molecules that collide with the surface are reactively taken up into the particle. Uptake coefficients provide insights into the kinetics between the gas and condensed phases. Further conclusions on how the structure or chemical properties of the gas and condensed phases affects the magnitude of these measured uptake coefficients can be drawn. In the study of amines with citric and humic acids, uptake coefficients ranged from $(6 - 7) \times 10^{-3}$ and $(5 - 10) \times 10^{-5}$ for citric and humic acids, respectively.[123] Even with these acid–base reactions, uptake coefficients are far less than unity. The reactive uptake for ozone on mixed oleic/steric acid and oleic acid particles are also on the order of 10^{-3}.[147, 148] Therefore, it is essential to determine uptake coefficients for different reaction systems relevant to the atmosphere. However, it is difficult to experimentally measure uptake coefficients. For example, if solid substrates are utilized, considerations of the gas phase concentrations must be taken into account as to not rapidly saturate the surface of the substrate.[149, 150] Other issues with measuring uptake coefficients of gas phase species onto solid substrates is accounting for diffusion into multiple layers of the solid if more than a monolayer of the solid is present.

VI. Project Goals

The goal of this project is to measure uptake coefficients for a variety of different gas phase species and substrates to determine if there exists a relationship between the structure of the two species and uptake. These heterogeneous reactions are relevant to the atmosphere so that a molecular level understanding of the chemistry behind uptake of the gas phase species onto the condensed phase can be formulated. On a larger scope, the ultimate goal is to build a database of

uptake coefficients for a wide range of scenarios to help make predictions for different systems based on molecular properties. Ultimately, these structure–activity relationships will help atmospheric modelers incorporate these uptake coefficients into their models to better account for the complex chemistry in the atmosphere.

Model systems chosen for study include (1) gas phase species of differing polarities onto low viscosity liquids and laboratory generated SOA. Initial studies of gas phase species onto low viscosity liquids were chosen to avoid complications of gas phase uptake such as diffusion limitations. Isobutyl nitrate, hydroxyacetone, acetone, and acetic acid were chosen as gas phase species due to their atmospheric relevance. Squalane and Fomblin ® were chosen as low viscosity model substrates. (2) Reactions of amines with solid diacids using two techniques – a flow reactor and a Knudsen cell, both coupled to a quadrupole mass spectrometer. In the former, first order rate constants are used to derive uptake coefficients. Knudsen cell studies are able to measure uptake coefficients using the intensity of the amine before and after introduction to the diacid surface. The goal of the amine–diacid system is to determine if the structure of the amine and/or the diacid has an effect on the measured uptake coefficients and to provide molecular level information on factors that determine net uptake.

CHAPTER 2: EXPERIMENTAL METHODS

I. Uptake of Gas Phase Species with Single Compounds as Models for SOA

Uptake of gas phase species onto selected substrates was characterized using a Nicolet 6700 (Thermo Scientific) Fourier transform infrared (FTIR) spectrometer. The substrate was applied to a germanium (Ge) attenuated total reflectance (ATR) crystal (Pike Technologies, 80 mm x 10 mm x 4 cm, 10 reflections) and enclosed in a horizontal flow–through ATR holder (Pike Technologies). In order to obtain absorbance spectra, a background spectrum (S_0) of a clean crystal was taken; another spectrum was taken of the substrate on top of the ATR crystal (S_1). The resulting IR spectrum was plotted as $\log_{10}(S_0/S_1)$. Background spectra in uptake experiments were that of the substrate on the ATR crystal (S_0). Spectra were taken as soon as the gas phase species was introduced to the substrate (S_1) and the resulting absorbance spectrum will indicate any changes between S_1 and S_0. All experiments were performed at 4 cm^{-1} resolution.

Two liquid–phase substrates were used in these studies (Figure 2-1). Squalane (Sigma-Aldrich, 99%), a long chain hydrocarbon proxy for primary organic aerosol particles[151] was utilized along with Fomblin ® (Solvay Solexis, Y25/6), a substrate with more polar groups and a low vapor pressure. Their properties are summarized in Table 2-1.

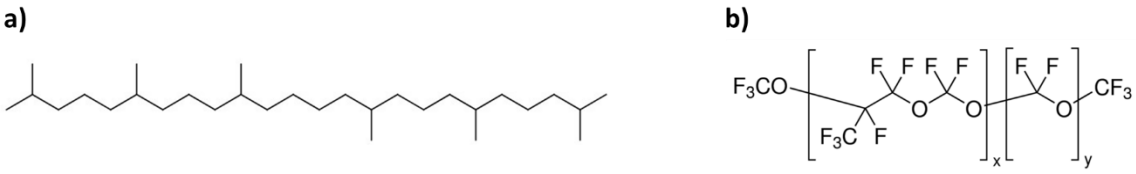

Figure 2-1. Structures of squalane and Fomblin ®.

Table 2-1. Physical and chemical properties of squalane and Fomblin ®.

	Squalane	Fomblin ®
Molar mass (g mol^{-1})	422	3300 [a, b]
Density (g cm^{-3})	0.81 [152]	1.9 [a]
Viscosity (Pa s)	3.1×10^{-2} [152]	0.5 [a]
Vapor pressure (atm)	10^{-11} [152]	7.9×10^{-11} [a]
Refractive index	1.4 [152]	1.3 [153]
Diffusion coefficient (cm^2 s^{-1})	10^{-6} [c]	10^{-7} [37 c]

[a] Values from Solvay SDS.
[b] Average molecular weight.
[c] Estimated using the viscosity of Fomblin ® or squalane and Figure 1 in Koop et al.[37]

Both compounds were deposited onto the Ge crystal either by deposition of a solution containing the liquid substrate dissolved in solvent and letting it evaporate to produce a thick film, or by nebulization of the neat solution giving liquid droplets. For a thick film of squalane, a known volume of squalane was dissolved in 1 mL heptane. The volume of squalane needed to dissolve in heptane was calculated using the area of the crystal opening on the ATR holder and the desired film thickness (90 μm). Particle size distributions of the squalane droplets were

measured using a scanning mobility particle sizer (SMPS; TSI 3080) equipped with a differential mobility analyzer (TSI 3081) and condensation particle counter (TSI 3025A). The diameter of the mode of the nebulized squalane particles was 400 nm. This diameter was used because larger particles in the size distribution were not captured due to the cut–off of the instrument (700 nm). Because Fomblin ® has a slightly higher viscosity, it was easier to spread throughout the crystal and therefore 0.15 mL of neat Fomblin ® was used to coat the ATR crystal giving a thickness of 400 μm.

Atmospherically relevant gas phase species were used to determine uptake and solubility into the substrate. These include isobutyl nitrate (IBN), hydroxyacetone (HA), acetic acid, and acetone (Figure 2-2).

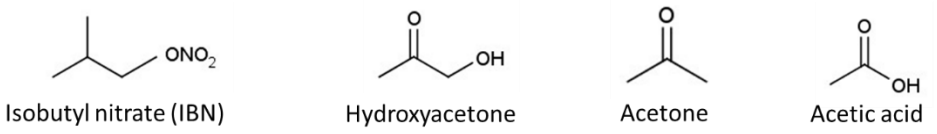

Figure 2-2. Structures of gas phase species used in ATR uptake studies.

IBN serves as a representative for organic nitrates that are formed from the oxidation of hydrocarbons via NO_x ($NO + NO_2 + NO_3$).[154-158] Organic nitrates are thermally stable and typically have long atmospheric lifetimes (on the order of hours to days),[156-160] and can ultimately produce NO_2.[155, 161] Hydroxyacetone is often observed as a second generation oxidation product of isoprene.[162, 163] Acetone is ubiquitous in the atmosphere with sources from biomass burning, oxidation of hydrocarbons, and biogenic emissions.[164-166] Acetic acid, along

with formic acid, is the most common monocarboxylic acid found in the gas phase (ppb levels) around various atmospheric environments.[167-171]

All four compounds are commercially available in liquid form. The desired compound is introduced in the gas phase via a syringe pump (Pump Systems Inc., NE-1000) which pumps liquid at a constant rate into a 5 L mixing bulb filled with ultra–zero air (Praxair, 19.5–23.5% oxygen, < 2 ppm water, < 0.1 ppm total hydrocarbons, < 0.5 ppm carbon monoxide, < 0.5 ppm carbon dioxide, balance nitrogen). A known concentration of the gas phase species exits the mixing bulb and is directed to a UV–Vis spectrometer (HP 8452A) to monitor the concentration out of the bulb. From the UV–Vis spectrometer, the flow is then directed into the ATR cell to measure uptake into the substrate.

During the experiment, the IR beam interrogates the coated Ge ATR crystal shown in Figure 2-3.

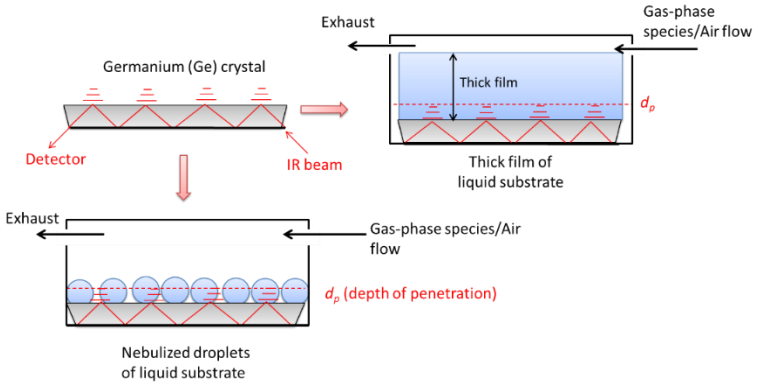

Figure 2-3. Schematic of two different types of squalane coatings on the Ge ATR crystal.

How much the IR beam penetrates the liquid substrate can be calculated using the depth of penetration (d_p),

$$d_p = \frac{\lambda_1}{2\pi(sin^2\theta - {n_{21}}^2)^{1/2}} \quad \textbf{2.1}$$

where n_1 and n_2 are the refractive indices of the crystal and liquid substrate, respectively, λ_1 is the ratio of the desired wavelength of the specific compound (liquid substrate) over n_1, n_{21} is the ratio of n_2 over n_1, and θ is the angle of incidence.[172] Using the reported refractive indices for squalane and Fomblin ® (Table 2-1) the depth of penetration for both substrates can be derived. The depth of penetration for squalane is 0.23 μm at 2800 cm^{-1}, corresponding to the –CH stretch. The depth of penetration for Fomblin ® at 1230 cm^{-1}, reflecting the $–CF_3$ stretch, is 0.52 μm. Based on these values for the depths of penetration for squalane and Fomblin ®, only a small portion of the thick films is being interrogated.

II. Generation and Uptake of Gas Phase Species onto SOA

Uptake experiments were repeated using laboratory generated SOA in order to see if the dependence of uptake on chemical composition and viscosity holds true for SOA. SOA was generated using a stainless steel, large volume flow reactor[173] using 1 ppm α-pinene and ~ 500 ppb ozone as the gas phase precursors. The total flow in the reactor was 20 L min^{-1}. SOA was impacted onto a Ge ATR crystal using a custom–built impactor described in detail previously and shown in Figure 2-4.[56]

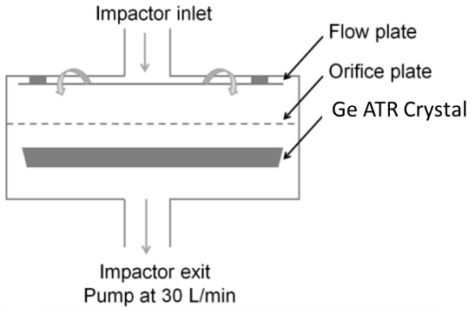

Figure 2-4. Schematic of impactor used in SOA ATR studies. Figure adapted from Kidd et al.[56]

Briefly, a large inlet (10 mm) directs particles through an aluminum plate with evenly spaced holes that form a centerline along this plate.[56] The flow of particles is pumped through the impactor at 30 L min^{-1} and particles with enough momentum will impact onto the ATR crystal while smaller particles will travel along the edges of the crystal and out into the airstream.[56] Particles exiting at the end of the flow reactor were impacted onto the ATR crystal as a function of impaction time, with longer impaction times collecting more mass and giving a stronger IR signal of the asymmetric $–CH_3$ stretch as shown in Figure 2-5. In these experiments, SOA collected for 10 minutes and 180 minutes impaction times were used in order to determine the effect of thickness on uptake of gas phase species.

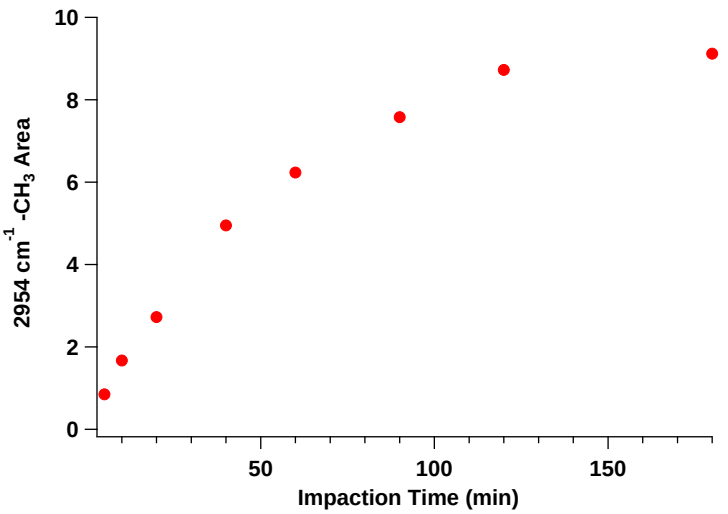

Figure 2-5. Plot of the $–CH_3$ stretch peak areas for SOA as a function of impaction time.

III. The Use of Self-Assembled Monolayers to Avoid Uptake onto Clean Crystal Surfaces

Self–assembled monolayers (SAMs) consist of a trichlorosilane group that attaches to a silanol surface with the alkyl chain exposed to the interface. The SAM used in these experiments was made from octadecyltrichlorosilane (C18 alkyl SAM; 97% Gelest Inc.) as shown in Figure 2-6.

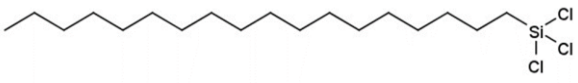

Figure 2-6. Structure of octadecyltrichlorosilane (C18 alkyl SAM).

As discussed in Chapter 3, Section III, uptake of polar gases onto the clean Ge crystal was observed. Therefore, SAMs were employed to shield the crystal from the incoming polar gas phase species. The C18 alkyl terminated SAM was deposited onto a silicon (Si) ATR crystal

(Pike Technologies, 80 mm x 10 mm x 4mm, 10 reflections) that was boiled in isopropyl alcohol prior to use. The crystal was placed inside a custom–built Teflon holder that has an open slot exposing the surface of the ATR crystal. To achieve a concentration of 2.15 mM, 6.8 μL of the C18 alkyl SAM was dissolved in 8 mL hexadecane. The 2.15 mM SAM solution was used to fill the open area of the Teflon holder containing the Si ATR crystal. The SAM solution was left to react with the Si ATR surface for approximately 45 min. The crystal was then removed from the holder and boiled in dichloromethane to remove any unreacted SAM. This procedure was repeated two more times to ensure a complete and even coating of the SAM onto the Si ATR crystal. In preparation for experiments, the C18 coated Si ATR crystal was placed in a commercially available horizontal flow–through ATR holder and purged with ultra–zero (Praxair, 19.5–23.5% oxygen, < 2 ppm water, < 0.1 ppm total hydrocarbons, < 0.5 ppm carbon monoxide, < 0.5 ppm carbon dioxide, balance nitrogen) air to eliminate impurities and achieve a "dry" system. A thick film of Fomblin was then used to coat the C18 coated Si ATR crystal. A volume of 0.15 mL Fomblin ® was used as described in Chapter 2 Section I to give a 400 μm estimated thickness.

IV. Reaction of Gas Phase Amines with Soild Dicarboxylic Acids Using a Custom–Built Flow System

The design of the borosilicate glass flow system is shown in Figure 2-7.

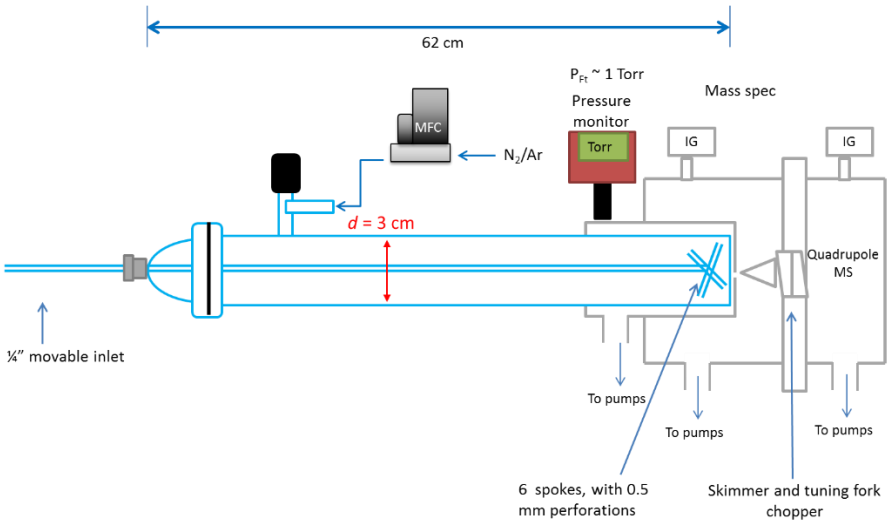

Figure 2-7. Schematic of the flow reactor coupled to the QMS. IG = ion gauge. P_{FT} = total pressre in the flow reactor (Torr). MFC = mass flow controller.

The total length of the flow reactor is 62 cm, with an inside diameter of 3 cm and it is interfaced to a quadrupole mass spectrometer (QMS, Extrel Core Mass Spectrometers). Coatings of the dicarboxylic acids (diacids) include oxalic (C2; Sigma–Aldrich), malonic (C3; Alfa–Aesar, Sigma–Aldrich), succinic (C4; Sigma–Aldrich), and glutaric (C5; Sigma–Aldrich) acids (Figure 2-8), all with a stated purity of ≥ 99%, and were used as received. The flow reactor was not water cooled and therefore all experiments were performed at ambient temperatures.

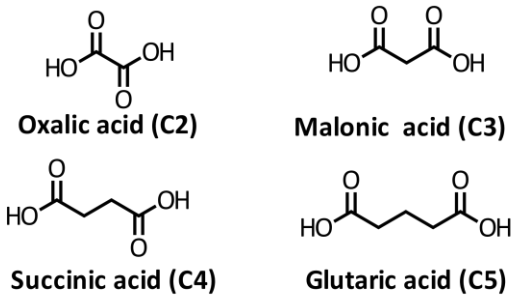

Figure 2-8. Structures of diacids used in flow reactor studies.

Milli–Q ™ water (Mili–Pore, 18.2 MΩ cm) was used to wet the inside of the flow reactor. The diacid of interest was then deposited onto the inner wall of the flow reactor and dispersed by rolling a plastic tube around the inside of the flow reactor. A flow of dry nitrogen (Praxair, 99.999%) was used to dry the excess water from the diacid.

The reactions of amines with solid diacids were studied to measure their uptake coefficients. A moveable inlet with six 0.5 mm perforated spokes was used to introduce the gas phase reactant whose loss is followed with time to obtain first–order kinetics as it reacts with the solid substrate coating the flow reactor. The amines used in this study were *n*–butylamine (BA) and *sec*–butylamine (sBA) (Figure 2-9).

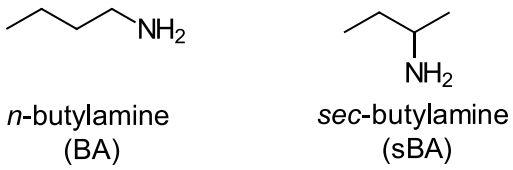

Figure 2-9. Structures of gas phase amines used in flow reactor studies.

Gas phase species were introduced from a trap containing liquid BA (Sigma–Aldrich, 99%) or sBA (Sigma–Aldrich, 99%), where helium (Praxair, 99.999%) flowed over the headspace. The gas travels through a flowmeter (Matheson 610A), which was calibrated using a Gilibrator (Sensidyne) as a function of the black ball reading on the flowmeter (Figure 2-10). The flow of the gas phase species was controlled with various needle valves.

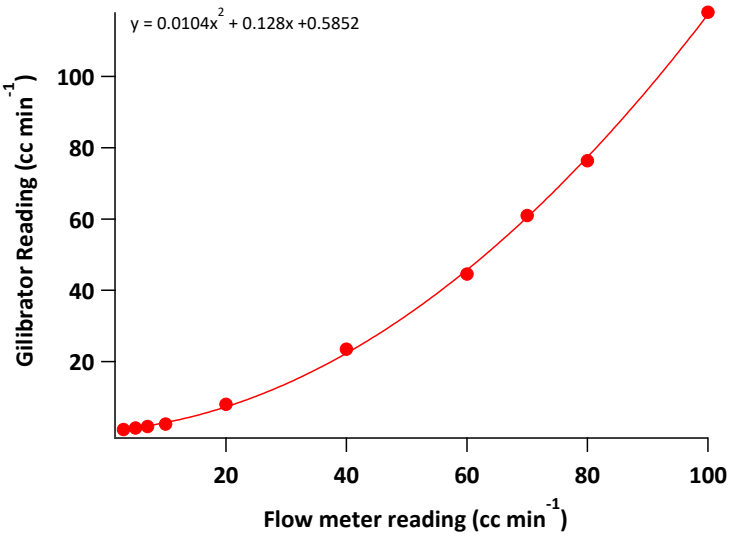

Figure 2-10. Calibration curve for 610A flow meter using Helium.

Nitrogen (Praxair, 99.999%) or argon (Praxair, 99.999%) was introduced through a stop–cock upstream from the QMS as a bulk carrier gas at a flow rate of 190 – 200 cc min^{-1} based on the desired concentration of the amine, giving total pressures of 0.8 – 1.0 Torr inside the reactor. Average flow speeds in the reactor were calculated to be 414 ± 20 cm s^{-1} (2σ) using the equation $\frac{P_0 F_{tot}}{A P_{FT}}$, where A is the area of the flow reactor (cm^2), P_{Ft} is the total pressure in the flow reactor (atm), P_0 is the pressure of the gas phase species at 1 atm, and F_{tot} is the total flow rate in the flow reactor. Recall that experiments in the flow reactor were conducted at ambient

temperatures. Initial concentrations of the amines ranged from $(3 – 30) \times 10^{13}$ molecules cm^{-3}. The amine was allowed to condition the system until a steady amine signal was achieved. No uptake of the amines on a clean flow reactor was observed.

The flow of gas molecules exiting the flow reactor entered the QMS via a pinhole of 1 mm in diameter. The molecular beam then passed through a 2 mm diameter skimmer to narrowly direct the beam into the ionizing region. The beam of amine molecules exiting the skimmer was then chopped with an 800 Hz tuning fork chopper (American Time Products, L40CB, model 5AR driver,) connected to a lock–in amplifier (Princeton-Applied Research, Model 5209). This allows for only those components that are chopped at 800 Hz to be measured by the lock–in amplifier, thus improving signal–to–noise. Operation of the mass spectrometer was controlled using Merlin Automation Data System software (Extrel, Version 3.0). The amine signal was monitored using the $H_2C{=}NH_2^+$ fragment ion at *m/z* 30 for BA and $H_2C{=}NH(CH_3)^+$ at the *m/z* 44 fragment ion for sBA.[174]

The signal of the amine peak as a function of time was monitored using the Merlin Automation Software. The average signal ($I_{measured}$) and background signal ($I_{background}$) at t = 0 s (I_0) and time, t, were subtracted to give the total signal (I_{total}). A plot of $\ln(I_{total,t})/(I_0)$ against reaction time was used to measure first–order rate constants for the amines on each diacid. Uptake coefficients are subsequently measured using Equation 2.2.

$$\gamma \frac{A}{V}\sqrt{\frac{RT}{2\pi M}} = k \qquad \textbf{2.2}$$

Equation 2.2 takes into account the geometric surface area of the diacid (A, cm^2), the reacted volume of the flow reactor (V, cm^3), the measured first–order rate constant (k, s^{-1}), the uptake coefficient (γ), and R, T, and M are the gas constant ($J\ K^{-1}\ mol^{-1}$), temperature (K), and molar mass ($kg\ mol^{-1}$), respectively.

All parameters except for the surface area of the diacids were easily measured. The maximum total surface area of the diacid was calculated using Equation 2.3.

$$A = l^2 * 5 * N \qquad \textbf{2.3}$$

The crystals were assumed to be cubic in structure. The length of the edge of a diacid crystal is represented by l, five indicates the sides available for reaction, and N is the number of crystals on the flow reactor coating. These variables were all measured independently. First the surface area of one crystal was calculated by measuring one edge of the crystal. Dial calipers were used to measure the edge of a crystal and an average length of 20 crystals was used to obtain average lengths as shown in Table 2-2.

Table 2-2. Diacid edge lengths measured using dial calipers. Averages are of 20 crystals.

Diacid	Edge Length (l) μm ± 1σ
Oxalic (C2)	690 ± 340
Malonic (C3)	700 ± 370
Succinic (C4)	680 ± 230
Glutaric (C5)	780 ± 480

Next, the total number of crystals was measured using the ratio of the total volume of the diacid on the flow reactor and the volume of a single diacid crystal. The volume of a diacid crystal was calculated using the average edge length of the crystal. The total volume of the diacid coating was obtained by taking the mass of the coating that was scrapped off after a run divided by the density of the diacid. Masses from initial studies with BA on malonic acid (C3) were obtained from rinsing off the coating with nanopure water and boiling the mixture to evaporate the water and subsequently taking the mass of the resulting solid. The temperatures of the heated aqueous solutions were around 90 °C. Malonic acid (C3) decomposes at 140 °C[175] and therefore, it can be assumed that all the malonic acid (C3) is recovered from the rinsed off coating. Due to the assumptions of nature of the coating, variability in coatings from sample to sample, and the large spread in edge lengths (Table 2-2), the largest source of uncertainty in the uptake coefficients stem from the diacid surface area.

Method validation for the flow reactor was performed by looking at the uptake of HNO_3 on NaCl and comparing the uptake coefficient to literature values. Nitrogen was flowed through a trap containing a 70% solution of HNO_3 (Sigma-Aldrich, 99%) and passed through the same

configuration as discussed above. The flow reactor was coated with NaCl (Fisher-Scientific, certified ACS crystalline) using the procedure stated previously. The average length of the NaCl crystals was 550 μm. The concentration of HNO_3 in the flow reactor was ~ 2×10^{14} molecules cm^{-3} giving an uptake coefficient of $(3 \pm 2) \times 10^{-3}$ ($\pm 1\sigma$) which is in good agreement with the accepted value of approximately 10^{-3} to 10^{-2} measured from various studies.[176-179]

V. Uptake of Gas Phase Amines on Diacid Slurries

Continuous flow reactor experiments on solid diacids and NaCl coatings gave rise to a buildup of salt around where the pinhole mounts in the front chamber. In addition, experiments with solid coatings resulted in large uncertainties due to assumptions made regarding the shape and arrangement of the crystals. Therefore, the coating method was altered to a slurry coating.

Supersaturated solutions of malonic (C3) and glutaric (C5) acids were created in nanopure water and heated to near boiling. These solutions were considered supersaturated when diacid crystals were no longer dissolved in the solution. A cloth glove was dipped into the solution and used to evenly spread the saturated solution onto the flow reactor walls. Excess solution was poured out of the flow reactor and the reactor was subsequently dried with nitrogen (Praxair, 99.999%). Once dried, a thin coating of the diacid was left behind, rather than solid crystals fixed to the flow reactor walls. The "slurry" coatings have the benefit of eliminating the uncertainty in the surface area because the error in accounting for the number of crystals and available sides for reaction is not involved. Instead, the surface area of the flow reactor was used as the reactive surface area.

Coatings of oxalic (C2) and succinic (C4) acids were not as straightforward. For oxalic acid (C2), a saturated solution was prepared as mentioned for the odd carbon diacids, and subsequently heated. A cork was placed at the end of the flow reactor and the hot solution was poured inside and swirled. This rinsing method was repeated a few times and excess solution was poured out and nitrogen (Praxiar, 99.999%) was flowed through the reactor to dry the coating. It is important to note that leaving an oxalic acid (C2) coated flow reactor interfaced to the QMS for extended periods of time pumped off the thin coating. This could be due to its very high vapor pressure (1.1×10^{-7} atm at 296 K)[136] compared to the other diacids. A similar method was used to coat succinic acid (C4) onto the flow reactor.

Uptake coefficients were calculated using Equation 2.2, however assumptions for the reactive surface area were different for the slurry experiments than for the solid coatings. It was assumed that there was an even coating on the flow reactor walls. Therefore, the surface area of the flow reactor was used in Equation 2.2.

VI. Knudsen Cell Studies of Amines/Ammonia on Diacids

A second approach using a Knudsen cell was applied to obtain uptake coefficients for amines on diacids. The Knudsen cell was interfaced to a quadrupole the QMS which has been described in detail previously.[176] Orifice diameters of either 1.40 or 6.28 mm were used in these experiments (Figure 2-11).

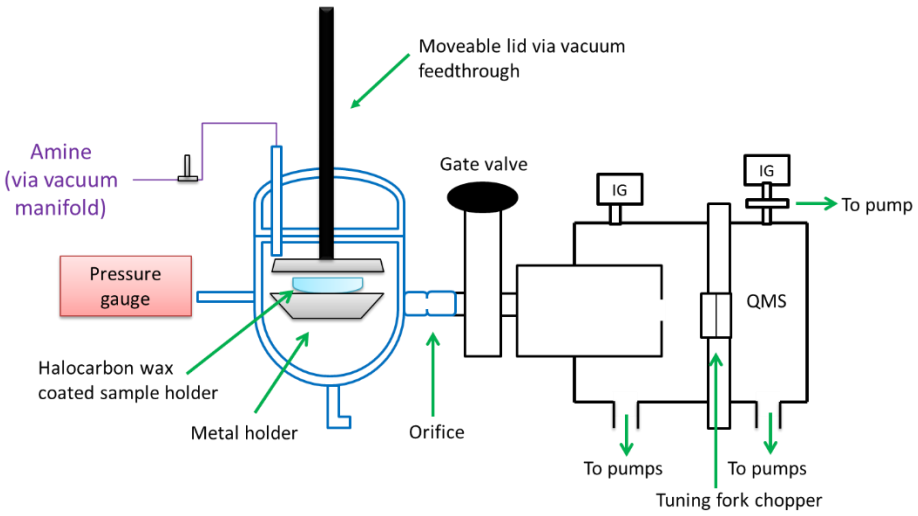

Figure 2-11. Schematic of the Knudsen cell interfaced to the QMS. IG = ion gauge.

Total pressure in the cell was measured using a Pirani pressure gauge (Edwards) with an active gauge controller (Edwards) and was maintained at ≤ 0.3 mTorr to stay in the free molecular regime.[180-182] All experiments were performed at ambient temperature (296 ± 1 K). A modified Petri dish, coated with halocarbon wax (Halocarbon Products Corporation, Series 1500), was used to hold the diacid crystals. Malonic acid (C3), succinic acid (C4), glutaric acid (C5), adipic acid (C6), pimelic acid (C7), and suberic acid (C8) (Figure 2-12), all with a stated purity of ≥ 99% (Sigma-Aldrich), were sieved using two mesh sizes (U.S. Standard) and the crystals which passed through the larger mesh, but not the smaller, were used.

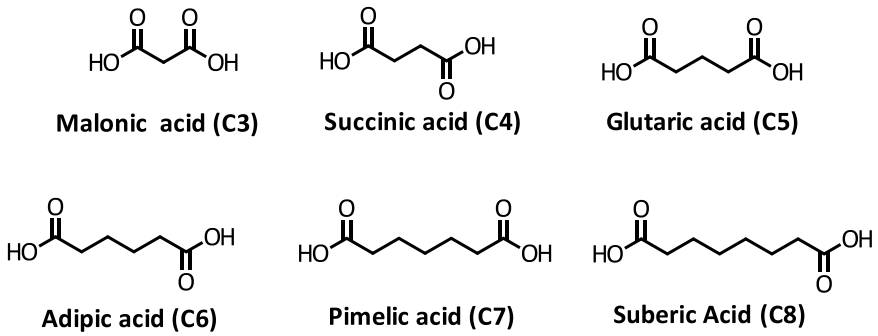

Figure 2-12. Structures of diacids used in Knudsen cell studies.

This gave average crystal sizes over a narrower size range than from unsieved samples (Table 2-3). Sieves used in these experiments gave particles with average sizes in the range from 125 to 850 μm, depending on the diacid.

Table 2-3. Sieve sizes and corresponding average lengths of each diacid crystal. Average lengths were derived from a sample size of 20 crystals.

Diacid	Sieve Sizes (μm)	Length ± 2σ (μm)
Malonic (C3)	425 – 500	519 ± 222
Succinic (C4)	425 – 500	443 ± 114
Glutaric (C5)	500 – 850	856 ± 338
Adipic (C6)	125 – 250	173 ± 82
Pimelic (C7)	500 – 850	742 ± 326
Suberic (C8)	125 – 250	132 ± 86

For all experiments, the solid diacid crystals formed less than a monolayer of crystals on the sample holder. This is a significant advantage because the diffusion of the amine into

multiple layers of the diacid does not have to be taken into account. The diacids were isolated from the rest of the cell by a moveable lid mounted on a vacuum feedthrough that could be raised to expose, or lowered to isolate, the diacid from the amine. Before the introduction of amine, each diacid sample was pumped on for 20 minutes to remove loosely bound water.

Introduction of the amine into the Knudsen cell was accomplished via a vacuum manifold. Figure 2-13 shows the gas phase amines and ammonia used in the Knudsen cell experiments.

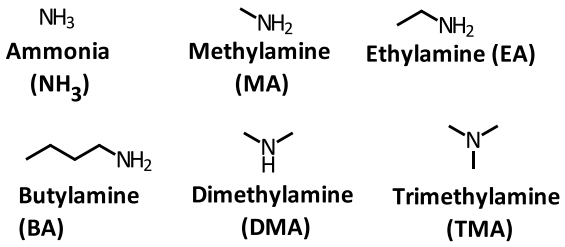

Figure 2-13. Gas phase amines and ammonia used in Knudsen cell studies.

The sources and purities were as follows: methylamine (MA; Sigma-Aldrich, ≥ 98%), ethylamine (EA; Sigma-Aldrich, 97%), dimethylamine (DMA; Sigma-Aldrich, ≥ 99%), trimethylamine (TMA; Sigma-Aldrich, ≥ 99%), and ammonia (Matheson, 99.99%). For experiments at concentrations of $(3 – 6) \times 10^{12}$ molecules cm^{-3} the gas phase species was placed in a 5 L evacuated bulb. Liquid BA was placed in a 50 mL bulb and underwent three freeze–pump–thaw cycles before filling the manifold and an attached 5 L evacuated bulb. Experiments performed at concentrations of $(3 – 5) \times 10^{11}$ molecules cm^{-3} amine or ammonia involved diluting the pure gas phase species with helium (Praxair, 99.999%) in the 5 L bulb. The gas

phase amine or ammonia was introduced into the cell via a stainless steel needle valve and allowed to condition the cell and QMS until a steady signal was observed in the mass spectrum. The volume of the manifold and mixing bulb was sufficiently large that only small drops in the monitored driving pressure was observed with the needle valve open during the course of these experiments.

The following fragments were monitored on the QMS: for MA, EA, and BA *m/z* 30 ($H_2C{=}NH_2^+$); DMA *m/z* 44 ($H_2C{=}NH(CH_3)^+$); TMA *m/z* 58 ($H_2C{=}N(CH_3)_2^+$). The background intensity of *m/z* 17, which corresponds to the most intense fragment of ammonia (NH_3^+), was significant without added ammonia due to background water. Therefore, the ion at *m/z* 16 (NH_2^+) for ammonia was used instead. There was still a contribution from background water at this mass, but it was about an order of magnitude smaller than that at *m/z* 17.

Uptake coefficients (γ) were calculated using Equation 2.4[3, 180] by monitoring the background corrected signal intensity of the amine when the moveable lid was closed (I_0) to cover the diacid sample and the signal intensity when the lid was opened (I_r) to expose the diacid to the amine:

$$\gamma = \left(\frac{I_0}{I_r} - 1\right)\left(\frac{A_{orifice}}{A_{surf}}\right) \qquad \textbf{2.4}$$

$A_{orifice}$ and A_{surf} are the areas of the orifice and diacid surface area, respectively. Note that these are effective uptake coefficients that are calculated using assumed geometric crystal surface areas. As discussed below, the actual reactive surface areas may be different.

By measuring the average length of 20 sieved diacid crystals with dial calipers, and assuming a cubic structure with five sides that can react, the average exposed surface area of a single crystal was estimated. The total surface area was then calculated using the average exposed surface area for one crystal multiplied by the total number of crystals for each sample. For C3, C4, C5, and C7 diacids, the total number of crystals in an experiment was calculated from the measured total mass (Sartorius scale model 1702, ± 0.0001 g) of diacid and the average mass per crystal. The mass per crystal was derived separately by counting the number of crystals used to obtain a measured mass of the order of 0.01 g. However, for adipic (C6) and suberic (C8) acids, the crystals were much smaller in size and photographs of the samples of mass ~0.01 g were used to physically count the number of crystals and thus obtain the average mass per crystal.

Sources of uncertainties in the calculated uptake coefficient arise in the variability of the signal intensities, the number of crystals, and the measured diameters of the orifices. However, the major source of uncertainty was the estimated total exposed surface area, which is dependent on the average measured size of sieved crystals and the assumption of a cubic crystal with five sides exposed for reaction. As shown in Table 2-3, the 2σ uncertainties in crystal size were as large as 65%. In addition, if crystals were assumed to be spherical instead of cubic, the surface area would be smaller by 60%, resulting in a corresponding increase in uptake coefficient. All

sources of uncertainty were treated as independent and the cumulative uncertainty in the uptake coefficient was determined using propagation of errors.[183]

VII. Formation of Aminium Salts and Viscosity Measurements

Evaporation of aqueous mixtures of amines with C2, C3, and C5 *mono*carboxylic acids have been previously shown to form ionic liquids (ILs).[184] In order to determine whether or not the amines and/or ammonia and *di*carboxylic acids form ionic liquids, 2:1 and 1:1 molar ratios of aqueous amine–diacid mixtures were prepared in Mili–Q ™ water (Mili–Pore, 18.2 MΩ cm). For BA, the pure liquid was used and for all other amines and ammonia aqueous solutions of MA (Sigma-Aldrich, 40% wt. in H_2O), EA (Sigma-Aldrich, 66.0 – 72.0% wt. in H_2O), DMA (Sigma-Aldrich, 40% wt. in H_2O), TMA (Sigma-Aldrich, 45% wt. in H_2O), and ammonium hydroxide (Fisher Scientific, 29% wt.) were used. Solutions were placed in a rotovap (Wheaton, SPIN-VAP) where water was evaporated off at 80 – 90 ^oC. The resulting extracts were stored under either nitrogen (Praxair, 99.999%) or ultra-zero air (Praxair, 19.5–23.5% oxygen, < 2 ppm water, < 0.1 ppm total hydrocarbons, < 0.5 ppm carbon monoxide, < 0.5 ppm carbon dioxide, balance nitrogen). As described below, these procedures resulted in solid salts in some cases, and viscous liquids in others.

For mixtures resulting in liquids, viscosity was measured using the falling sphere viscometer technique. Briefly, the liquid is placed in a graduated cylinder and a 4.36 mm metal sphere of known density (7.96×10^3 kg m^{-3}) was allowed to fall through the liquid. The relationship between velocity of the falling sphere and viscosity of the liquid is given by Equation 2.5,[185]

$$\mu = \frac{2gr^2(\rho_s - \rho_f)}{9V} \quad \textbf{2.5}$$

where μ is the viscosity of the fluid (Pa s), g is the gravitational constant (9.8 m s^{-2}), r is the radius of the sphere (m), ρ_s and ρ_f are the densities of the sphere and fluid (kg m^{-3}), respectively, and V is the velocity of the sphere falling through the liquid (m s^{-1}). Videos of the sphere falling through the viscometer next to a ruler and stopwatch were recorded. Playback of the videos in slow-motion allowed for determination of the sphere's velocity by recording the distance travelled and the time. The density of the fluid was calculated separately from the measured mass of the liquid and the volume measured in a graduated cylinder.

VIII. Reaction of Amines and Diacids Using a Flow Reactor and Direct Analysis in Real Time Mass Spectrometry (DART-MS)

Reactions of TMA and BA with the diacids were also investigated using a flow reactor followed by analysis using direct analysis in real time mass spectrometry (DART–MS).[186] DART–MS is an atmospheric pressure, soft ionization technique in which the configuration allows for online analysis by direct introduction of the particle stream exiting the flow reactor as shown in Figure 2-14 (inset).

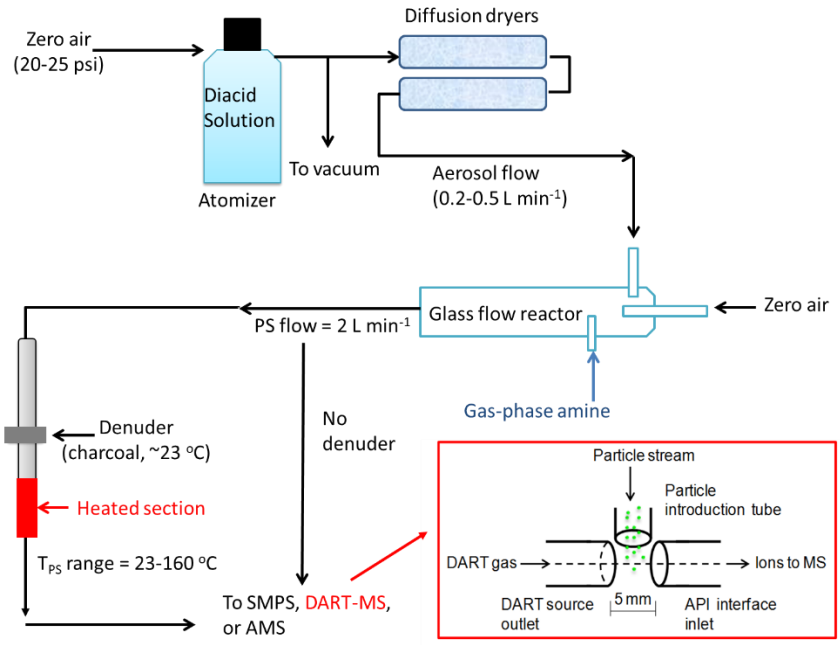

Figure 2-14. Schematic of the flow reactor used to measure reactions of amines with diacids. Inset is the DART interface. Adapted from Zhao et al.[186]

Diacid particles were generated by atomizing a 1 g L^{-1} solution in nanopure water using an atomizer (TSI, 3076) and passing them through a series of two diffusion dryers (TSI, 3062). The dessicant inside the dryers was replaced daily to maximize the efficiency of minimizing the amount of water associated with the particles. Gas phase TMA was generated by flowing 1.0 L min^{-1} clean, dry ultra–zero air (Praxair, 19.5–23.5% oxygen, < 2 ppm water, < 0.1 ppm total hydrocarbons, < 0.5 ppm carbon monoxide, < 0.5 ppm carbon dioxide, balance nitrogen) through a U–shaped holder housing a permeation tube containing the pure liquid (VICI Metronics Inc.). BA in the gas phase was achieved by injecting a 1% (v/v) solution in nanopure water using a syringe pump into a flow of 0.5 L min^{-1} dry air. The concentration of TMA was measured by collection of the gas phase amine onto a weak cation exchange resin followed by analysis using ion chromatography as described elsewhere.[85] BA concentrations were calculated using the rate

of aqueous solution injected, while taking into account the dilution of BA, and the total flow in the reactor. Both amines were at concentrations of 50 ppb. The total flow in the reactor was 2.0 L min^{-1} giving a residence time of 44 s.

The particle stream was then passed through a denuder to measure particle phase amines exiting the flow reactor or directly into the DART source to measure gas + particle bound amines. These values were used to determine the particle phase fraction of amine taken up into the diacid, F_p, and thus compare uptake of amines based on their structure, as well as the structure of the diacid.

CHAPTER 3: RESULTS – REACTIONS OF GAS PHASE SPECIES ON SOA MODELS

The uptake of gas phase species of differing polarities onto low viscosity liquids was chosen in order to study the rapid diffusion of the gas phase species into the liquid substrates, without diffusion limitations. Next, uptake of the gas phase species into laboratory generated SOA was conducted to analyze the effects of increasing the viscosity of the substrate. Lastly, uptake of the gases into low viscosity liquids containing a differing number of polar groups was carried out to determine the effect of uptake on increased presence of polar functional groups.

I. Characterization of Squalane Coatings

Figure 3-1 shows the IR spectrum of squalane droplets, prepared as described in Chapter 2 Section I, with specific stretches for squalane including the $–CH_3$ stretch observed at 2952 cm^{-1} and $–CH_2$ stretches observed at 2933 and 2852 cm^{-1}.[187]

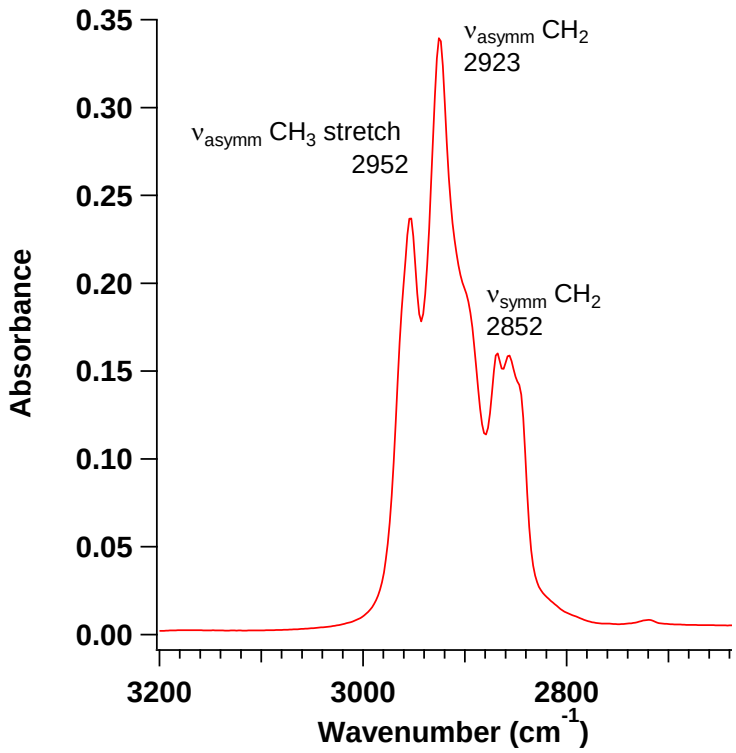

Figure 3-1. IR spectrum of squalane droplets.

The intensity of the $-CH_3$ and $-CH_2$ stretches differed for nebulized droplets vs. a 90 μm thick film of squalane. Figure 3-2 shows the peak height of the asymmetric $-CH_3$ stretch as a function coating thickness as indicated by the number of nebulized coats on the ATR crystal. Ten coats of squalane was used to coat the crystal for subsequent experiments as it is well below the plateau. Thick coatings at the plateau are not fully interrogated by the IR beam and the surface where gas uptake takes place is most likely above the depth of penetration. Asymmetric $-CH_3$ intensities for a 90 μm thick film of squalane are equal to the plateau region for nebulized droplets.

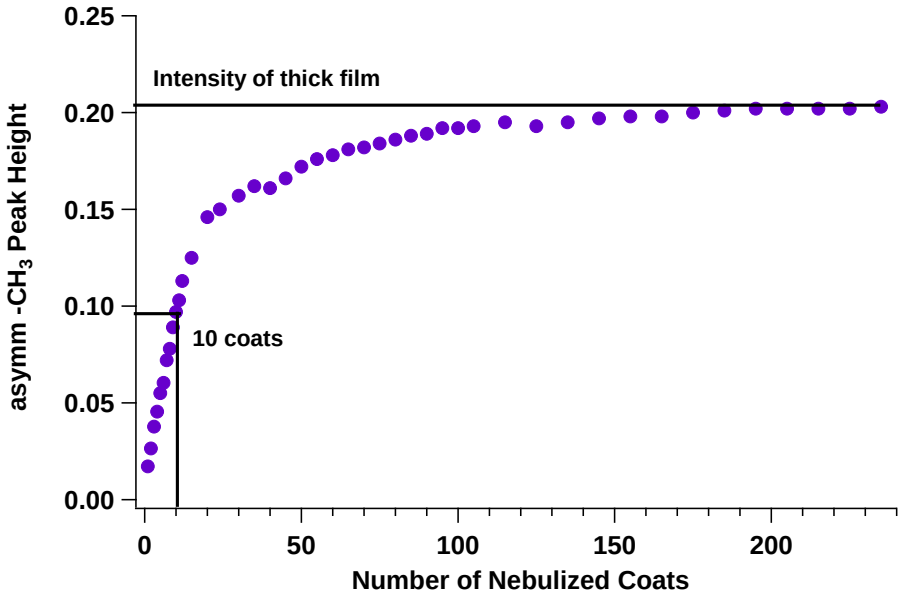

Figure 3-2. Peak height of the asymmetric $–CH_3$ stretch for nebulized squalane droplets as a function of coats on the ATR crystal.

II. Uptake of Non–Polar Gases on SOA and SOA Models

Figure 3-3 shows the IR spectrum of neat IBN taken using a transmission cell. The characteristic peaks of organic nitrates appear at 1630 and 1230 cm^{-1}, corresponding to the asymmetric and symmetric $–ONO_2$ stretches, respectively.[187, 188]

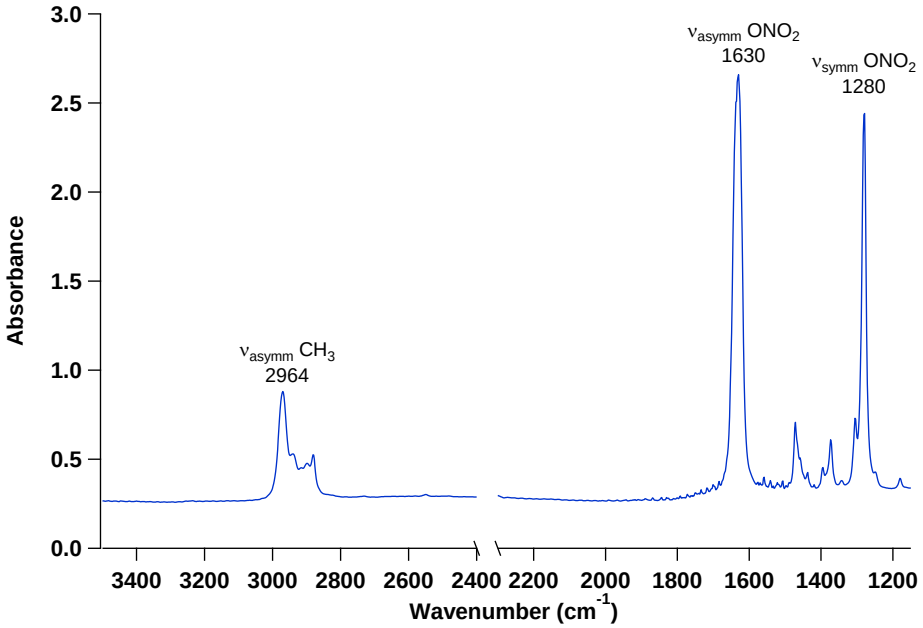

Figure 3-3. IR spectrum of neat IBN using a transmission cell with CaF_2 windows.

Gas phase IBN (20 ppm, 4.9×10^{14} molecules cm^{-3}) in 1 atm of air was introduced in the flow cell via syringe pump and mixing bulb, as described in Chapter 2, Section I, at room temperature (298 K) under dry conditions. Figure 3-4 shows the presence of the asymmetric and symmetric $–ONO_2$ peaks at 1630 and 1280 cm^{-1} respectively, only during IBN flow for both a thick film (Figure 3-4a) and squalane droplets (Figure 3-4b).

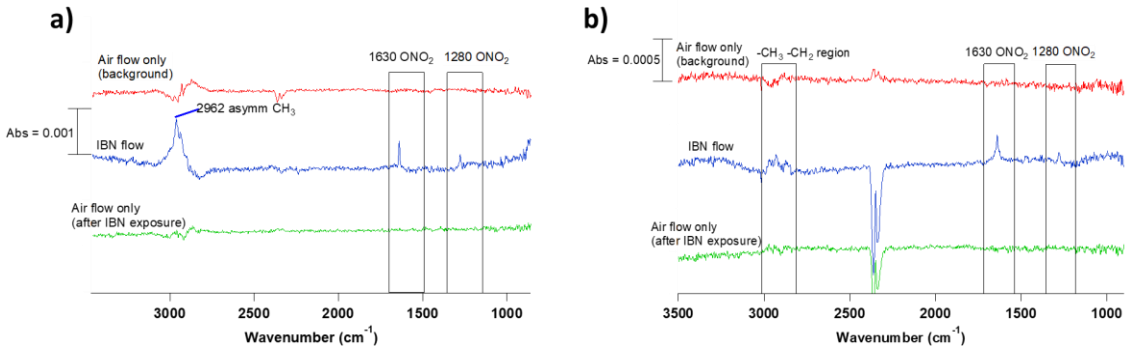

Figure 3-4. Spectra showing uptake of 20 ppm IBN on a) a thick film and b) squalane droplets. Baselines adjusted for clarity.

The absorbance of the 1280 cm^{-1} $–ONO_2$ peaks was converted to number of IBN molecules in a thick film of squalane. First, the volume of squalane on the crystal was calculated using the effective thickness (0.46 μm) and the area of the crystal containing the thick film of squalane (3.75 cm^2). The effective thickness was calculated by taking the average of the relative effective thicknesses for perpendicular and parallel polarization using Equations and 3.1and 3.2, respectively.[172] Variables include n_1 and n_2, which are the refractive indices of the crystal and squalane, respectively, λ_1 is the ratio of the desired wavelength of the specific compound (squalane) over n_1, n_{21} is the ratio of n_2 over n_1, and θ is the angle of incidence.[172]

$$d_{e,\perp} = \frac{\lambda_1 n_{21} cos\theta}{\pi(1-n_{21}^2)(\sin^2\theta - n_{21}^2)^{\frac{1}{2}}} \qquad \textbf{3.1}$$

$$d_{e,\parallel} = \frac{\lambda_1 n_{21} cos\theta(2\sin^2\theta - n_{21}^2)}{\pi(1-n_{21}^2)[(1+n_{21}^2)\sin^2\theta - n_{21}^2](\sin^2\theta - n_{21}^2)^{\frac{1}{2}}} \qquad \textbf{3.2}$$

Next, the number of squalane molecules in the thick film was calculated using the volume, density, and molar mass of squalane (Table 2-1). Since squalane has eight methyl groups, the total number of methyl groups in a given volume of squalane can also be computed by multiplying eight by the total number of squalane molecules. The ratio of the $–CH_3$ stretch in the IBN + squalane spectrum to squalane only and the total number of methyl groups in a molecule of squalane were used to calculated the number of IBN molecules in a given sample of squalane. From there, the number of IBN molecules in a thick film of squalane can be plotted as a function of time shown for a typical set of data in Figure 3-5a.

The number of IBN molecules in squalane droplets (Figure 3-5b) was derived in a different manner. First, to find the total number of squalane molecules in the droplets, the total number of squalane molecules in a thick film was multiplied by the ratio of the $–CH_3$ absorbances of the droplets to the thick film. The total number of $–CH_3$ groups in the droplets was calculated by multiplying the total number of squalane molecules in the droplets by eight, since there are eight methyl groups in squalane. Next, the total number of methyl groups attributed to IBN in squalane is equal to the total number of IBN molecules multiplied by two, since there are two methyl groups in IBN. Rearrangement of this equality allows for the calculation of IBN molecules in squalane.

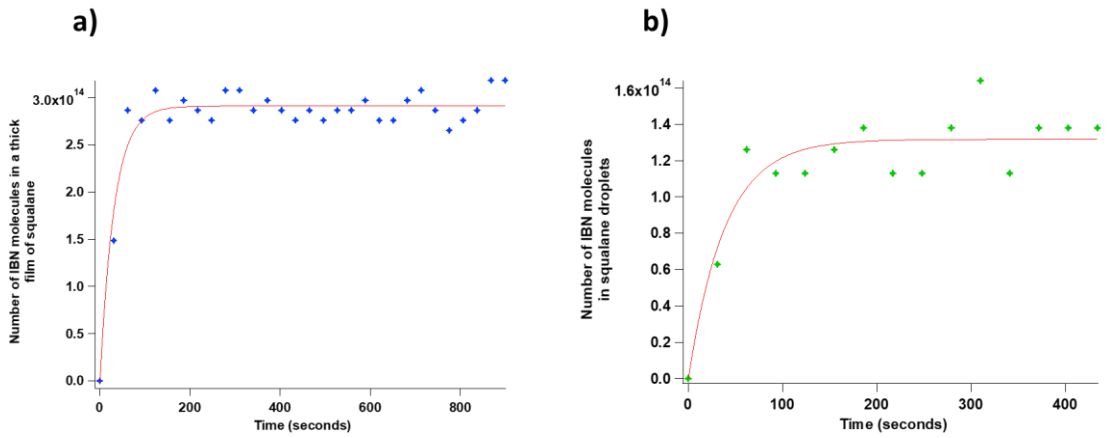

Figure 3-5. Typical plots of the number of IBN molecules in a) a thick film and b) squalane droplets as a function of time.

Using these plots, the Henry's law constant (solubility) of IBN at equilibrium and the uptake coefficient of IBN on squalane can be determined. The Henry's law constant for a gas in a liquid droplet can be calculated using Equation 3.3,[3]

$$[x] = H_x P_x \qquad \textbf{3.3}$$

where $[x]$ is the equilibrium concentration of species x in solution (mol L^{-1}), H_x is the Henry's law constant (M atm^{-1}), and P_x is the partial pressure of the gas at equilibrium (atm). The concentration of IBN at equilibrium can be calculated using the moles of IBN at equilibrium from the number of molecules at equilibrium for both a thick film and squalane droplets (Figure 3-5a and b, respectively) keeping in mind that the volume of squalane differs for a thick film and squalane droplets. The partial pressure of 20 ppm IBN at equilibrium was the same for both cases of squalane and converted into units of atm (20×10^{-6} atm). Table 3-1 shows the calculated Henry's law constants for a thick film and droplets of squalane.

Table 3-1. Measured Henry's law constants[a]

Squalane Coating	H_x (M atm^{-1})
20 ppm IBN on thick film of squalane	147 ± 23 (2σ)
20 ppm IBN on squalane droplets	122 ± 11 (2σ)

[a] Using $[x] = H_x P_x$

As observed in Table 3-1, there is not a significant difference in the Henry's law constants between the two films. This is expected since the measurement of the Henry's law constant is a measure of solubility, and it both cases, it measures solubility of IBN in squalane. Since there is no significant difference in the measured Henry's law constants for a thick film and droplets of squalane, it suggests that IBN rapidly diffuses down to the depth of penetration in a thick film of squalane, consistent with rapid diffusion due to the low viscosity of squalane. For comparison, a study of Henry's law constants for synthesized hydroxy nitrates range from (5 – 36) × 10^3 M atm^{-1} in water.[160, 189] The increased polar groups help facilitate solubility in water, thus giving higher Henry's law constants that would be expected for IBN in a non–polar solvent such as squalane.

The Henry's law constant was also calculated using the initial rate of uptake by plotting Equation 3.4,[3]

$$rate = [IBN]HRT\sqrt{\frac{D_l}{\pi t}} \quad \textbf{3.4}$$

where H is the Henry's law constant in units of M atm^{-1}, D_l is the self–diffusion coefficient for squalane (10^{-6} cm^2 s^{-1}), R is the gas constant (82.06 cm^3 atm mol^{-1} K^{-1}), and T is the temperature (298 K). The rate (molecules cm^{-2} s^{-1}) was calculated using the exponential curve fit from the plot of IBN molecules vs. time (Figure 3-5a and b) and taking the slope at each point. The rate was then plotted against $t^{-1/2}$ (Figure 3-6) where the slope of the line is equal to $[IBN]HRT\sqrt{\frac{D_l}{\pi}}$. All other constants are known and thus Henry's law constant can be determined. Henry's law constants for other atmospherically relevant gases have been derived previously using variations of this method.[190-192]

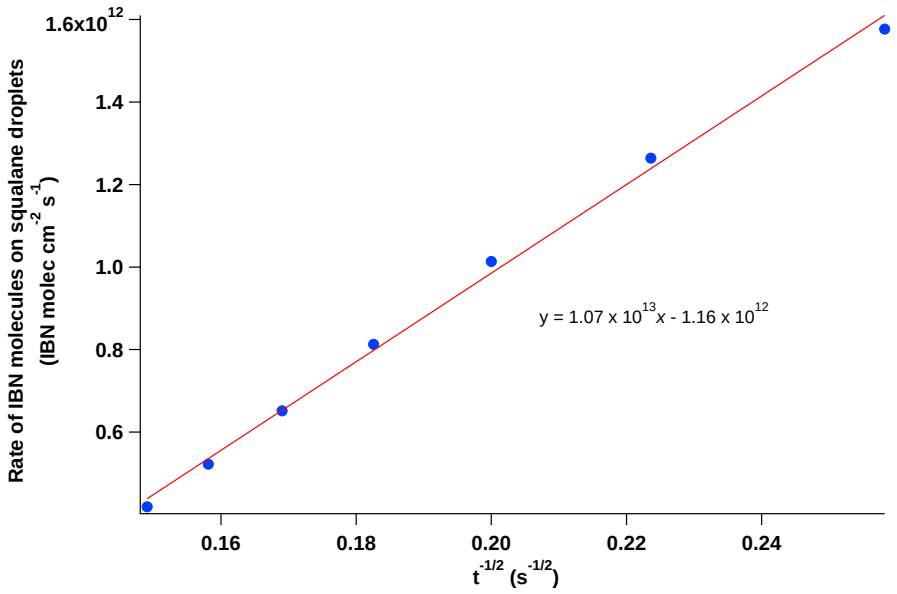

Figure 3-6. Plot of the rate of IBN molecules on squalane droplets per area vs. $t^{-1/2}$ of for the linear uptake region.

The plot of rate of IBN molecules on a thick film of squalane vs $t^{-1/2}$ was not linear and thus an accurate determination of the Henry's law constant was not achieved. The Henry's law constant for 20 ppm IBN on squalane droplets using the initial region was calculated as $H = 1.1 \pm 0.9$ (2σ) M atm^{-1}. This value is about 100 times smaller than the Henry's law constant determined using the concentration of IBN in squalane at equilibrium (Table 3-1). Reasons for this difference are discussed as the following. According Koop et al.,[37] for a particle with a diameter of ~ 400 nm and diffusion coefficient of ~10^{-6} cm^2 s^{-1} (corresponds to low viscosity liquid such as squalane), the equilibrium time is around 1 ms. However, according to the first data point in Figure 3-5b, IBN has not yet established equilibrium with squalane even though this data point is at t = 30 seconds. This may be due coagulation of squalane droplets causing a larger distance for IBN to diffuse into, which would give longer equilibrium times than that estimated using the diameter of the nebulized droplets. Second, it is assumed that the nebulized

droplets are spherical in nature, however since squalane is a low viscosity liquid, the droplets most likely flattening as the hit the crystal. Therefore, at the first IR scan, the system is at an "intermediate" state where gradient of IBN diffusion and evaporation is established. At this point in the experiment, the amount of IBN entering the coagulated squalane droplets is greater than what is coming out as shown in Figure 3-7.

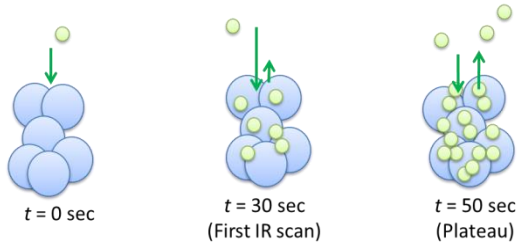

Figure 3-7. Schematic representation of IBN coming to equilibrium with squalane droplets.

The uptake coefficient for 20 ppm IBN in squalane droplets was determined using the plot in Figure 3-5b. The slope extrapolated at t = 0 seconds was used for the rate and the uptake coefficient, γ, was calculated using Equation 3.5,[3]

$$Rate = \gamma A [IBN] \sqrt{\frac{RT}{2\pi M}} \qquad \textbf{3.5}$$

where *A* is the area (cm^2) of the squalane droplets, and M is the molar mass (g mol^{-1}) of IBN, *R*, *T*, and *M* are the gas constant (J K^{-1} mol^{-1}), temperature (K), and molar mass (kg mol^{-1}), respectively. The slope at t = 0 seconds was used because after t = 0, the data points start to plateau, due to the system establishing equilibrium. The average uptake coefficient for 20 ppm

IBN on squalane droplets was calculated as $\gamma = (7.5 \pm 5) \times 10^{-7}$ (2σ). Again, because the uptake coefficient was calculated using the initial uptake region, this average value is considered a lower limit due to a small amount of IBN evaporating out as shown in Figure 3-7.

The uptake of IBN onto a liquid substrate containing more polar groups was then carried out. Figure 3-8 shows the IR spectrum of a thick film of Fomblin ® (400 μm) with the only peaks present due to the CF groups of polyfluorinated compounds in the 1360-1090 cm^{-1} region.[187]

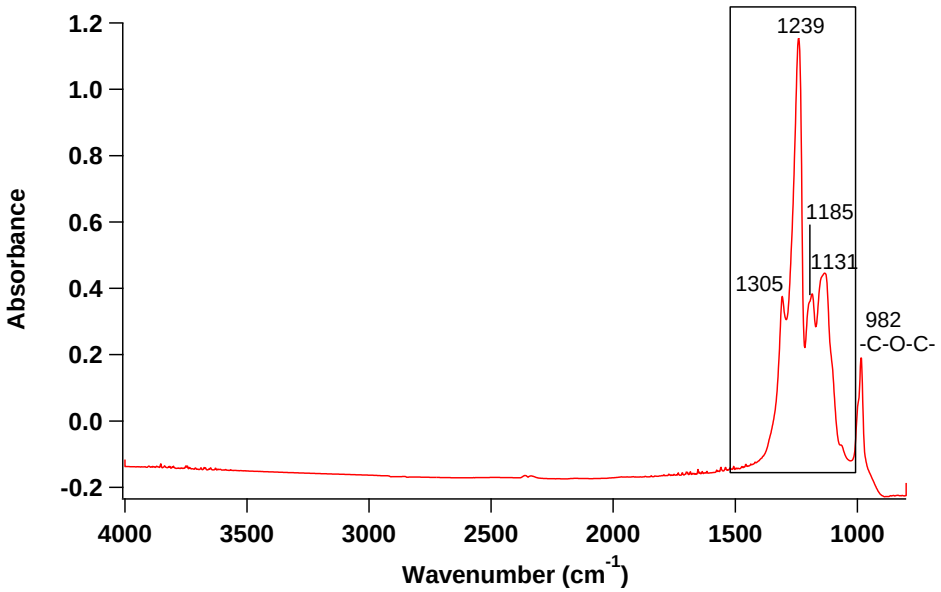

Figure 3-8. IR spectrum of a thick film of Fomblin ®.

During the flow of IBN, the asymmetric $-ONO_2$ peak at 1648 cm^{-1} was only visible when the IBN flow (100 ppm, 2.5×10^{15} molecules cm^{-3}) was on (Figure 3-9a). The peak was followed as a function of time with and without the IBN flow (Figure 3-9b).

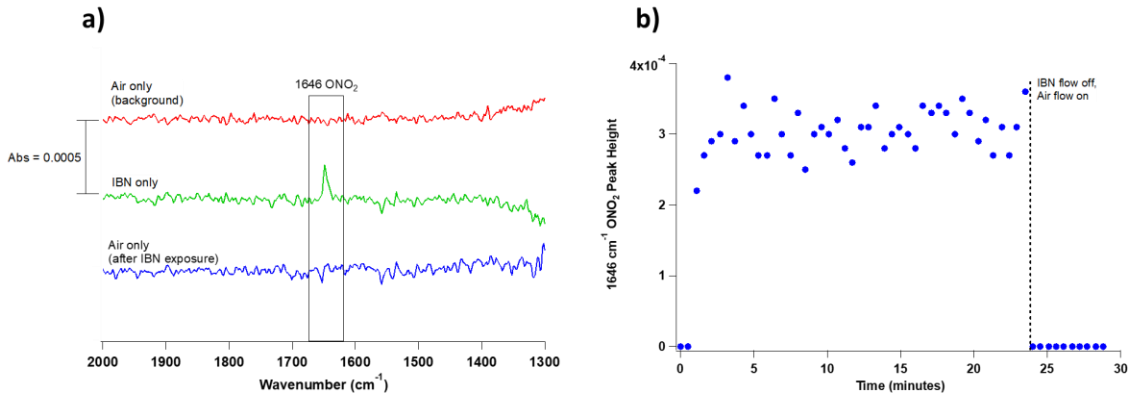

Figure 3-9. a) Uptake of 100 ppm IBN on a thick film of Fomblin ®. Baselines are adjusted for clarity. b) Absorbance of the asymmetric $–ONO_2$ peak as a function of time.

Quantification of how much IBN was present in a thick film of Fomblin ® proved to be difficult. Since Fomblin ® does not have a $–CH_3$ stretch, it is not possible to calculate the fraction of IBN molecules in Fomblin ® using the same method as described with squalane. One method that was attempted was to create a calibration curve of the peak height of the $–ONO_2$ peak at 1648 cm^{-1} vs. moles IBN per liter of Fomblin ®. For that, a demountable liquid cell was used in which the cell consisted of KBr windows sandwiched together with a Teflon spacer. Figure 3-10 shows the resulting calibration curve.

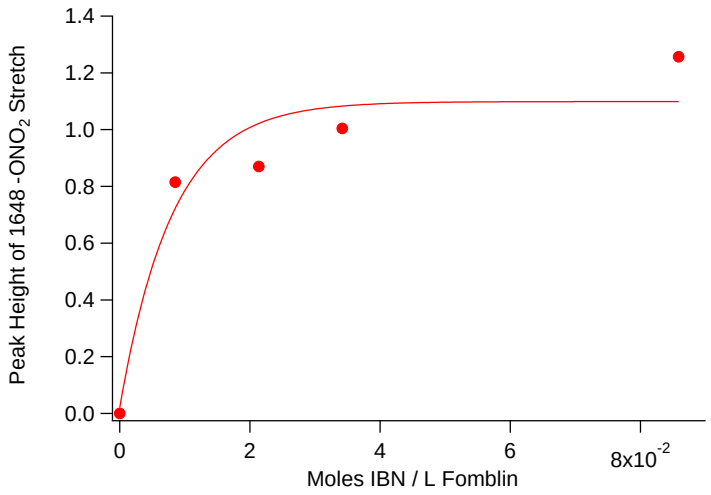

Figure 3-10. Calibration curve of moles of IBN in 1 mL Fomblin ®.

As seen in Figure 3-10, the resulting calibration curve is not linear. Many different factors can be contributing to this non-linearity. First, IBN has a vapor pressure of 9.1×10^{-3} atm[193] and thus evaporates fairly quickly. At small volumes of IBN (1 µL – 10 µL) it is likely that some of IBN is evaporating from the IBN/Fomblin ® mixture. The volumes of IBN cannot exceed 10 µL because at absorbances greater than 1.0, deviations from Beer's Law start to occur due to high concentrations. Equal volumes of IBN in Fomblin ®, which would correspond to points beyond the last point in Figure 3-10, produced two separate layers even after mixing indicating IBN is not soluble in Fomblin ®, shown in Figure 3-11.

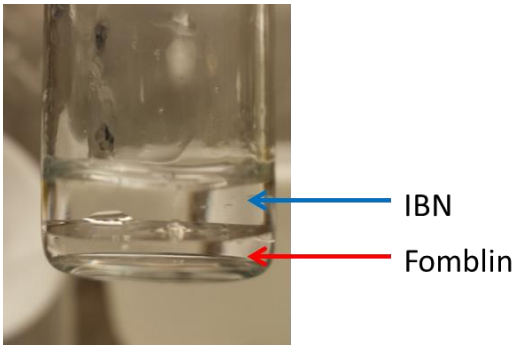

Figure 3-11. Equal volumes of IBN and Fomblin ® after mixing.

The plateau on the calibration curve may be due to IBN reaching saturation in Fomblin ®. Only a qualitative approach on the solubility of IBN in Fomblin ® can thus be determined at this point. The solubility of IBN in Fomblin ® is determined to be less than that of IBN in squalane due to the formation of two separate layers with equal volumes of IBN and Fomblin ®. The mixing of equal volumes of IBN and squalane results in a single layer indicating that IBN is soluble in squalane. The difference in the solubility of IBN in Fomblin ® is also indicative in that a higher concentration of IBN (100 ppm) was needed to see uptake in Fomblin ® compared to squalane (20 ppm). It is expected that IBN should be less soluble in Fomblin ® than squalane due to the increased number of polar functional groups on Fomblin ®.

Since IBN was not soluble in Fomblin ®, SOA was then used as a polar substrate. SOA was generated and impacted onto a Ge ATR crystal for 10 minutes and placed in a horizontal flow–through ATR holder as described in Chapter 2, Section II. Ultra–zero air was used to purge the system of any impurities and water. The resulting spectrum is shown in Figure 3-12.

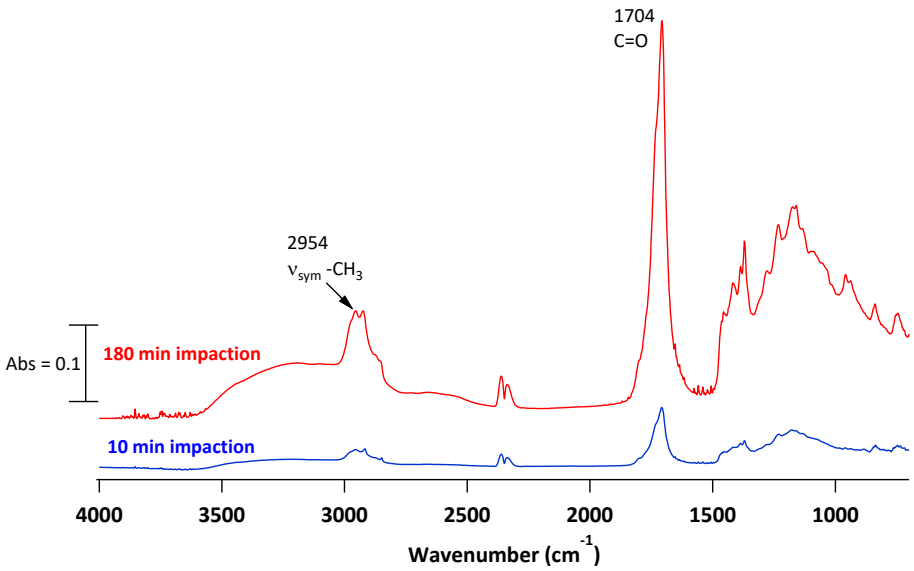

Figure 3-12. IR spectrum of α-pinene/O_3 SOA impacted for 10 minutes (blue) and 180 minutes (red).

A concentration of 100 ppm (2.5×10^{15} molecules cm^{-3}) IBN was used to measure uptake onto SOA because no nitrate stretches were observed in the spectra with concentrations lower than 100 ppm. Experiments were performed at 100 scans and 50 cc min^{-1} of the IBN/air mixtures. The intensity of the 1280 cm^{-1} –ONO_2 peak was monitored as a function of time (Figure 3-13a) to monitor the uptake of IBN into SOA, with Figure 3-13b showing the intensity of the nitrate peak as a function of time. The trend in uptake of IBN onto "thin" SOA is similar to that on squalane and Fomblin ®: fast diffusion in and fast diffusion out.

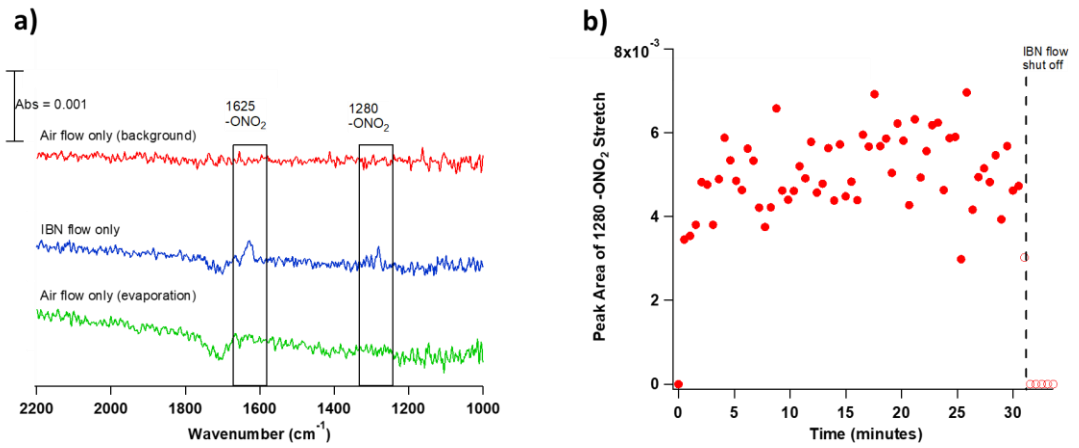

Figure 3-13. a) IR spectrum of 100 ppm IBN in 10 min. impacted SOA. b) Peak area of the nitrate stretch at 1280 cm^{-1} as a function of time.

In order to determine if thickness has any effect on uptake, SOA that was impacted for 180 minutes was used. As stated previously, the area of the asymmetric $-CH_2$ stretch is higher the longer the impaction time (Figure 2-5), which translates to a thicker layer of SOA on the ATR crystal. Figure 3-12 shows the IR spectrum of SOA impacted at 180 minutes. The number of scans remained at 100 and 100 ppm of IBN at 50 cc min^{-1} was used to measure uptake. Figure 3-14a shows the IR spectrum of the uptake of IBN onto SOA impacted for 180 minutes. As seen in Figure 3-14b, there are striking differences on the uptake of IBN onto a thicker layer of SOA. First, diffusion into SOA occurs on much longer time scales than for squalane, Fomblin ®, or even a thin (10 min impaction) layer of SOA. Second, the time to reach equilibrium is much longer, about 5 hours and 45 minutes. Lastly, IBN is slow to diffuse out of SOA impacted for 180 minutes compared to squalane, Fomblin ®, and a thin layer of SOA. This is consistent with the higher viscosity of α–pinene SOA ($10^5 – 10^{14}$ Pa s)[62, 194] compared to squalane (3.1×10^{-2} Pa s) and Fomblin ® (0.5 Pa s)

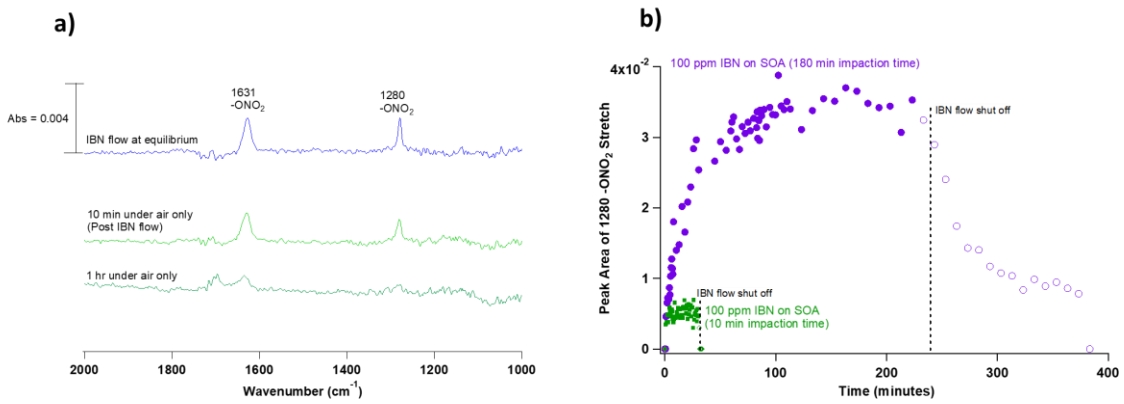

Figure 3-14. IR difference spectrum of IBN on SOA impacted for 180 minutes under flow conditions. B) Peak area of the nitrate stretch as a function of time on 180 min. impacted SOA (purple) and 10 min. impacted SOA (green).

III. Uptake of Polar Gases on SOA Models

The uptake of 20 ppm hydroxyacetone (HA) on a thick film of squalane was carried out using the method stated above. Figure 3-15 shows the IR spectrum of HA with the most prominent peaks coming from the carbonyl (1724 cm^{-1}) and the –OH stretch (3426 cm^{-1}).[12]

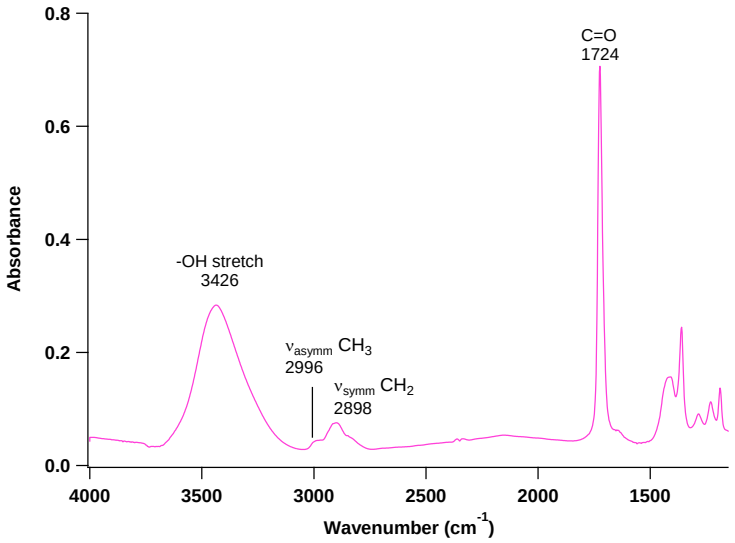

Figure 3-15. IR spectrum of pure liquid hydroxyacetone (HA) using a transmission cell with CaF_2 windows.

Peak heights for the C=O stretch were very low when HA flow was introduced, as shown in Figure 3-16a. Another interesting behavior of HA is that it remained even after the HA flow was shut off and air flow was introduced (Figure 3-16b). Unlike IBN, hydroxyacetone sticks to the surface of the Ge crystal. One reason for this is that the more polar hydroxyacetone has a higher affinity for the Ge surface rather than the hydrophobic squalane.

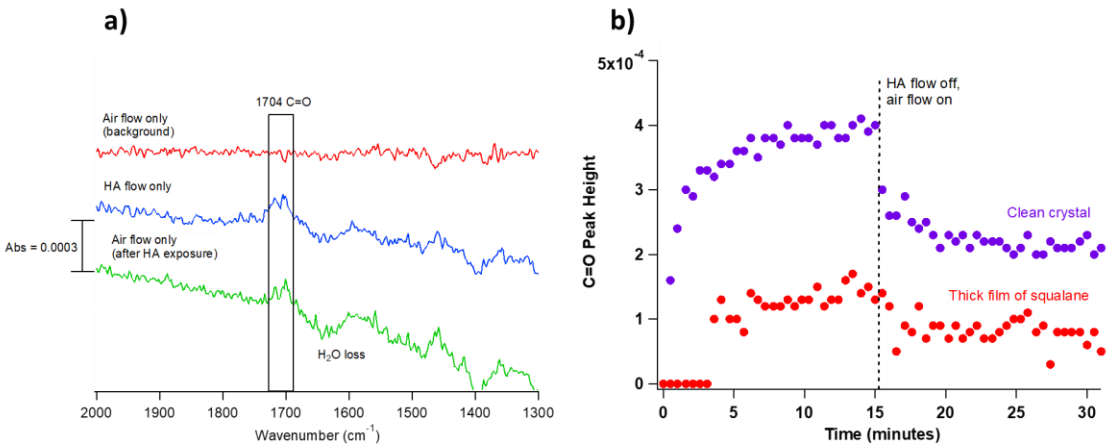

Figure 3-16. a) Peak at 1704 cm^{-1} due to HA uptake into a thick film of squalane. b) Trend of C=O peak height as a function of gas flow.

Because of the preference of HA for the Ge crystal, a different polar gas phase species was chosen. Figure 3-17 shows the IR spectrum of acetone, which is similar to HA in that the most prominent peak is due to the C=O stretch.

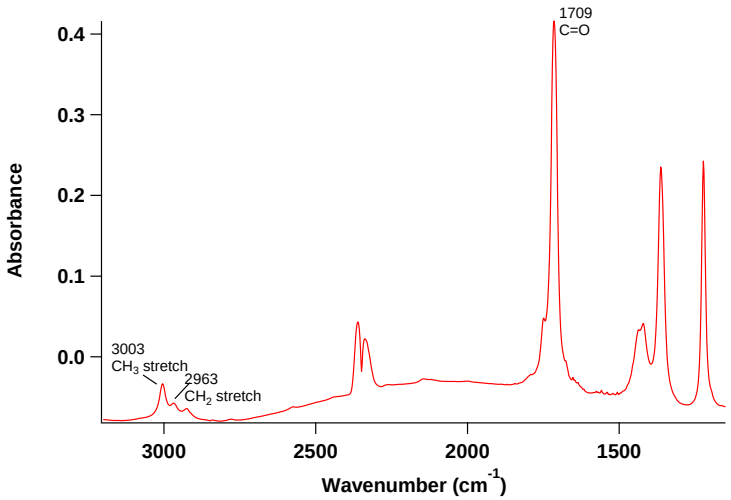

Figure 3-17. IR spectrum of neat acetone using a transmission cell with CaF_2 windows.

The uptake of acetone on a thick film of squalane was also carried out; however, the intensity of the carbonyl stretch was low, with a high standard deviation of the signal. The acetone signal, much like hydroxyacetone, remained even after acetone flow was shut off and air flow resumed, making reliable quantification difficult.

Another possible factor that could be affecting the uptake of acetone is the vapor pressure. Acetone has a vapor pressure of 0.3 atm,[195, 196] which is 2 orders of magnitude higher than the vapor pressure of IBN (9×10^{-3} atm).[193] In order to eliminate the variable of vapor pressure and still compare polarities, acetic acid was chosen to measure differences in uptake (vapor pressure = 1×10^{-2} atm).[195, 196]

Next, a polar gas phase species was paired with a polar substrate. It was expected that because the two are of the same polarity, that the uptake and diffusion out will be rapid. It was also hypothesized that the polar gas phase species will have a higher affinity for the polar substrate, rather than the Ge ATR crystal. Again, Fomblin ® was chosen as the substrate and acetic acid as the gas phase compound, due to its vapor pressure being on the same order of magnitude as IBN. The IR spectrum of acetic acid is shown in Figure 3-18.

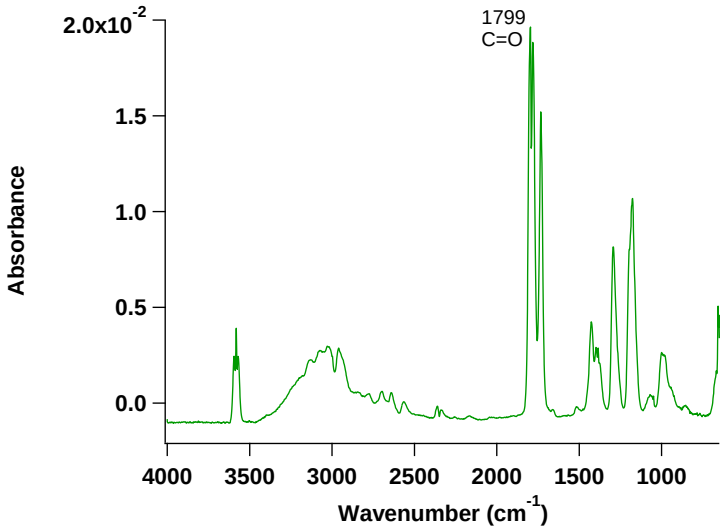

Figure 3-18. Gas phase IR spectrum of 200 ppm (4.9×10^{15} molecules cm^{-3}) acetic acid in ultra zero air. Pathlength of cell = 9 cm. T = 295 K. P_{tot} = 1 atm.

A thick film of Fomblin ® was applied to the Ge ATR crystal as described previously to give a 400 μm thick coating. A concentration of 100 ppm acetic acid at a flow rate of 50 cc min^{-1} was used. Figure 3-19 shows the peak area of the C=O stretch for uptake of acetic acid on a thick film of Fomblin ® (red trace). Much like the uptake of HA and acetone on squalane, the acetic acid remains in the Fomblin ® once the flow is switched to air (open circles). Another interesting note is that even in the scenario of a polar gas/polar substrate, there is still considerable uptake onto a clean Ge ATR crystal (green trace).

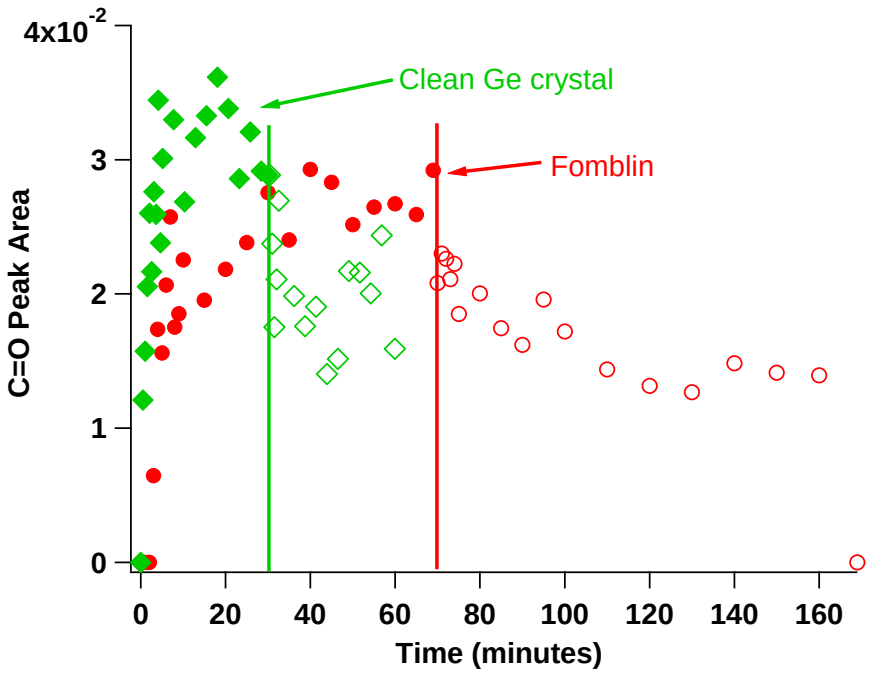

Figure 3-19. Peak area of C=O stretch for 100 ppm acetic acid in a thick film (400 μm) of Fomblin ® (red) and on a clean Ge ATR crystal (green). Line indicates the swtich of gas phase acetic acid flow to only air flow. Open symbols represent evaporation.

In order to potentially shield the ATR crystal surface from the polar gas phase speices, a SAM was deposited on the crystal surface as described in Chapter 2 Section III. Figure 3-20 shows the trend of the C=O stretch for acetic acid on the C18 SAM deposited on a Si ATR crystal (purple). A rapid uptake onto the SAM was observed, leading to the conclusion that the acetic acid molecules may be sufficiently small in size and may be penetrating in between the SAM chains, indicating an increase in the C=O peak area when the IR spectrum is subtracted from the SAM alone. Since the acetic acid signal did not fall to zero once the flow was switched to air only suggests that the acetic acid molecules may be trapped inside the SAM chains. Note that experiments involving the SAM were done on a Si ATR crystal and a blank of acetic acid on a clean Si crystal without a SAM was not conducted. However, since both the Ge and Si

surfaces are expected to be polar, the acetic acid is expected to have an affinity for the clean Si ATR crystal surface.

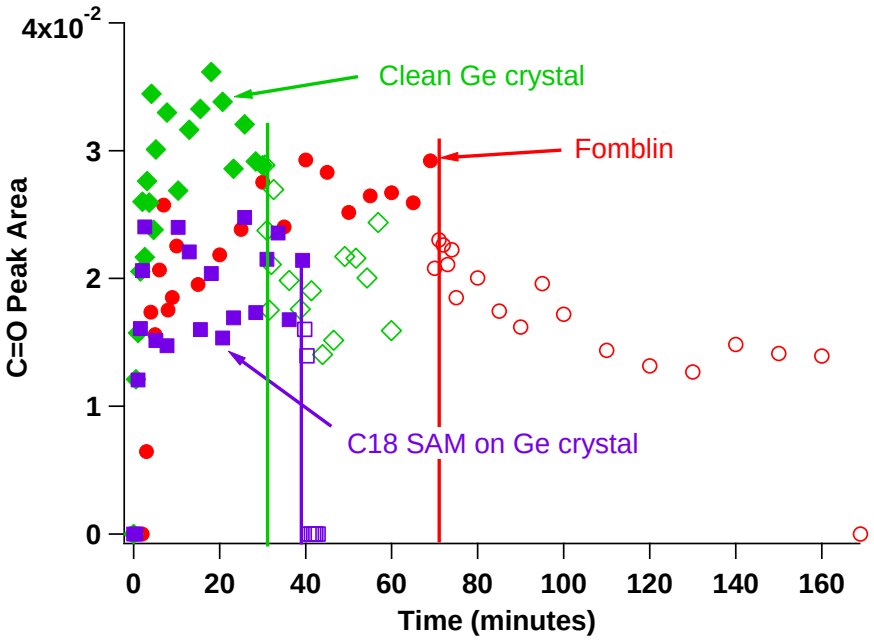

Figure 3-20. Peak areas of C=O stretch for acetic acid onto Fomblin ® (red) on a Ge crystal, a clean Ge ATR crystal (green), and the C18 SAM on the Si ATR crystal (purple). Line indicates the swtich of gas phase acetic acid flow to only air flow. Open symbols represent evaporation.

IV. Conclusions

The goal of the ATR–FTIR experiments was to characterize the uptake of gas phase species of differing polarities onto low viscosity liquids and laboratory generated SOA. The differing polarities of the gas phase species as well as the difference in viscosities of squalane, Fomblin ®, and SOA were analyzed to determine if the chemical properties of both the gas and condensed phases affect how the gas phase species are taken up into the substrates.

ATR–FTIR proved to be useful for studying uptake of a low polarity gas phase species onto a non–polar liquid substrate, such as squalane. However, the uptake was rapid, in that the time dependence of the initial uptake region could not fully be captured. At the time that the first IR scan is taken, evaporation of IBN could be occurring simultaneously with uptake. Because of this occurrence, we only estimate a lower limit for the uptake coefficient. Uptake of IBN onto Fomblin ® was also rapid, as was the diffusion out of the substrate which agrees with the fact that Fomblin ® is a low viscosity liquid. However, there was a difference in uptake and diffusion out of SOA for IBN when SOA was impacted at two different times. This was due to the much higher viscosity of SOA compared to squalane and Fomblin ®.

The uptake of polar gases onto the ATR crystal was greater than that on the substrate of interest. Even with an attempt to utilize a SAM to coat the crystal surface, small, polar gas molecules such as acetic acid, were able to penetrate in between the SAM alkyl chains. The combination of rapid uptake of gases onto non–polar substrates and the affinity of polar gases for the crystal rendered ATR–FTIR difficult to proceed with quantifying uptake coefficients.

CHAPTER 4: RESULTS – REACTION OF AMINES ON DIACIDS USING A FLOW REACTOR

A different approach was chosen to study the kinetics of heterogeneous reactions. The difficulty in coating ATR crystals with solid substrates lead to the use of a flow reactor coupled to a mass spectrometer. Flow reactors are typically used in kinetics studies due to the ability to obtain rate constants, which can be subsequently used to derive uptake coefficients. In these experiments, the kinetics of the reactions between amines and dicarboxylic acids (diacids) were studied.

I. Uptake of BA on Solid Diacids

Typical MS plots for flow reactor experiments follow the signal of the gas phase amine. As the inlet is pulled back, a decrease in the amine signal is observed indicating uptake or reaction. Figure 4-1 shows typical uptake profiles for $(5 – 9) \times 10^{13}$ molecules cm^{-3} BA on solid C2 – C5 diacids. As shown in Figure 4-1, both odd carbon diacids show that uptake continues on the coating after the first trial. Uptake on a second trial on a coat of oxalic acid (C2) is also observed, however, the change in signal when the inlet is pulled back is less distinct. Only succinic acid (C4) shows signs of surface saturation as indicated by the increase in amine signal as the inlet is held at a given position, and minimal uptake occurs when the inlet is pulled back for a second trial. These differences in behavior of uptake of BA onto the diacids show that there may be differences in reactivity between odd and even carbon diacids.

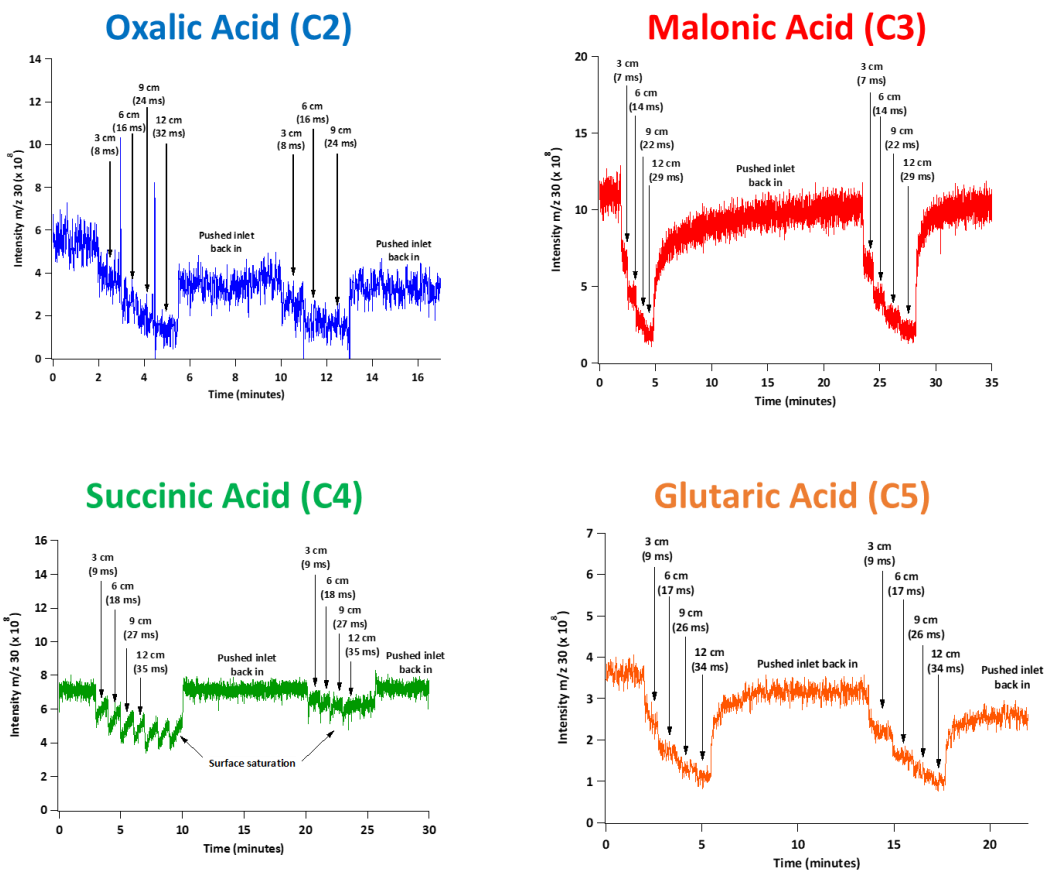

Figure 4-1. Uptake of (5 – 9) × 10^{13} molecules cm^{-3} BA on solid C2 – C5 diacids in a flow reactor. Total pressure (P_{FT}) in the reactor = 0.8 – 1.0 Torr.

First–order rate plots of $\ln(I/I_0)$ as a function of reaction time provide values of the pseudo–first order rate constant, *k*, from which values of the uptake coefficients can be obtained using Equation 2.2. As discussed above, the surface area of the diacids was calculated using the total number of crystals in a coating multiplied by five times the surface area of a single crystal face, assuming a cubic structure. Figure 4-2 shows typical first–order rate plots for (5 – 9) × 10^{13} molecules cm^{-3} BA on solid C2 – C5 diacids. Rate constants for malonic (C3) and glutaric (C5) appear to be similar, while the rate constant for oxalic acid (C2) is largest and that for succinic acid (C4) is the smallest.

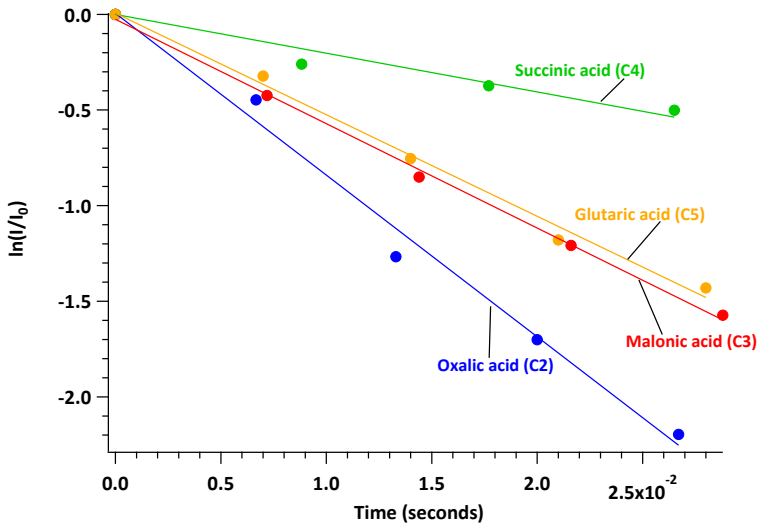

Figure 4-2. Typical first-order kinetics plot for (5 – 9) × 10^{13} molecules cm^{-3} BA on solid C2 – C5 diacids.

Table 4-1 shows the experimental conditions and uptake coefficients for BA on C2 – C5 solid diacids. The uptake coefficients for malonic (C3) and glutaric (C5) acids are larger than those for succinic acid (C4). Oxalic acid (C2) has similar uptake coefficients compared to those for malonic (C3) and glutaric (C5) acids. However, oxalic acid (C2) has the highest vapor pressure of the diacids (1.1×10^{-7} atm at 296 K),[136] therefore contributions from reactions with gas phase oxalic acid (C2) may be affecting the measured uptake coefficient. This may be evident in a "frosting" effect that is observed around the edge of the flow reactor and on the spokes after reaction with amine as shown in Figure 4-3.

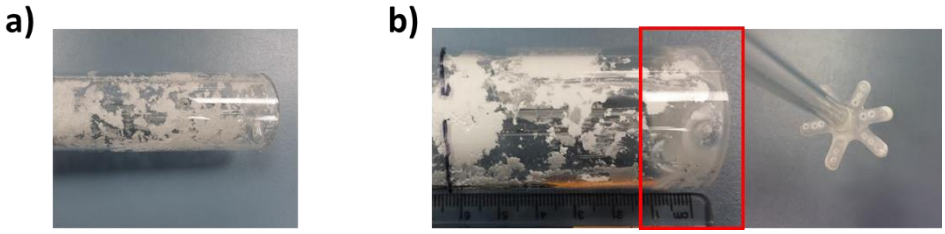

Figure 4-3. Photos of oxalic acid (C2) coated flow reactor A) before and B) after amine exposure. The flow reactor shows a frosted outline of the spokes at the end of the flow reacotr (red box) as well as frosting on the perforated spokes.

Table 4-1. Summary of experimental conditions and uptake coefficients for BA on solid diacids.

Diacid	$[BA]_0 \times 10^{14} \pm 2\sigma^a$ (molecules cm^{-3})	Diacid Area $\pm 2\sigma^a$ (cm^2)	$k \pm 2\sigma^a$ (s^{-1})	$\gamma \pm 2\sigma^a$
Oxalic	0.51 ± 0.12	65.6 ± 15.7	72.5 ± 15.7	$(1.4 \pm 0.4) \times 10^{-2}$ [d]
(C2)	1.3[b]	89.5 ± 39.1	46.6 ± 12.2	$(0.69 \pm 0.16) \times 10^{-2}$ [d]
Malonic	0.74 ± 0.30	47.3 ± 2.4[c]	48.5 ± 17.5	$(1.6 \pm 1.0) \times 10^{-2}$
(C3)	1.4 ± 0.3	57.6 ± 20.2	59.9 ± 4.5	$(1.4 \pm 0.2) \times 10^{-2}$
	2.3 ± 0.3	65.6 ± 6.5	69.3 ± 4.3	$(1.2 \pm 0.2) \times 10^{-2}$
Succinic	0.74 ± 0.56	167.1 ± 49.6	21.5 ± 4.9	$(0.77 \pm 0.34) \times 10^{-2}$ [d]
(C4)	1.3 ± 0.3	48.5 ± 30.1	24.9 ± 1.7	$(0.58 \pm 0.47) \times 10^{-2}$ [d]
	2.4 ± 0.2	53.2 ± 20.9	– [e]	– [e]
Glutaric	0.49 ± 0.08	18.2 ± 10.7	44.6 ± 19.1	$(2.2 \pm 0.5) \times 10^{-2}$
(C5)	1.3 ± 0.1	60.6 ± 10.2	60.7 ± 7.5	$(1.3 \pm 0.2) \times 10^{-2}$
	2.3 ± 0.1	41.2 ± 28.5	67.8 ± 17.2	$(2.0 \pm 1.0) \times 10^{-2}$

[a] Represents two sample standard deviations based on each replicate. [b] Amine concentrations were constant for all runs. [c] Surface area of half the samples were obtained by rinsing the coating off the flow reactor and evaporating off the water to obtain the mass. Averages reported are those from scrapping the coating and measuring the mass. Both methods of obtaining the mass of diacid showed no significant difference in calculated uptake coefficients. [d] Uptake coefficients decreased with time and those reported are for the first trial of each sample. [e] First–order rate plots were not linear, which may be due to surface saturation as discussed in the text.

The potential dependence of uptake coefficients on carbon chain length may lie in the availability and accessibility of the –COOH groups. Ruehl et al.[197] proposed that the orientation of diacids on the surface of aqueous ammonium sulfate particles depended on their structure, with the odd carbon diacids having one –COOH group pointing outside the particle while even

carbon diacids have both -COOH groups buried inside the liquid interface. However, these orientations correspond to aqueous particles and the surface structure will not be the same for solid particles.

Another possibility is the difference in crystal structures between the odd and even carbon diacids. In general, diacid chains link end–to–end via hydrogen bonding between –COOH groups.[138] Adjacent chains are held via hydrophobic interactions between methylene chains.[138] In odd carbon diacids, the chains are twisted and thus create a high energy lattice with torsional strain along the methylene chains, while even carbon diacids are offset and thus are more stable.[138] Higher energetics of odd carbon diacids contributes to lower melting points for odd carbon diacids compared to even carbon diacids.[138] The twist of the odd carbon diacid lattice creates more space in between chains, contrary to the tightly packed even carbon lattices.[139] The larger spacing between diacids is thought to explain why odd carbon diacids have higher solubilities in water[139] and organic solvents.[140] Amine molecules may penetrate the odd carbon diacid lattices more readily than even carbon diacids, thus giving larger uptake coefficients. Lastly, the formation of an ionic liquid layer stemming from the reaction of odd carbon diacids with amines has been shown to occur. Details of this reaction and the implication on the kinetics for the amine–diacid system are discussed in detail in Chapter 5.

The dependence of uptake coefficients on amine concentration was also investigated. Figure 4-4 shows the uptake of 1×10^{14} molecules cm^{-3} BA on solid oxalic acid (C2). Compared to uptake at 5×10^{13} molecules cm^{-3} (Figure 4-1), surface saturation is more evident at the higher concentration as the inlet is held at a given position of the flow reactor. This results

in a lower uptake coefficient compared to an amine concentration of 5×10^{13} molecules cm^{-3} (Table 4-1).

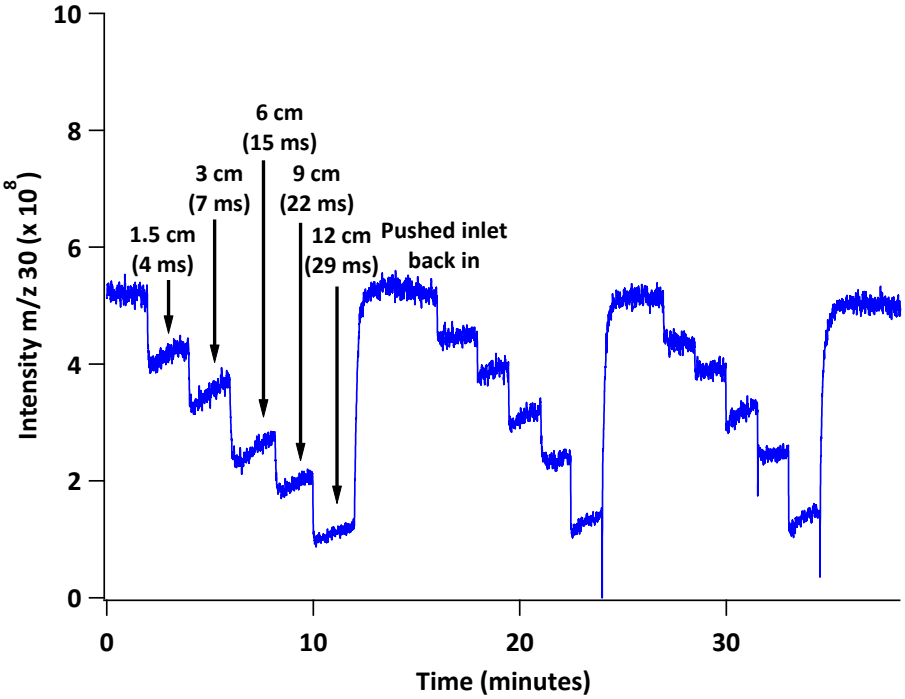

Figure 4-4. Uptake of 1×10^{14} molecules cm^{-3} BA on solid oxalic acid (C2) using a flow reactor. P_{FT} = 0.9 Torr.

Surface saturation is also evident for concentrations of $(1 – 2) \times 10^{14}$ molecules cm^{-3} BA on succinic acid (C4) as shown in Figure 4-5. A decrease in uptake as the concentration of the gas phase species is expected for typical gas–solid reactions. With an increase in concentration, the number of collisions increase, leading to more rapid depletion of surface sites. Other amine molecules thus cannot react with the diacid surface, which would give an increase in amine signal as the inlet is fixed at a given position. Reactions between amines and carboxylic acids result in their respective aminium salt. Formation of a salt product layer on the surface of the

even carbon diacids would effectively shut down the reaction as the solid product layer on the surface prevent amine molecules from encountering fresh diacid, i.e. passivation of the surface occurs.

It is interesting to note that there is no dependence of the uptake coefficient on the BA concentration for odd carbon diacids. There are no signs of surface saturation for the odd carbon diacids as the concentration of BA increases (Figure 4-5) which may be attributed to ionic liquid formation on the surface of the odd diacid. This provides a layer in which continuous uptake of the amine is possible. Details on this mechanism are provided in Chapter 5.

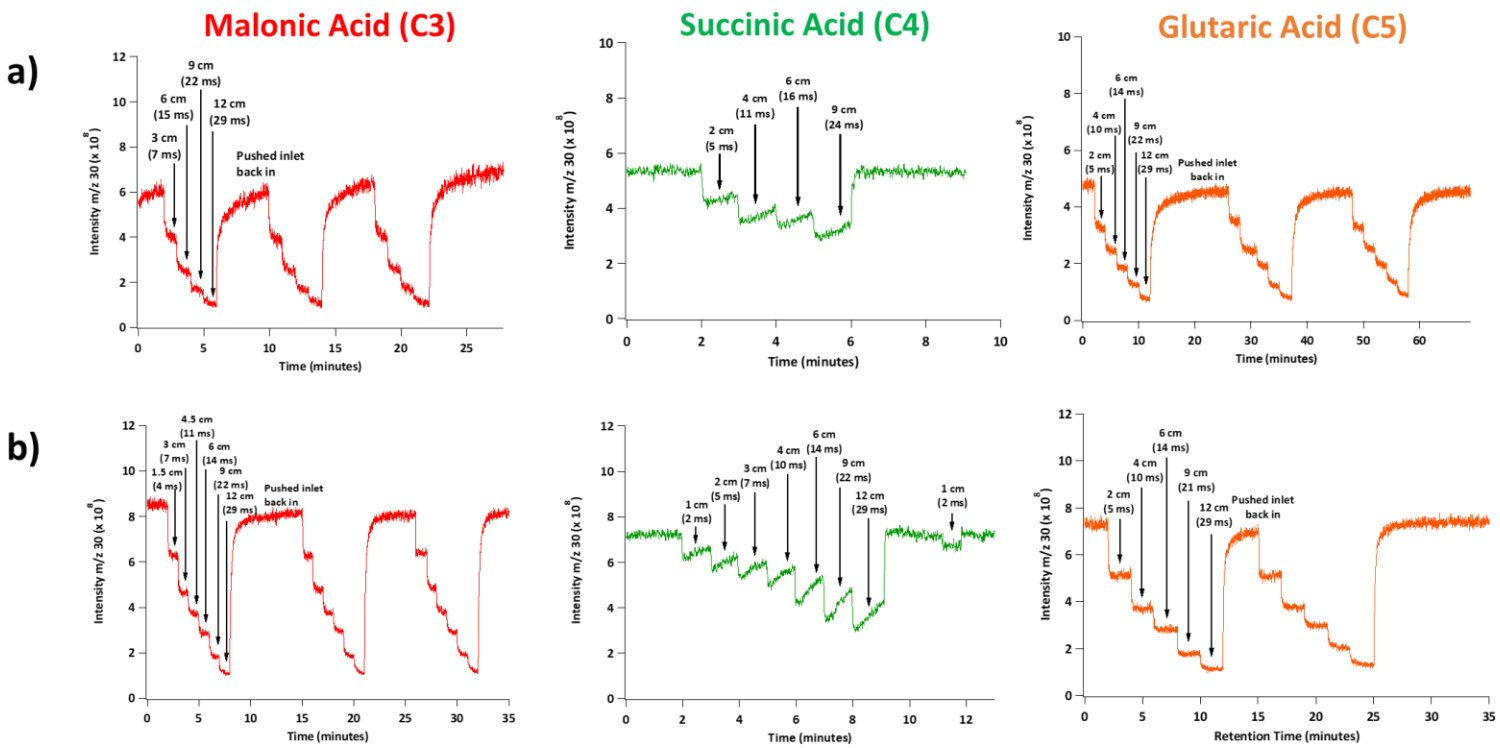

Figure 4-5. Uptake profiles of C3 – C5 solid diacids with a) 1×10^{14} molecules cm^{-3} and b) 2×10^{14} molecules cm^{-3} BA using a flow reactor. P_{FT} = 0.9 Torr.

II. Uptake of sBA on Solid Diacids

In order to determine if amine structure plays a role in uptake onto the solid diacids, the isomer of BA, sBA, was chosen, since sBA is a secondary amine. Figure 4-6 shows the uptake of $(7 – 9) \times 10^{13}$ molecules cm^{-3} sBA on the solid diacids. Similar trends are observed in comparing uptake behavior of sBA with BA (Figure 4-1) in that succinic acid (C4) exhibits signs of surface saturation. As with BA, both odd carbon diacids (C3 and C5) show no signs of surface saturation in that subsequent trials on a single coat can be measured with no difference in uptake coefficients. Uptake coefficients were calculated in the same manner as with BA. First order rate plots of $\ln(I/I_0)$ as a function of reaction time are shown in Figure 4-7.

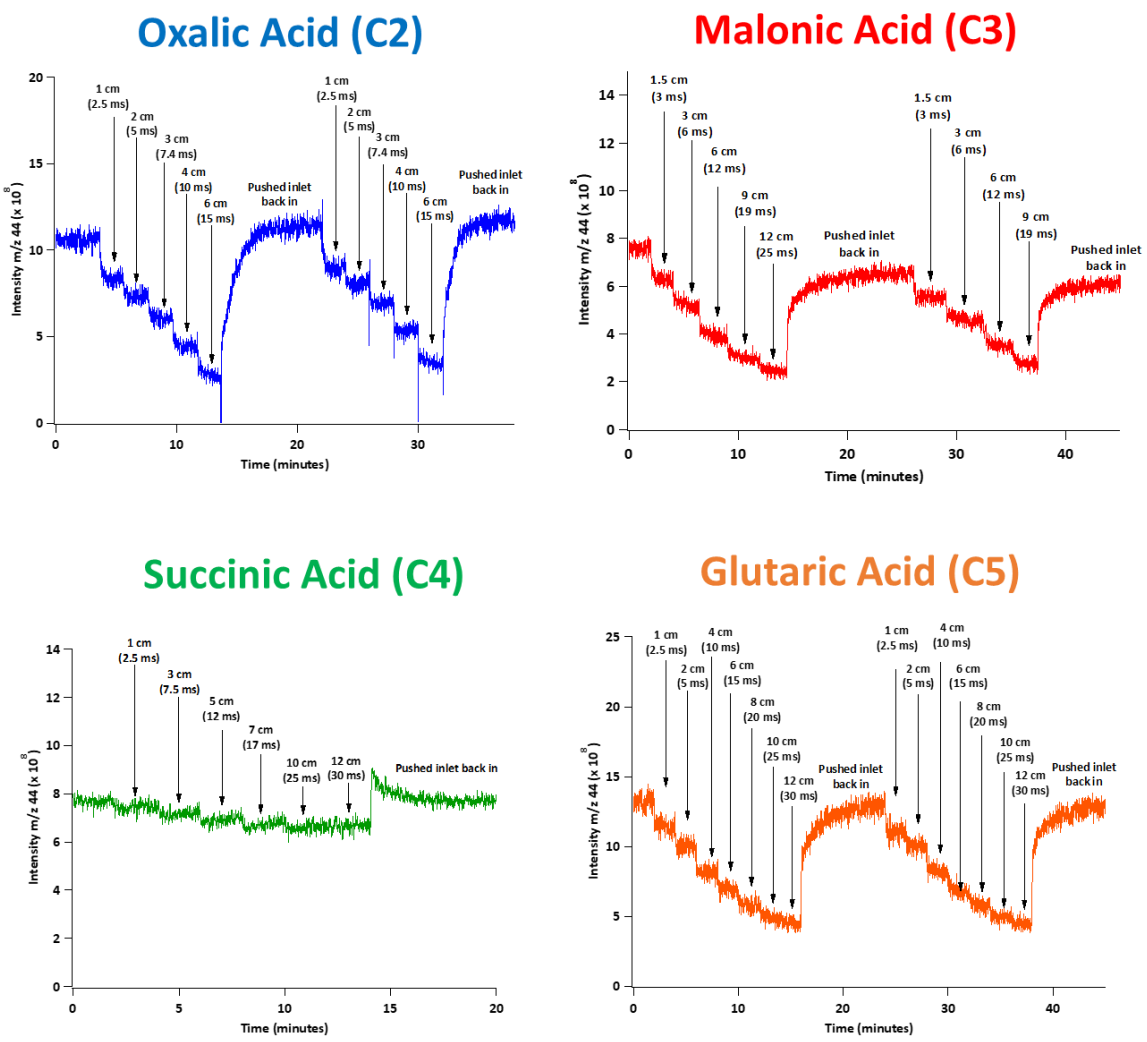

Figure 4-6. Uptake profiles for (7 – 9) × 10^{13} molecules cm^{-3} sBA on solid C2 – C5 diacids using a flow reactor. P_{FT} = 0.8 – 0.9 Torr.

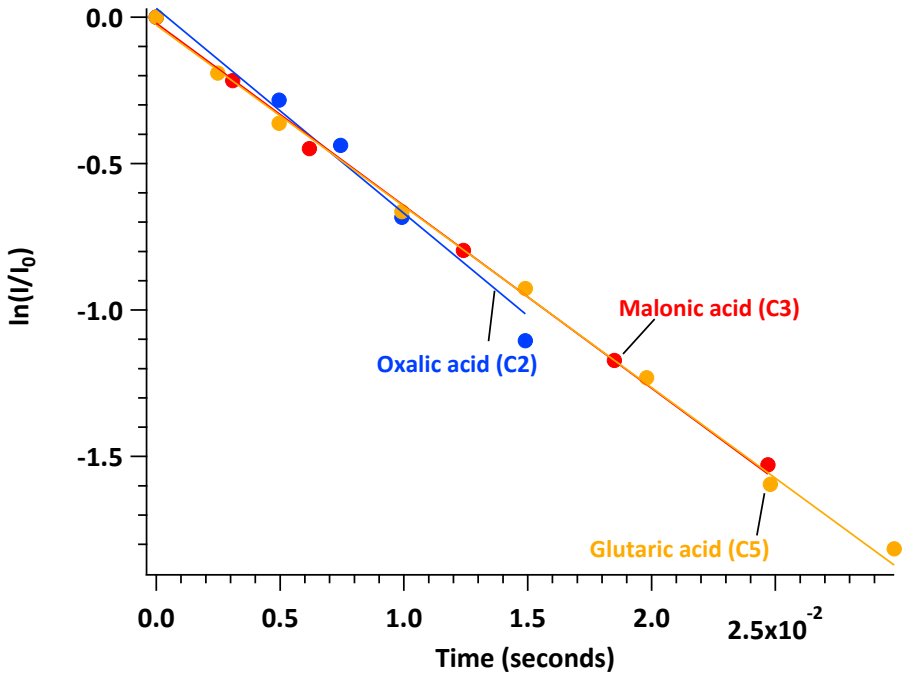

Figure 4-7. First order rate plots for (7 – 9) × 10^{13} molecules cm^{-3} sBA on C2, C3, and C5 solid diacids.

Table 4-2 summarizes experimental conditions and uptake coefficients for sBA on the diacids. In experiments where rate constants and uptake coefficients were obtained, there appears to be no significant difference between diacids (C2, C3, and C5), similar to trends seen with BA (Table 4-1). As with BA on oxalic acid (C2), due to the high vapor pressure of oxalic acid (C2), the uptake coefficients measured may include contributions from the reactions with gas phase oxalic acid (C2).

Concentration dependence was also investigated with sBA and uptake profiles for $(1 – 2) \times 10^{14}$ molecules cm^{-3} sBA on C2, C3, and C5 diacids are shown in Figure 4-8. Oxalic acid (C2) shows a difference in the uptake behavior between the two higher concentrations compared to the lower concentration. At the two higher concentrations, surface saturation becomes evident, giving slightly lower uptake coefficients. With malonic (C3) and glutaric (C5) acids, there is no observable difference in uptake between the three concentrations. Measuring uptake coefficients for succinic acid (C4) at both concentrations was less direct. As shown in Figure 4-6, the same saw–toothed pattern was observed when the inlet was pulled back at different increments, much like with BA. This pattern continued when the concentration was increased to 1×10^{14} molecules cm^{-3} (Figure 4-9).

Table 4-2. Summary of experimental conditions for sBA on solid C2 – C5 diacids.

Diacid	$[sBA]_0 \times 10^{14} \pm 2\sigma^a$ (molecules cm^{-3})	Diacid Area $\pm 2\sigma^a$ (cm^2)	$k \pm 2\sigma^a$ (s^{-1})	$\gamma \pm 2\sigma^a$
Oxalic (C2)	0.81 ± 0.01	54.2 ± 15.2	66.7 ± 11.6	$(1.1 \pm 0.5) \times 10^{-2}$
	1.3 ± 0.2	33.7 ± 6.7	66.2 ± 4.0	$(0.76 \pm 0.14) \times 10^{-2}$
	2.0 ± 0.1	35.0 ± 17.3	67.9 ± 28.1	$(0.76 \pm 0.17) \times 10^{-2}$ [c]
Malonic (C3)	0.92 ± 0.11	67.7 ± 7.4	66.4 ± 18.9	$(0.95 \pm 0.21) \times 10^{-2}$
	1.7 [b]	46.8 ± 1.9	79.1 ± 7.3	$(1.4 \pm 0.1) \times 10^{-2}$
	2.4 ± 0.1	56.3 ± 17.8	73.1 ± 11.2	$(1.1 \pm 0.3) \times 10^{-2}$
Succinic (C4)	0.67 ± 0.04	65.5 ± 10.9	– [d]	– [d]
	1.3 ± 0.1	59.9 ± 31.3	– [d]	– [d]
Glutaric (C5)	0.78 ± 0.21	45.4 ± 24.9	61.0 ± 5.4	$(1.6 \pm 0.7) \times 10^{-2}$
	1.3 ± 0.1	59.2 ± 16.4	63.1 ± 20.9	$(1.3 \pm 0.7) \times 10^{-2}$
	2.0 ± 0.1	67.2 ± 33.8	70.5 ± 18.4	$(1.2 \pm 0.3) \times 10^{-2}$

[a] Represents two sample standard deviations based on each replicate. [b] Amine concentrations were the same for all runs. [c] Uptake coefficients decreased with time and those reported are for the first trial of each sample. [d] First-order rate plots were not linear, which may be due to surface saturation as described in the text.

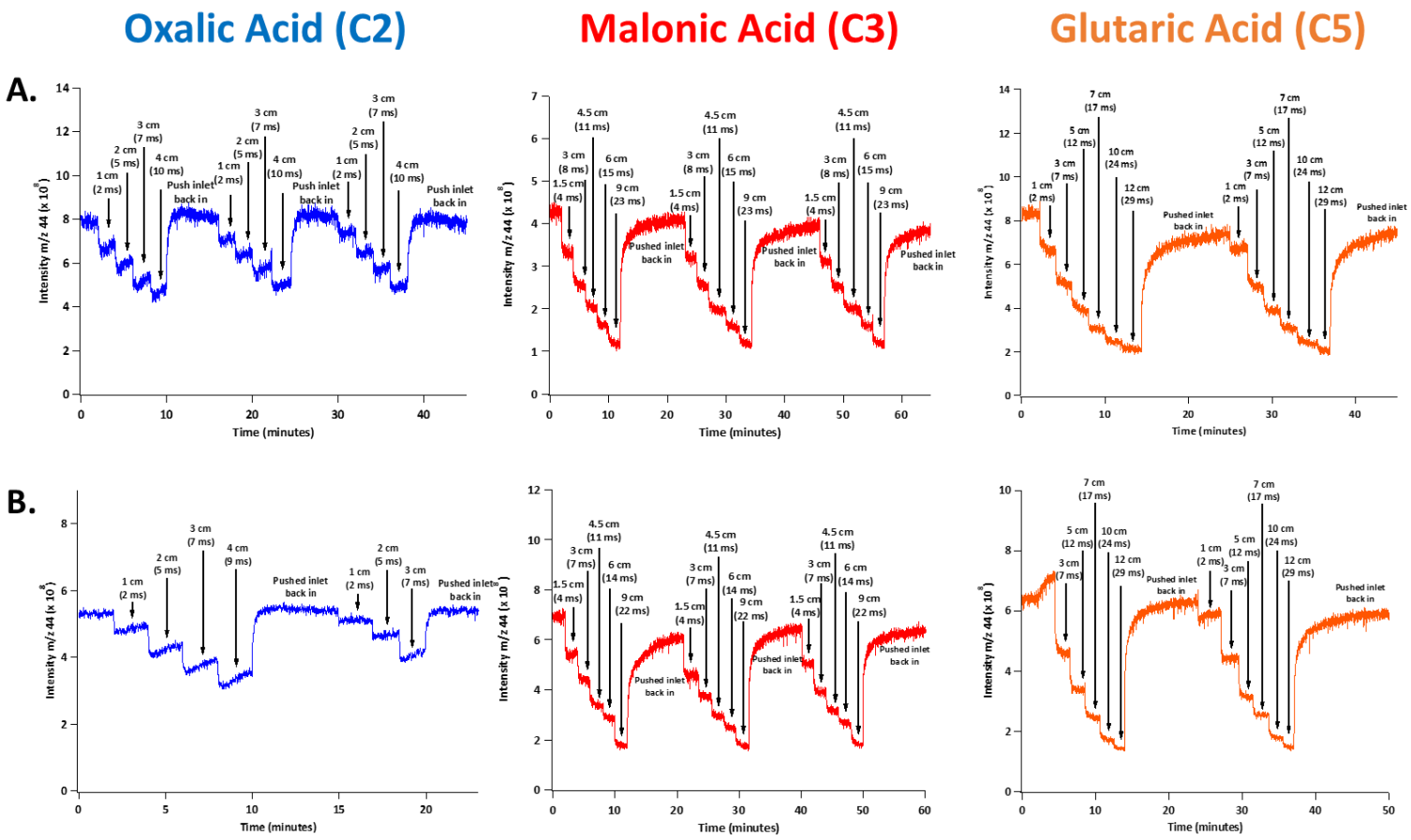

Figure 4-8. Uptake profiles for C2, C3, and C5 diacids at sBA concentrations of a) 1×10^{14} molecules cm^{-3} and b) 2×10^{14} molecules cm^{-3} in the flow reactor. P_{FT} = 0.8 – 0.9 Torr.

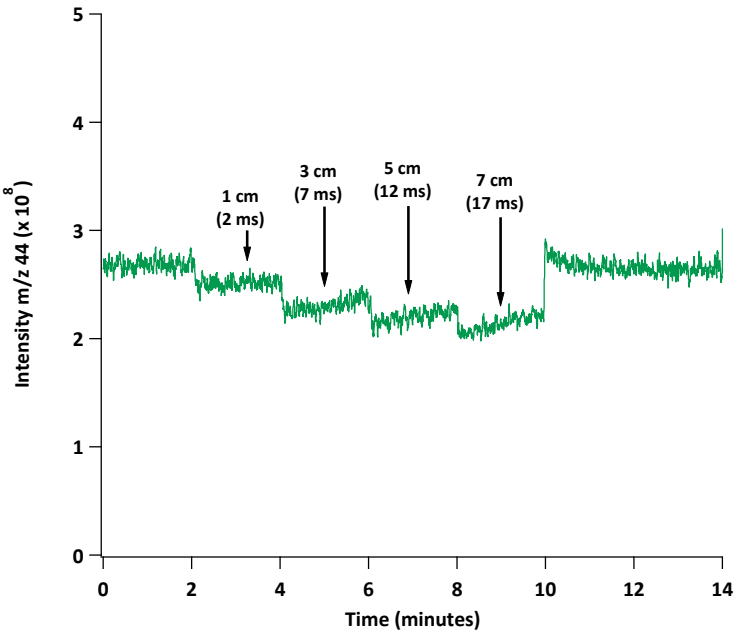

Figure 4-9. Uptake of 1×10^{14} molecules cm^{-3} sBA on solid succinic acid (C4) in the flow reactor. P_{FT} = 0.9 Torr.

However, when the intensities at the lowest point was taken to obtain first–order kinetics, plots were not linear when all inlet distances were included as shown in Figure 4-10. In flow reactor studies, as the inlet or injector is pulled back, the gas phase species is exposed to the surface for a longer time. Therefore, the intensity of the gas should decrease in a linear fashion, if the reaction follows first–order kinetics. The last couple of points cause the loss of linearity, and excluding the non–linear points still does not result in a linear fit. Possible causes of this non–linearity are discussed below.

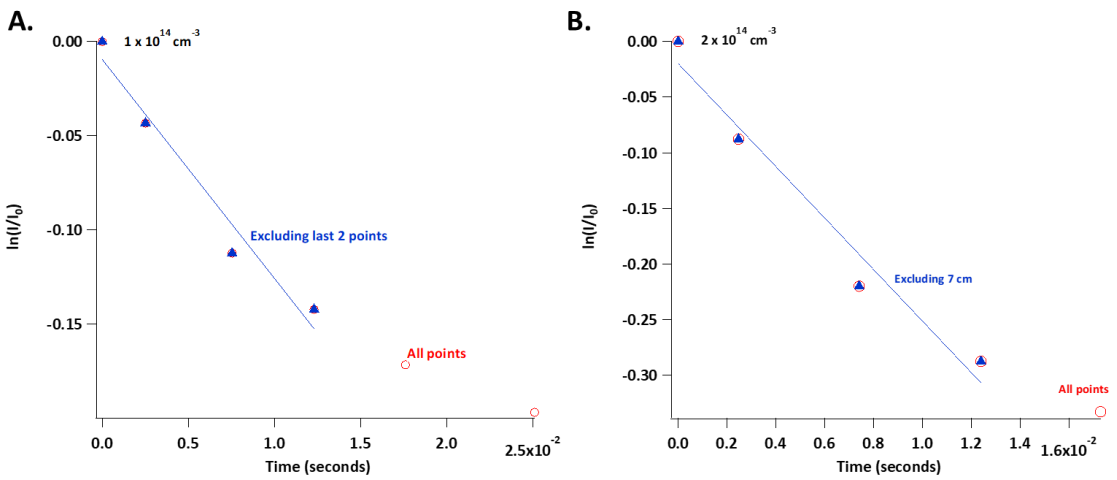

Figure 4-10. First-order rate plots for a) 1×10^{14} molecules cm^{-3} and b) 2×10^{14} molecules cm^{-3} sBA on succinic acid (C4).

Pulling back the inlet in a coated flow reactor should result in a decrease in the gas phase signal due to uptake/reaction of the gas onto the substrate. However, in the case of sBA at both concentrations, the decrease in amine signal as the inlet is pulled back further and further does not decrease linearly with increasing inlet distance. If there is no linear decrease in signal intensity of the amine as the inlet is pulled back, it indicates that the supposed "fresh" surface is not fresh and may have less available reactive sites as the previous section has once the inlet is pulled back.

Second, the main reason for the non–linearity for succinic acid (C4) with sBA, and BA, may be due to surface saturation already occurring at the first inlet position. The time resolution of our experiments may be too slow to capture the true, initial uptake of the amine onto the diacid, and thus the points taken to obtain first–order kinetics already represent surface saturation. Decreasing the response time for acquisition of data comes at the expense of

increasing the amount of noise, which in some cases, will make the change in amine signal upon pulling back the inlet indistinguishable.

III. Conclusions for Flow Reactor Experiments using Solid Diacids

The coating method for experiments with solid diacids provided some challenges. First, there is a large uncertainty in the surface area due to the large distribution in edge lengths as well as the collection of the coating to obtain the mass of the coating. Second, the coatings may not be uniform along the flow reactor and the assumption that the crystals are cubic with five sides available for reaction may be an overestimate since crystals may stick together. Lastly, a significant amount of noise can be seen for some uptake profiles, due to the increased sensitivity scale for experiments with oxalic acid (C2). In addition, the slower time constant made quantification difficult. Therefore, a new coating method was employed to improve on measuring uptake coefficients with the flow reactor.

IV. Uptake of BA on Diacid Slurry

The pinhole on the QMS was decreased from 1 mm to 0.2 mm and better alignment of the quadrupole was also achieved. The coating method was switched from solid to "slurry" in order to obtain a more uniform coating and rather than calculating the surface area of diacid crystals, the reacted area was assumed to be that of the flow reactor. Images of diacid coatings using slurries are shown in Figure 4-11. As evident in Figure 4-11, some diacid slurries result in a more intact, even coating, while others are more uneven and sparse. Also, it is interesting to note is that frosting on the inlet not only occurs with oxalic acid (C2), but to some extent with all diacids.

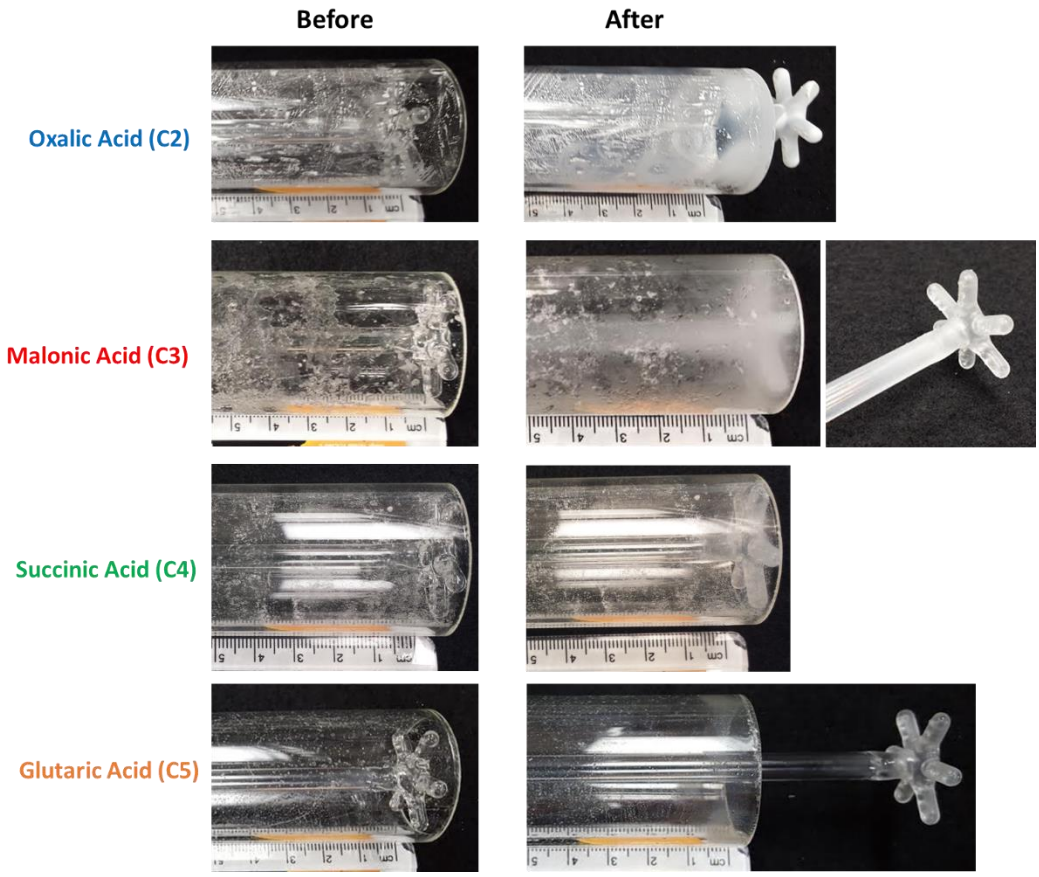

Figure 4-11. Photos of C2 – C5 diacid slurry coatings before and after exposure to BA.

Figure 4-12 shows typical uptake profiles for concentrations of (7 – 30) × 10^{13} molecules cm^{-3} BA on malonic acid (C3). The first behavior that is distinctly different from BA on the first diacid coating method (Chapter 4, Section I) is that at most concentrations, there are signs of surface saturation present while the inlet is held at a certain position as well as decreasing uptake with subsequent trials. At concentrations of 7 × 10^{13} molecules cm^{-3}, it appears that the signal of the amine remains relatively flat while the inlet is held at a given position. This trend was consistent and reproducible for experiments done at this concentration. With each increasing

trial, the initial uptake of the amine becomes more and more sharp, due to rapid depletion of reactive sites as the concentration of the gas phase species is increased.

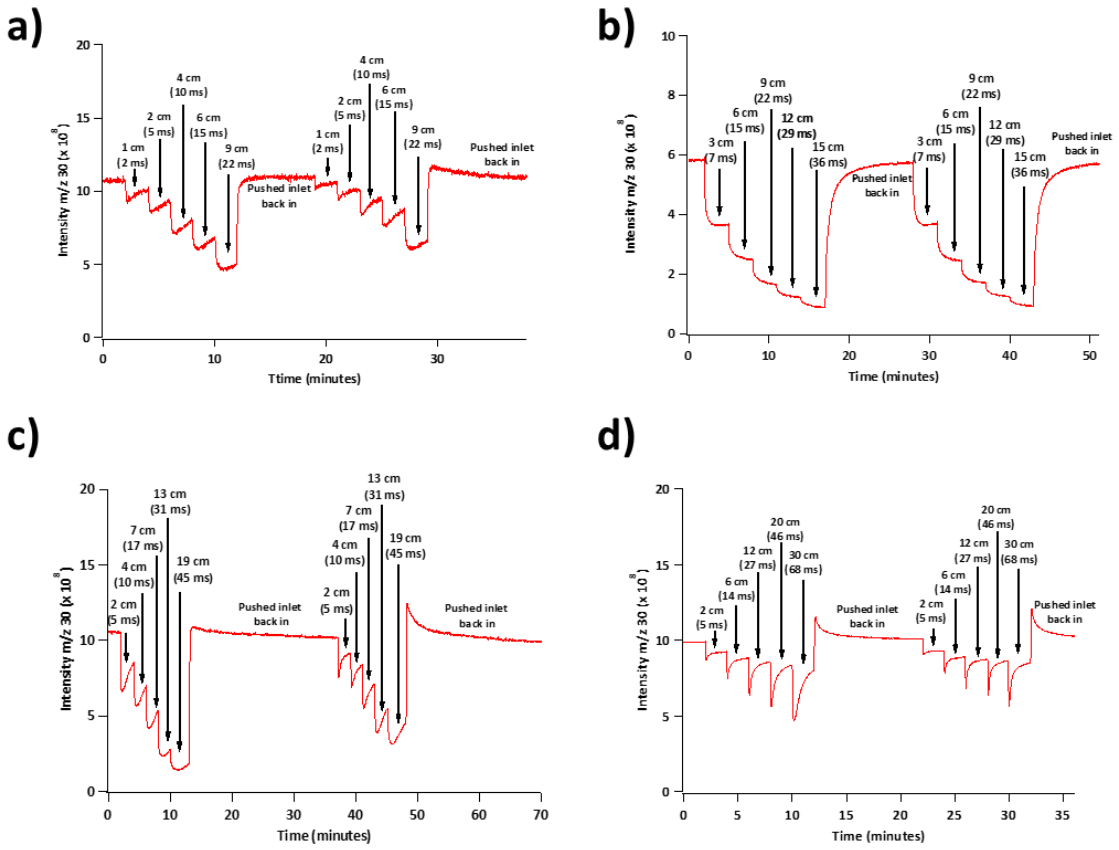

Figure 4-12. Uptake profiles for a) $(3 – 4) \times 10^{13}$ molecules cm^{-3}, b) $(7 – 8) \times 10^{13}$ molecules cm^{-3}, c) 2×10^{14} molecules cm^{-3}, and d) 3×10^{14} molecules cm^{-3} BA on malonic acid (C3) in the flow reactor. P_{FT} = 0.9 Torr.

First–order rate plots for BA concentrations of $(3 – 30) \times 10^{13}$ molecules cm^{-3} on malonic acid (C3) slurries are shown in Figure 4-13. The slopes and thus rate constants decrease with increasing trials for all concentrations except 7×10^{13} molecules cm^{-3} BA. Another trend that is different from uptake onto the first coating method is that the first order rate plots are not always linear, especially at higher concentrations. A large increase in pulling back the inlet in going

from 12 to 20 cm (27 to 46 ms) in Figure 4-12d results in a small change in intensity of the amine signal (Figure 4-13). As mentioned in Chapter 4 Section II, a small amount of amine flow may react away a portion of the diacid surface (Figure 4-3). However, in these experiments, the inlet is pulled back at a distance larger than one centimeter indicating that the next portion of the slurry coating can most likely be considered as a fresh surface.

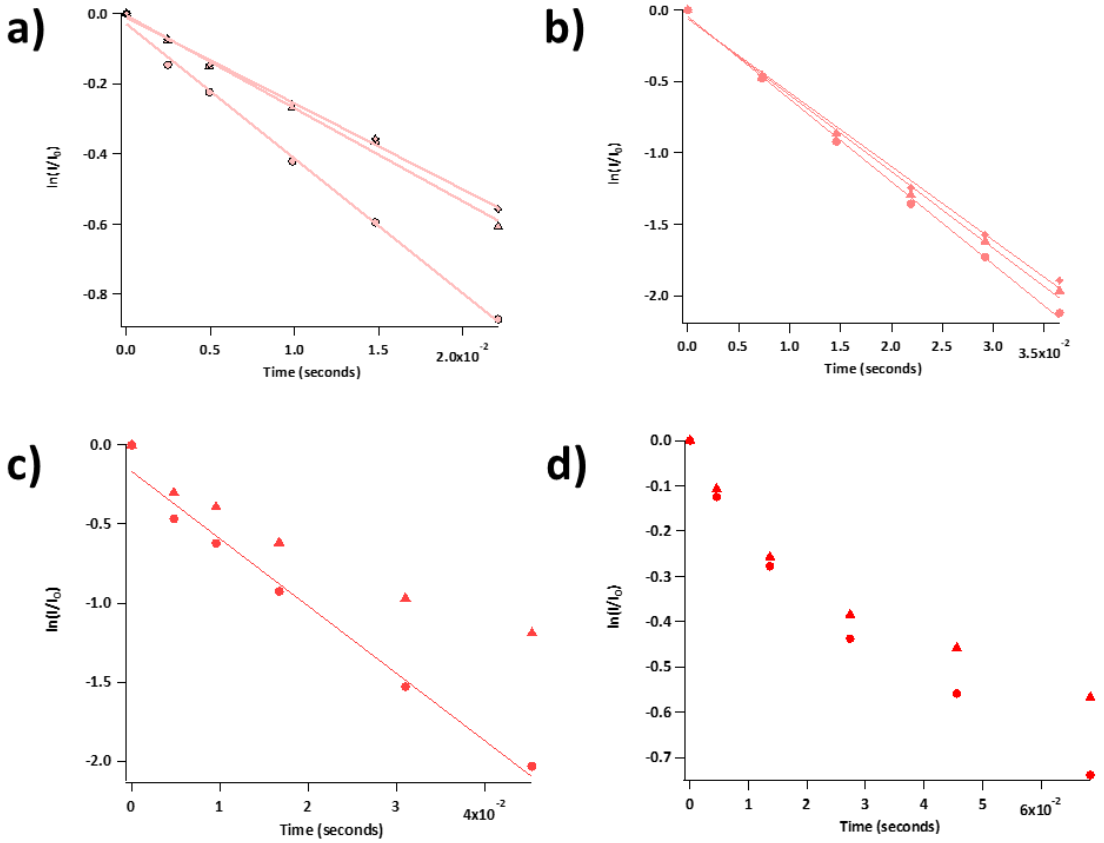

Figure 4-13. First–order rate plots for a) (3 – 4) × 10^{13} molecules cm^{-3}, b) (7 – 8) × 10^{13} molecules cm^{-3}, c) 2 × 10^{14} molecules cm^{-3}, and d) 3 × 10^{14} molecules cm^{-3} BA on malonic acid (C3) using the flow reactor. Each symbol represents a different trial.

The behavior of (7 – 30) × 10^{13} molecules cm^{-3} BA on glutaric acid (C5) showed similar behavior (Figure 4-14) as malonic acid (C3). However, unlike experiments with malonic acid

(C3), those with glutaric acid (C5) are reproducible in their saturation dependence on amine concentration. At the lowest concentration (Figure 4-14a), the first trial shows no indication of surface saturation, however with each subsequent trial, surface saturation occurs as is evident by the lower signal intensity compared to the previous inlet position and the lowered uptake with each progressing trial. At the two highest concentrations from $(1 – 3) \times 10^{14}$ molecules cm^{-3} BA, the decrease and subsequent recovery in the amine signal resulting from first pulling back the inlet is much sharper (Figure 4-14c and d), due to rapid depletion of reaction sites as the inlet is pulled back along the coating.

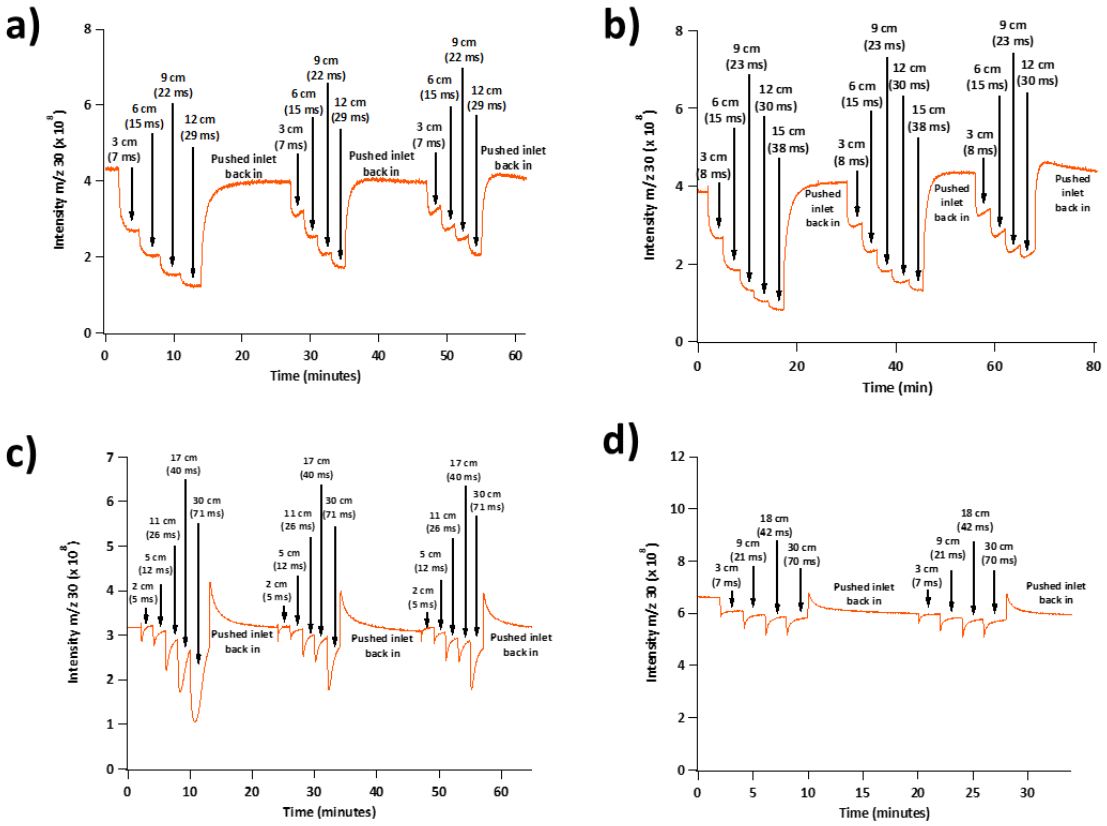

Figure 4-14. Uptake profiles for a) $(3 – 4) \times 10^{13}$ molecules cm^{-3}, b) $(7 – 8) \times 10^{13}$ molecules cm^{-3}, c) 2×10^{14} molecules cm^{-3}, and d) 3×10^{14} molecules cm^{-3} BA on glutaric acid (C5) using a flow reactor. P_{FT} = 0.9 Torr

As with malonic acid (C3), glutaric acid (C5) also does not exhibit linear first–order kinetics plots (Figure 4-15) at the higher concentrations. At the lowest amine concentration of $(3 – 4) \times 10^{13}$ molecules cm^{-3} all plots of $\ln(I/I_0)$ as a function of time are linear for all three trials, however, the slope decreases with each progressing trial, as a result of surface saturation observed in Figure 4-14a. However, as the concentration increases, linearity in the first–order plots also decreases. As evident in Figure 4-14, as the concentration increases, the drop and subsequent recovery of amine signal when the inlet is first pulled back becomes sharper and sharper, and in some cases, the drop in signal is lower than the previous inlet distance which in

turn affects the linearity. Varying drops in amine signal may be attributed to irregularities in the coatings (Figure 4-11).

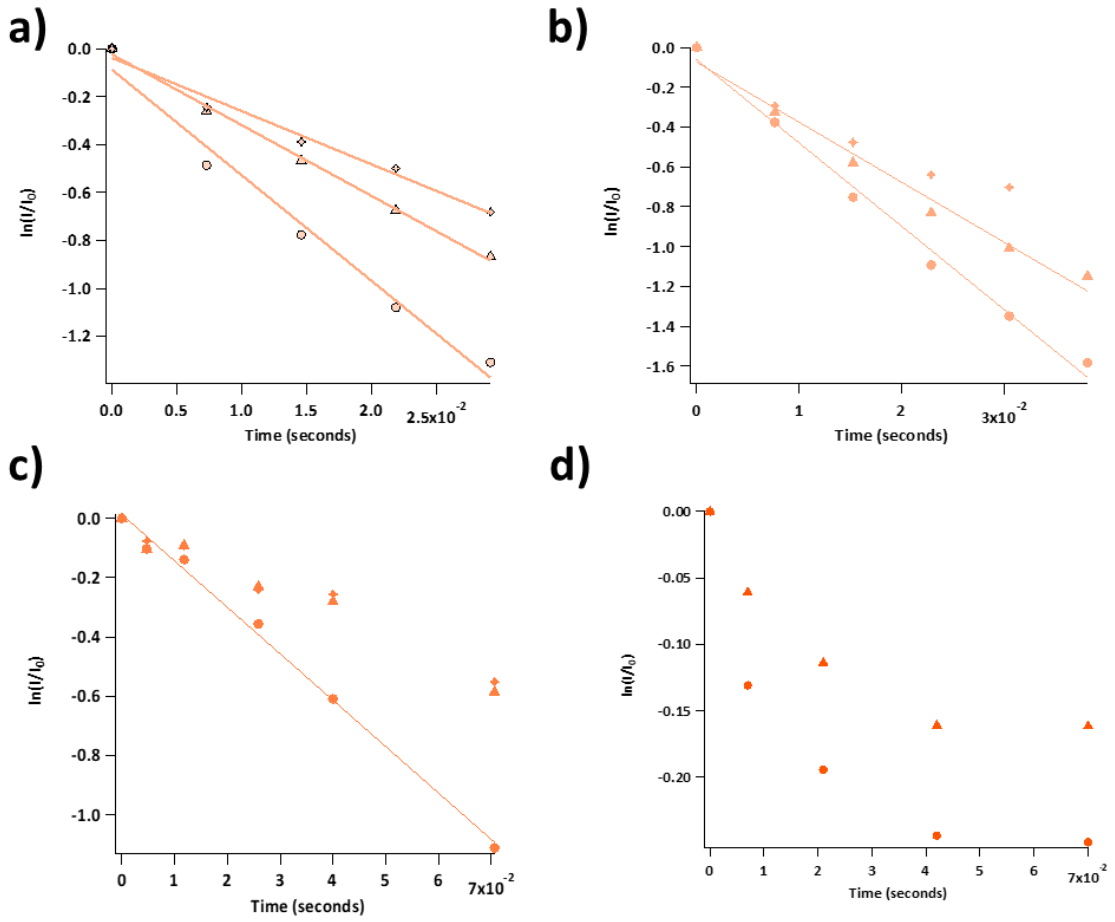

Figure 4-15. First–order rate plots for a) (3 – 4) × 10^{13} molecules cm^{-3}, b) (7 – 8) × 10^{13} molecules cm^{-3}, c) 2 × 10^{14} molecules cm^{-3}, and d) 3 × 10^{14} molecules cm^{-3} BA on glutaric acid (C5) using the flow reactor. Each symbol represents a different trial.

Significant differences in uptake were observed with increasing concentrations of BA on the succinic acid (C4) slurry as shown in Figure 4-16. Similar to uptake experiments on solid succinic acid (C4), subsequent trials on a single diacid coat are not possible. BA on succinic acid (C4) slurries also show saturation with increasing amine concentration. As observed with

BA on the malonic acid (C3) slurry, uptake of BA at 7×10^{13} molecules cm^{-3} on succinic acid (C4) appear to be an outlier compared to uptake at the other concentrations in Figure 4-16. The initial uptake of the amine as the inlet is pulled back becomes sharper and sharper as the concentration increases, which is attributed to rapid depletion of reactive sites as concentration of the gas phase increases.

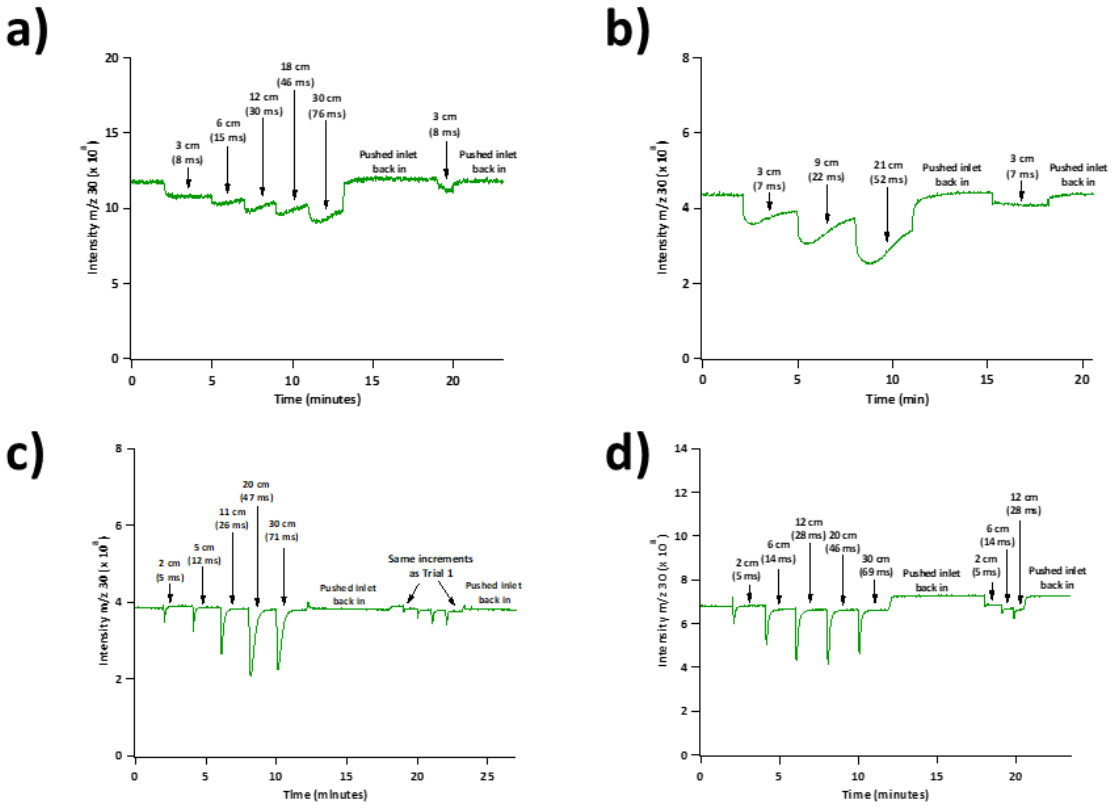

Figure 4-16. Uptake profiles for a) $(3 - 4) \times 10^{13}$ molecules cm^{-3}, b) $(7 - 8) \times 10^{13}$ molecules cm^{-3}, c) 2×10^{14} molecules cm^{-3}, and d) 3×10^{14} molecules cm^{-3} BA on succinic acid (C4) using the flow reactor. P_{FT} = 0.9 Torr.

As with sBA on solid succinic acid (C4) coatings, the kinetics for BA on slurries of succinic acid (C4) do not follow first order kinetics as shown in Figure 4-17. At the two lowest

concentrations of BA (Figure 4-17a and b), the data are better fit by a polynomial rather than a line. At the two highest concentrations, (Figure 4-17c and d), the last point has a lower intensity than the majority of points.

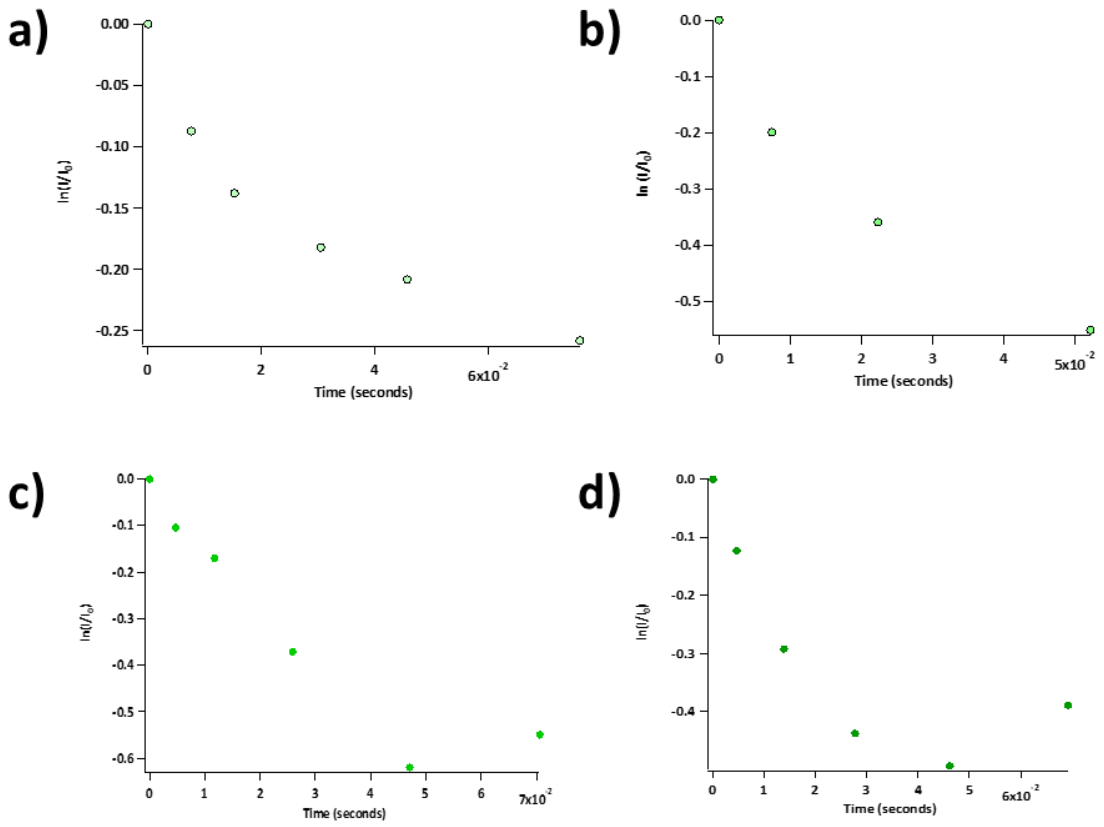

Figure 4-17. First–order rate plots for a) (3 – 4) × 10^{13} molecules cm^{-3}, b) (7 – 8) × 10^{13} molecules cm^{-3}, c) 2 × 10^{14} molecules cm^{-3}, and d) 3 × 10^{14} molecules cm^{-3} BA on succinic acid (C4) using the flow reactor.

Coatings of oxalic acid (C2) were not as uniform from sample to sample. Typical uptake profiles for (20 – 30) × 10^{13} molecules cm^{-3} BA are shown in Figure 4-18. The variations in data for oxalic acid (C2) may lie in the integrity of the coatings during the experiment. In some experiments, it was observed that after removing the flow reactor from the QMS, a portion or, in

some cases, all of the oxalic acid (C2) coating was pumped off. This was not observed with other diacid slurry coatings and may lie in the high vapor pressure of oxalic acid (C2).[136] Similar to the other diacid slurries, the kinetics plots were non–linear for concentrations of BA on oxalic acid (C2) as shown in Figure 4-19.

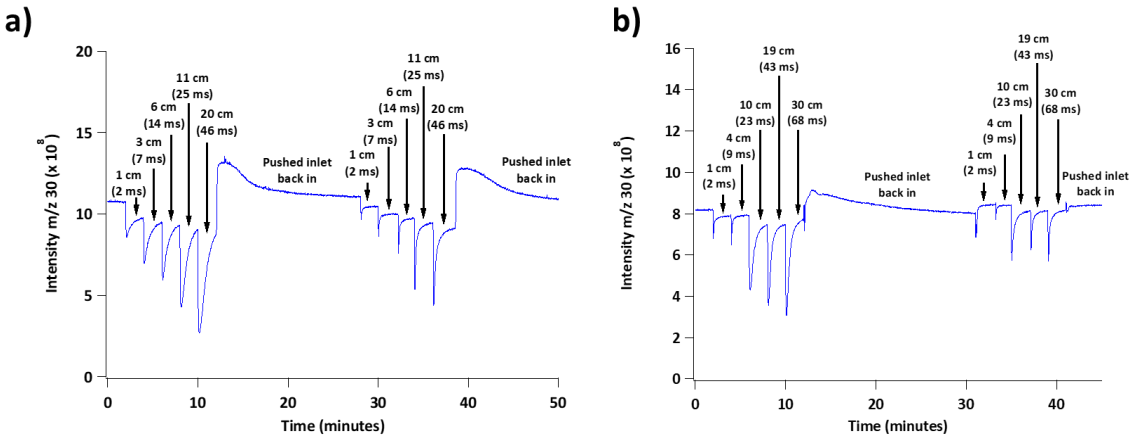

Figure 4-18. Uptake profiles for a) 2×10^{14} molecules cm^{-3}, and b) 3×10^{14} molecules cm^{-3} BA on oxalic acid (C2) using the flow reactor. P_{FT} = 0.8 – 0.9 Torr.

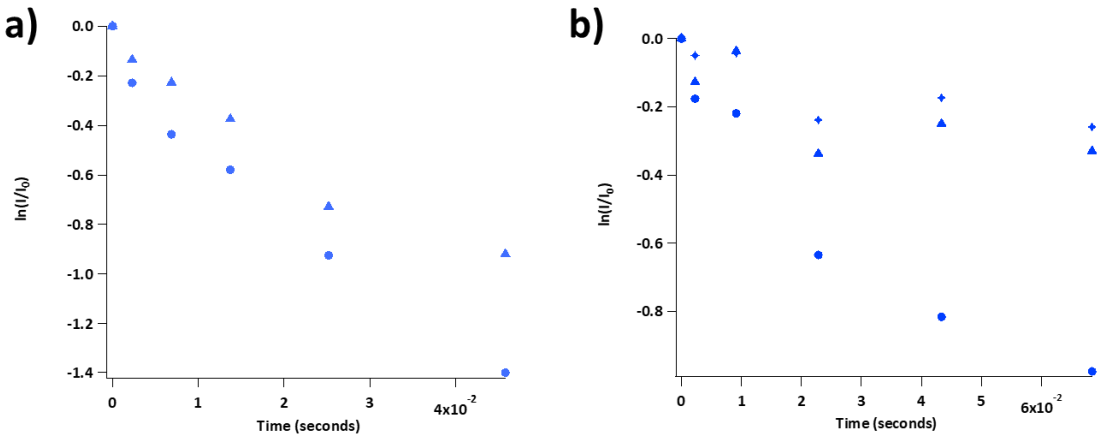

Figure 4-19. First–order rate plots for a) 2×10^{14} molecules cm^{-3}, and b) 3×10^{14} molecules cm^{-3} BA on oxalic acid (C2).

Due to the lack of linearity across experiments, quantifying uptake coefficients for several concentrations of amine on diacid slurries was less straightforward than experiments with solid diacid coatings. Therefore, a different approach to measuring uptake coefficients was utilized. As discussed above for amines on the solid diacid coatings, due to the time scales of these experiments, the surface may already be saturated, which is indicated by the exponential increase in the amine signal as the inlet is held at a given position. Therefore, an attempt to create an expression to extrapolate uptake coefficients using this exponential portion was carried out. Let θ represent the fraction of diacid monolayer reacted, therefore, we can represent the fraction of sites available for reaction as $(1 - \theta)$. These unreacted and reacted sites can be related to the behavior observed in the uptake profiles for the diacids.

Figure 4-20 shows a typical uptake profile for BA on diacids slurries. As the inlet is initially pulled back, it signifies the fraction of reacted sites approaching zero, corresponding to a fresh surface. At this point, the concentration of amine molecules is that at $t = 0$ or $[G]_0$. As the surface becomes saturated, the fraction of reacted sites approaches unity, i.e., there are no available sites for reaction. To derive an expression for the uptake coefficient, the kinetics at the surface must be taken into account.

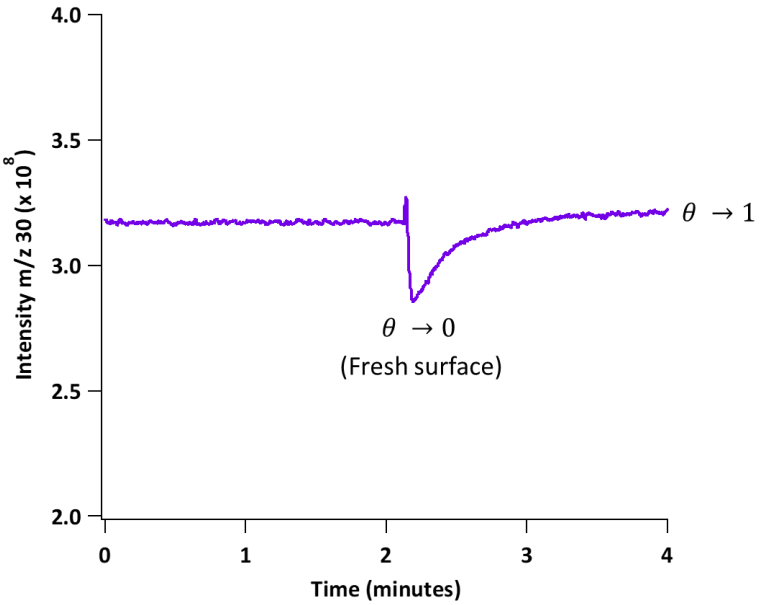

Figure 4-20. Zoomed in view of the initial drop in amine signal once the inlet is pulled back, followed by the exponential increase in amine signal, which is indicative of surface saturation.

The change in the number of reactions on a surface (N_s) per unit time can be represented using Equation 4.1.

$$\frac{dN_s}{dt} = \gamma A_0(1 - \theta)[G]\sqrt{\frac{RT}{2\pi M}} \qquad \textbf{4.1}$$

Variables in the equation include the initial reactive surface area of the diacid (A_0), the fraction of sites available for reaction ($1 - \theta$), concentration of the amine ($[G]_0$), the gas constant (R), temperature (T), and the molar mass of the amine (M). The change in surface sites as a function of time (θ^t) is also related to the change in the number of reactions of the amine onto the surface as a function of the maximum surface density of reactive sites (N_{max}) as written in Equation 4.2.

$$d\theta = \frac{dN_s}{N_{max}} \quad \textbf{4.2}$$

Combining Equation 4.2 with Equation 4.1 yields Equation 4.3.

$$\frac{d\theta}{dt} = \frac{dN_s}{dt}\frac{1}{N_{max}} = \frac{\gamma A_0(1-\theta)[G]}{N_{max}}\sqrt{\frac{RT}{2\pi M}} \quad \textbf{4.3}$$

Since we are interested in the change in reactive sites as a function of time, rearrangement of Equation 4.3 yields Equation 4.5, which can then be integrated in terms of θ and t. Equation 4.5 represents the integrated result of Equation 4.4, where $z = \frac{\gamma A_0[G]}{N_{max}}\sqrt{\frac{RT}{2\pi M}}$.

$$\int_0^{\theta} \frac{d\theta}{(1-\theta)} = \mathrm{z}\int_0^{t} dt \quad \textbf{4.4}$$

$$-\ln(1-\theta) = zt \quad \textbf{4.5}$$

Next, a derivation for the change in amine concentration is needed. Equation 4.1 represents the rate of gas phase molecules colliding with a surface per unit time. In this equation, A_0 is the initial reactive surface area at $t = 0$. At time, t, the area, A_t represents a fraction of surface area available for reaction, or $A_o(1 - \theta)$. Since the initial reactive surface area

is defined as the area of the flow reactor, Equation 4.1 can be written to express the change in amine molecules as a function of time in the volume of the flow reactor ($\pi r^2 L$).

$$\frac{\Delta[G]}{\Delta t} = -\frac{\gamma A_0(1-\theta)[G]}{\pi r^2 L}\sqrt{\frac{RT}{2\pi M}} \qquad \textbf{4.6}$$

Assuming L is 1 cm, simplification of Equation 4.6 in terms of the area and volume give Equation 4.7.

$$\frac{d[G]}{dt} = -\frac{2\gamma}{r}(1-\theta)[G]\sqrt{\frac{RT}{2\pi M}} \qquad \textbf{4.7}$$

Since we are interested in the change in amine concentration, Equation 4.7 can be rewritten as:

$$\frac{d[G]/[G]}{dt} = -\frac{2\gamma}{r}(1-\theta)\sqrt{\frac{RT}{2\pi M}} \qquad \textbf{4.8}$$

Rearrangement of Equation 4.8 yields Equation 4.9:

$$\frac{d[G]}{[G]} = \left[-\frac{2\gamma}{r}(1-\theta)\sqrt{\frac{RT}{2\pi M}}\right]dt \qquad \textbf{4.9}$$

Recall that Equation 4.5 can be written to express in terms of (1 – θ) to yield $(1-\theta) = e^{-zt}$. Substitution of this equality into Equation 4.9 gives Equation 4.10.

$$\frac{d[G]}{[G]} = -\frac{2\gamma}{r}\sqrt{\frac{RT}{2\pi M}}e^{-zt}\,dt \qquad \textbf{4.10}$$

Integration of both sides of Equation 4.10 yields:

$$ln\frac{[G]}{[G]_0} = -\frac{2\gamma}{zr}\sqrt{\frac{RT}{2\pi M}}(e^{-zt} - 1) \qquad \textbf{4.11}$$

Substituting *z* into Equation 4.11 and simplifying the rest of the constants leads to the final expression of Equation 4.12.

$$ln\frac{[G]}{[G]_0} = \left[\frac{2N_{max}}{rA_0[G]_0}\right](1 - e^{-zt}) \qquad \textbf{4.12}$$

All of the constants in the brackets are known, for example the radius of the flow reactor (*r*, 1.5 cm), the initial surface area (A_0) which is taken as the area of the flow reactor, and the initial amine concentration ($[G]_0$). The value of N_{max} is defined as the maximum surface density of reactive sites in a monolayer (1×10^{14} molecules cm^{-2}). For simplicity, the constants in the brackets will be defined as *Q*. Now Equation 4.12 takes the form as an equation that can be used to fit an exponential curve. Recall the uptake profiles for certain concentrations of BA on diacid slurries exhibit an exponential region after the first initial drop in amine signal once the inlet is pulled back. Since the concentration of the amine is proportional to the intensity of the amine measured by the QMS, plots of the natural log of the section of the sharp drop in signal once the

inlet is pulled back (I_0) and the rise of the signal as a function of time can be fit to an exponential curve with Equation 4.12 to find *Q* and *z* (Figure 4-21). Since γ is included in the *z* term, the exponential fit coefficient for *z* can be used to find γ for each increment at which the inlet was pulled back and an average uptake coefficient for a single trial can be obtained. This approach will yield a unique value for *Q* and *z*.

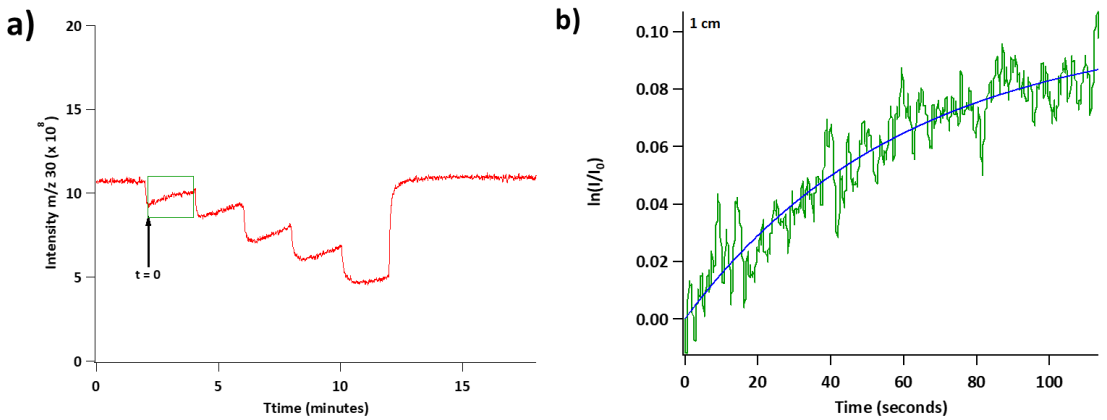

Figure 4-21. a) Uptake profile for $(3 – 4) \times 10^{13}$ molecules cm^{-3} BA on malonic acid (C3). b) Zoomed in view of intensity of the amine while the inlet is held at 1 cm with fit of Equation 4.12.

Curve fits were obtained for $(3 – 4) \times 10^{13}$ and 30×10^{13} molecules cm^{-3} BA on the diacid slurries. Uptake coefficients at these two concentrations are all on the order of 10^{-6} with no apparent trend in odd or even carbon diacids. These uptake coefficients are several orders of magnitude lower than those measured for BA on solid diacid coatings. Such low values of uptake coefficients do not make physical sense in that a value of 10^{-6} would indicate that the gas phase species has little to no affinity for the surface. However, as shown in all the uptake profiles for BA on the diacid slurries, there is a distinct, measurable drop in the signal as the inlet

is pulled back on the coating. As stated in the Chapter 2 Section IV, no uptake was observed on a clean flow reactor.

The low values for uptake coefficients may lie in the assumptions used to derive the equation for the change in concentration of the amine and the change in surface sites as a function of time. Fractional coverages of surface sites are usually used to represent reactions on solid surfaces, however with the diacid slurries, they were prepared from saturated, aqueous solutions. The fact these coatings are not pure solids, could have altered the nature and accuracy of the estimation of the surface. If the surface is more liquid–like, even though excess water was dried and pumped off, assumptions based on solid surfaces may lead to inaccuratly measured uptake coefficients.

V. Conclusions

The magnitude of uptake coefficients for BA and sBA on solid diacid coatings using the flow reactor were around 10^{-2}. A trend in uptake based on odd or even number of carbons on the diacid chain may exist. No differences between uptake of BA and sBA on diacids were observed. The uncertainties in surface area of the diacid crystals and assumptions made to calculate surface area contributed to the largest uncertainity in measuring uptake coefficients. Therefore, slurry coatings were used in order to achieve a more uniform coating. However, the kinetics behind the reaction onto the diacid slurries were not linear in any respect and attempts to derive an expression to measure uptake coefficients led to values of 10^{-6}. Assumptions made in the derived uptake coefficient expression stem from principles in surface chemistry of solids. In

the case of the slurries, the nature of the surface may be altered because the coatings are based on supersaturated, aqueous solutions.

Although uptake coefficients for the solid coating method are more reasonable, experiments for both coating methods may be reflecting surface saturation. The time constant used in both experiments may be too slow to fully capture the initial uptake of this reaction system. Therefore, the data presented may reflect saturation, which is evident in the exponential rise in amine signal when the inlet is held at a given position, as well as the non–linearity in the first–order kinetics plots.

CHAPTER 5: RESULTS – UPTAKE OF AMINES/AMMONIA ON DIACIDS USING KNUDSEN CELL

Knudsen cell studies have been used for a variety of reactions to measure uptake coefficients for heterogeneous reactions. The benefit to using a Knudsen cell over the flow reactor is the surface area of the diacid crystals is better defined using the Knudsen cell. Second, an issue in the time resolution of the flow reactor experiments was also suspected, in that the time constant used was too slow to capture the initial uptake of the amine onto the diacid. Therefore using the Knudsen cell, which has proved to be a successful technique in this lab,[176, 178, 198-201] was utilized. Due to the interesting properties of the diacids, the amine–diacid reaction system was further probed to determine if uptake coefficients do in fact depend on the number of carbons in the diacid chain and if the structure of the amine also governs its uptake and reaction with the diacid.

I. Uptake of BA onto C3 – C8 Diacids

Figure 5-1 shows typical uptake traces for BA on C3–C8 diacids at $[BA]_0 = (3 – 5) \times 10^{11}$ molecules cm^{-3}. There was no uptake observed on suberic acid (C8) or on a clean, halocarbon wax coated sample holder. The difference between the signal intensity with the lid closed compared to when it is open is a measure of the uptake coefficient (Equation 2.4). Table 5-1 summarizes the uptake coefficients for all experiments.

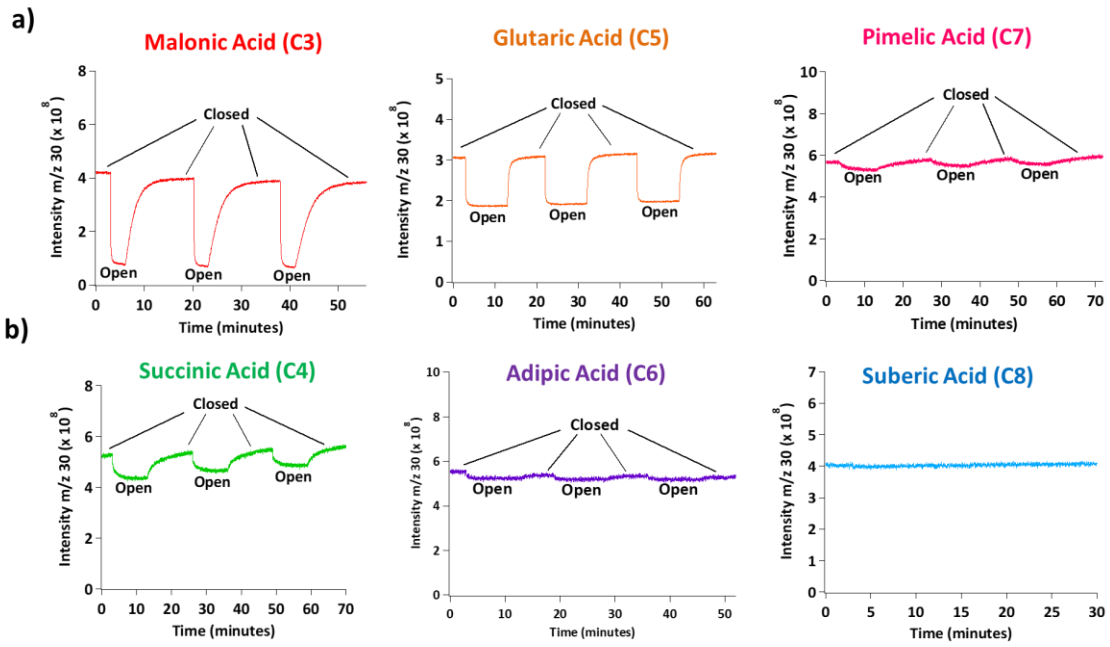

Figure 5-1. a) Uptake profiles for odd carbon diacids: malonic acid (C3), glutaric acid (C5), and pimelic acid (C7). b) Uptake profiles for even carbon diacids: succinic acid (C4), adipic acid (C6), and suberic acid (C8). $[BA]_0 = (3 – 5) \times 10^{11}$ molecules cm^{-3} for all experiments. Sensivitiy on the lock–in amplifier for experiments with malonic (C3) and glutaric (C5) acids was 100 mV. For experiments with succinic (C4), adipic (C6), pimelic (C7), and suberic (C8) acids, sensitivity was increased to 10 mV.

Table 5-1. Uptake coefficients (γ) for different concentrations of *n*-butylamine on different surface areas of diacids.

	Surface area $\pm 2\sigma$ [a] (cm^2)	$[BA]_0$ ($\times 10^{12}$) $\pm 2\sigma$ [b] (molecules cm^{-3})	$\gamma \pm 2\sigma$ [d]
Malonic (C3)	2.0 ± 0.9	0.29 [c] (3)	0.65 ± 0.19
	4.2 ± 2.1	0.29 [c] (3)	0.60 ± 0.19
	1.8 ± 0.9	4.1 ± 0.2 (3)	0.77 ± 0.23
	4.4 ± 2.2	4.9 ± 0.3 (3)	0.91 ± 0.27
Succinic (C4)	21.3 ± 6.4	0.49 ± 0.07 (3)	$(1.7 \pm 0.6) \times 10^{-4}$ [e]
	21.4 ± 5.6	4.9 ± 0.5 (4)	$(3.3 \pm 0.9) \times 10^{-4}$ [e]
Glutaric (C5)	2.0 ± 0.7	0.32 ± 0.03 (5)	0.099 ± 0.026
	4.5 ± 1.5	0.31 ± 0.03 (6)	0.11 ± 0.022
	2.1 ± 1.0	3.7 ± 0.2 (3)	0.37 ± 0.17 [e]
	4.4 ± 1.9	4.1 ± 0.4 (3)	0.30 ± 0.14 [e]
Adipic (C6)	32.5 ± 15.5	0.44 ± 0.07 (3)	$(1.9 \pm 1.4) \times 10^{-5}$ [e]
	30.3 ± 12.6	4.2 ± 0.3 (3)	$(2.8 \pm 1.9) \times 10^{-5}$ [e]
Pimelic (C7)	9.6 ± 4.5	0.45 ± 0.04 (4)	$(1.1 \pm 0.54) \times 10^{-4}$ [e]
	9.4 ± 5.1	4.4 ± 1.1 (3)	$(1.1 \pm 0.64) \times 10^{-4}$ [e]
Suberic (C8)	16.0 ± 10.5	0.45 ± 0.05 (4)	$\leq 8 \times 10^{-6}$ [f]
	14.9 ± 11.6	4.5 ± 0.7 (3)	$\leq 6 \times 10^{-6}$ [f]

[a] Standard deviations represent 2σ for the distribution of crystal sizes in each sample. Orifice areas for all experiments were 0.31 cm^2, except for those with succinic (C4), adipic (C6), pimelic (C7), and suberic (C8) acids which were 0.015 cm^2. [b] Standard deviations represent 2σ for the variation in butylamine concentrations for those runs. Number of experiments given in parentheses. [c] Amine concentration for all samples was constant. [d] The errors are statistically determined standard deviations. However, due to the significant uncertainty in particle shape, which affects surface area, the overall uncertainty is estimated to be about a factor of two. [e] Uptake coefficient decreased with time; these values represent the average of the first trial for all samples. [f] Represents an upper limit.

An unexpected trend observed in Figure 5-1 is the prolonged steady and repeated uptake when the lid is opened, indicating a lack of surface saturation on both even and odd carbon diacids. Surface saturation commonly occurs with gas–solid reactions such as HNO_3 with

NaCl.[176-179, 202, 203] Saturation times for BA on the diacids, if it occurs, can be estimated as follows. The rate of reaction of amine molecules with the surface when the Knudsen cell lid is open is equal to the rate of loss of reactive sites:

$$\text{Rate of amine reaction } (\text{cm}^{-2}\ \text{s}^{-1}) = \text{Rate of loss of reactive sites } (\text{cm}^{-2}\ \text{s}^{-1})$$

This equality can be rewritten as Equation 5.1.

$$\frac{k_r}{A_{surf}} N_r = k' S_0 \qquad \textbf{5.1}$$

The variable k_r (s^{-1}) is the first–order rate constant for the amine molecules reacting with a surface, A_{surf} is the reactive surface area of the sample, N_r is the absolute steady–state number of amine molecules while the lid is open, k' (s^{-1}) is the first-order rate constant for the loss of acid reactive sites, and S_0 is the initial number density of the reactive (–COOH) sites per cm^2 of the sample surface. Approximate values of S_0 for malonic (C3) and succinic (C4) acids as examples of odd and even diacids respectively, were both obtained from published unit cell dimensions (each diacid containing 2 molecules per unit cell).[204, 205] The dimensions for malonic acid (C3) are a = 0.533 nm, b = 0.514 nm, and c = 1.125 nm.[204] Unit cell dimensions for succinic acid (C4) are a = 0.510 nm, b = 0.888 nm, and c = 0.761 nm.[205] This yields the number of diacid molecules per cm^2 (3.4×10^{14} cm^{-2} for malonic acid (C3) and 3.0×10^{14} cm^{-2} for succinic acid (C4)). S_0 values are obtained when these surface number densities are weighted by the fraction of surface area that are acidic reactive sites, the latter estimated from layer structures given in

Thalladi et al.[138] The weighting factor for malonic acid (C3) is 0.25 and for succinic acid (C4) is 0.24. Therefore, for malonic acid (C3) $S_0 = 8.5 \times 10^{13}$ cm^{-2} and for succinic acid (C4), $S_0 = 7.1 \times 10^{13}$ cm^{-2}.

The first–order rate constant, k_r, can be calculated from measured values and kinetic molecular theory via Equation 5.2.[3]

$$k_r = \gamma \frac{1}{V} A_{surf} \sqrt{\frac{RT}{2\pi M}} \qquad \textbf{5.2}$$

The variable γ is the uptake coefficient (i.e., the fraction of collisions leading to reaction), V is the volume of the Knudsen cell (cm^3), R is the gas constant (kg m^2 mol^{-1} s^{-2} K^{-1}), T is the absolute temperature (K), and M is the molar mass of BA (kg mol^{-1}). Since values of V (691 cm^3), R, T (296 K), and M (7.3×10^{-2} kg mol^{-1}) were the same for all experiments, only γ and A_{surf} depend on a given experiment. For example, using average values from Table 5-1, k_r was calculated for malonic acid (C3) to be $k_r = 14$ s^{-1} (using $\gamma = 0.65$, $A_{surf} = 2.0$ cm^2, $[BA]_0 = 2.9 \times 10^{11}$ molecules cm^{-3}) and for succinic acid (C4) $k_r = 3.8 \times 10^{-2}$ s^{-1} (using $\gamma = 1.7 \times 10^{-4}$, $A_{surf} =$ 21.3 cm^2, $[BA]_0$ 4.9×10^{11} molecules cm^{-3}).

The absolute steady–state number of amine molecules when the Knudsen cell lid is raised (N_r) can be calculated from experimental data using Equation 5.3,

$$N_r = V[BA]_0 \left(\frac{I_r}{I_0}\right) \quad \textbf{5.3}$$

in which the initial amine concentration before the lid is opened, $[BA]_0$, is reduced by the fractional change in the amine signal once the lid is raised (I_r/I_0). With values of k_r and N_r, and a reasonable estimate of S_0, Equation 5.1 can be solved for k', the first-order rate constant for reactive site loss. If surface saturation were to occur, then the reactive site density must decay with time as $S_t = S_0 e^{-k't}$. It follows then, that the reciprocal of k', solved from Equation 5.1 gives the lifetime of reactive sites, τ (s). For representative experiments, we obtain $\tau = 0.3$ s for malonic acid (C3) and $\tau = 145$ s for succinic acid (C4). However, malonic acid (C3) did not show signs of saturation over many minutes of uptake at concentrations of 10^{11} molecules cm^{-3} (Figure 5-1), suggesting that more than the surface is available for reaction. With succinic acid (C4), saturation is observed after the first 10 minutes when the lid is opened for a second time. Similar conclusions apply for the rest of the diacids. For comparison, the uptake of amines onto solid ammonium sulfate, bisulfate, nitrate, and chloride salts have been reported to show signs of surface saturation.[206] A limitation on the availability of reactive species at surfaces is also consistent with a size dependence for the replacement of dimethylamine on ammonium bisulfate clusters, where displacement of the ammonium ions from the clusters became more difficult as cluster size increased.[207]

A possible explanation may lie in the nature of the surface formed upon reaction. The interaction of a gas with a solid is initially with the surface layer. If the reaction is restricted to

the surface, passivation occurs when the surface becomes covered with the solid product, effectively shutting down the reaction. However, reaction of the surface layer disrupts it and makes it more disordered. This can allow penetration of incoming gas molecules deeper into the crystal structure. Note also that if surface saturation occurs, the calculated value of the uptake coefficient would be expected to decrease with time. The time for surface saturation would be large at low concentrations and smaller for higher concentrations.

As shown in Figure 5-2, odd carbon diacids have much larger uptake coefficients than even carbon diacids. Furthermore, within each series (odd or even carbon numbers), the uptake coefficient decreases with increasing chain length. Previous DART–MS (direct analysis in real time mass spectrometry) studies[186] did not find detectable amounts of amines on the surfaces of C4 and C6 diacids, consistent with only a few surface layers being available for reaction. The observations of Zhao et al.[186] are also consistent with greater incorporation of the amines into the odd carbon diacid particles, with a trend to decreasing incorporation as the chain lengths increased.

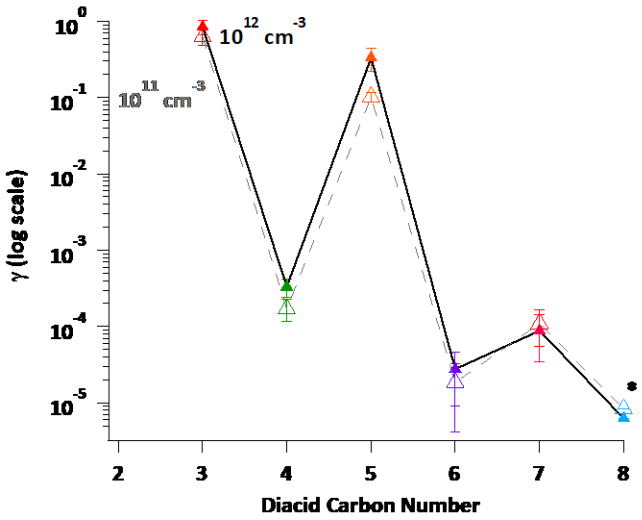

Figure 5-2. Summary of initial uptake coefficients, γ, for BA on C3–C8 diacids. Dashed lines are for BA concentrations of 10^{11} molecules cm^{-3} and solid lines are for 10^{12} molecules cm^{-3}. Error bars represent a propagation of errors (2σ). *Uptake coefficients for C8 represent an upper limit.

Both even and odd carbon diacids form intramolecular chains bound end–to–end by symmetric hydrogen bonds formed between –COOH end groups. Adjacent chains maintain the crystal structure due to dispersion forces between the methylene groups of the carbon chain as shown in Figure 5-3.[138] The decrease in uptake coefficient with increasing chain length within each series is consistent with greater diacid crystal stability due to increased dispersion forces,[138] making it more difficult to disrupt the surface in order to penetrate and react with the crystal lattice, thus leading to less reaction and lower effective uptake coefficients. Malonic acid (C3) has the shortest chain and hence smallest dispersion forces; in addition, its crystal structure is triclinic whereas all other diacids are monoclinic,[138] which may change its reactivity compared to the larger diacids.

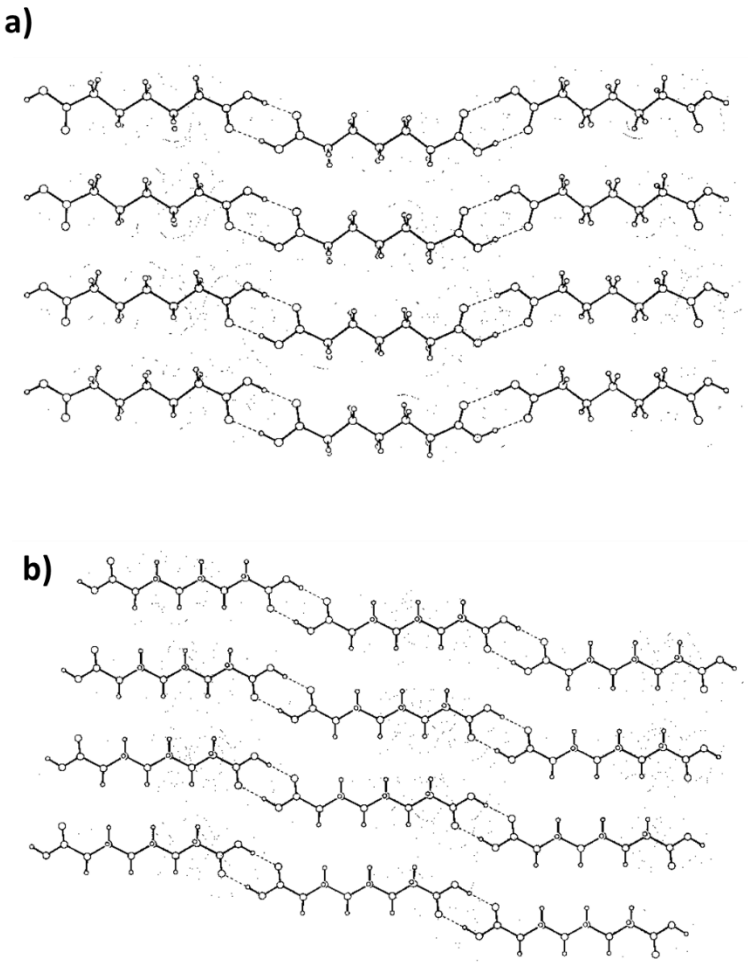

Figure 5-3. Arrangement of diacid lattice as reported by Thalladi et al.[138] for a) pimelic acid (C7) and b) suberic acid (C8). Chains are linked end–to–end via hydrogen bonding between –COOH groups and intramolecular chains are held together via dispersion forces between methylene groups. The odd carbon diacids have a twisted conformation and more torsional strain than the even carbon diacids.

Odd–even carbon alternations for diacids have been observed in physical properties such as vapor pressure,[135-137] melting point,[138] and solubility.[139, 140] One possibility for the increased reactivity of odd carbon diacids is the arrangement and stability of the crystal lattice. The odd carbon diacids adopt a trapezoidal arrangement due to the twisted conformation and torsional strain resulting from packing.[138] Even carbon diacids are offset to minimize interactions between

the carboxyl groups and are not twisted, resulting in a more stable parallelogram conformation.[138] These arrangements result in odd carbon diacid lattices having larger spacing in between the diacid chains and being less stable than the even carbon diacid lattices. As a result of the larger spacing, water molecules can more easily disrupt the packing structure of odd carbon diacids, which has been proposed to explain their higher aqueous solubility.[139] A similar effect was seen in their solubility in organic solvents.[140] Thus, butylamine may be able to disrupt the odd carbon lattices in an analogous manner, resulting in the higher reactivity of the odd carbon diacids.

Another contributing factor may be the orientation and thus the availability of the –COOH groups on the surface. Ruehl et al.[197] proposed that the orientation of diacids on the surface of aqueous ammonium sulfate particles depended on their structure, with the odd carbon diacids having one –COOH group pointing outside the particle while even carbon diacids have both –COOH groups buried inside the liquid interface. However, these orientations correspond to aqueous particles and the surface structure may not be the same for solid particles.

Finally, the higher uptake coefficients for the odd carbon diacids may be due to the nature of the aminium salts formed during reaction. Salts formed from amines and *mono*carboxylic acids have been shown to exist as viscous ionic liquids (ILs) at room temperature.[184] However, aminium *di*carboxylate salts formed from methyl- dimethyl- and trimethylamine with succinic (C4), adipic (C6), and azelaic (C9) acids were solids.[184] To test for the possible formation of ILs on the surface of the *di*carboxylic acid in the present experiments, butylaminium salts were synthesized from evaporated aqueous solutions of BA and C3–C8 diacids with 1:1 and 2:1 molar

ratios. Figure 5-4a shows that malonic (C3), glutaric (C5), and pimelic (C7) acids all form viscous liquids at room temperature in 2:1 BA molar ratios of the diacid. For 1:1 amine:diacid molar ratios, all three odd carbon diacid mixtures still form viscous liquids (Figure 5-4c), although pimelic acid (C7) solidified after several days. Given the ionic nature of the reaction products, these can be considered ionic liquids.[208, 209]

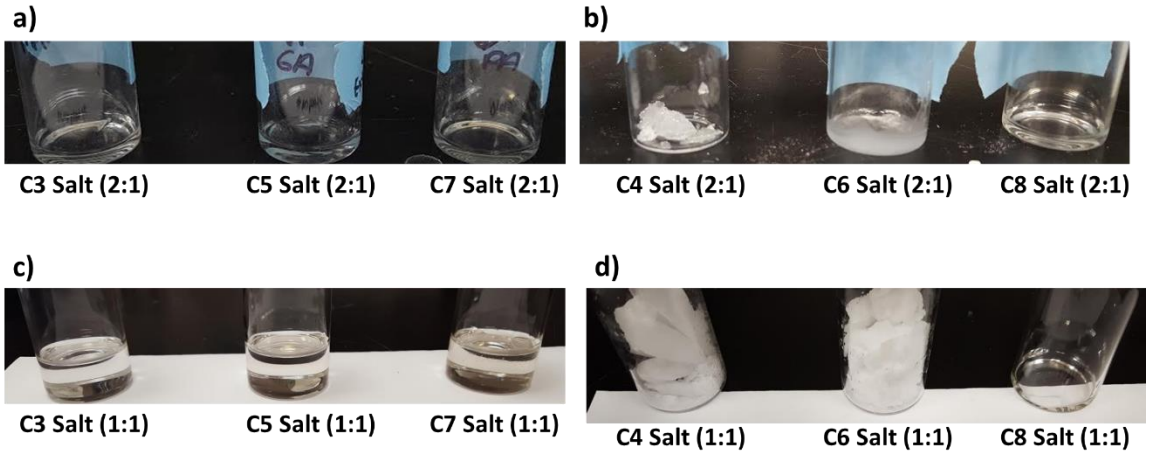

Figure 5-4. Formation of liquid and solid salts from aqueous mixtures of *n*-butylamine and diacids. 2:1 Butylaminium salts for a) odd carbon diacids and b) even carbon diacids. 1:1 Butylaminium salts for c) odd carbon diacids and d) even carbon diacids.

Measured viscosities for the mixtures from odd carbon diacids are reported in Table 5-2. For the 1:1 mixtures, the longer the diacid chain, the higher the measured viscosity. The trend is not continuous for the 2:1 mixtures but the viscosity for the C3 diacid is significantly smaller than for the C5 and C7 diacids. These observations are consistent with previous studies showing higher viscosities for longer carboxylate ions in ammonium–based ionic liquids.[208, 209] If the gas–solid reactions form an ionic liquid layer on the surface of these odd carbon diacids in the Knudsen cell, then continued uptake of the amine occurs into a liquid rather than with the surface

of a solid. In this case, the underlying diacid may dissolve into the liquid layer, allowing for continuous reaction on one sample without saturation.

Table 5-2. Measured viscosities (μ) and densities (ρ_f) for 2:1 and 1:1 amine:diacid mixtures.

	2:1		1:1	
n-butylamine/diacid mixture	μ (Pa·s) ± 2σ	ρ_f (units of 10^3 kg m^{-3})	μ (Pa·s) ± 2σ	ρ_f (units of 10^3 kg m^{-3})
Malonic (C3)	11 ± 0.6	1.1	5 ± 0.2	1.2
Glutaric (C5)	39 ± 6	1.1	9 ± 0.6	1.1
Pimelic (C7)	24 ± 4	1.0	12 ± 1.6	1.1

This hypothesis was further tested by exposing a sample of malonic acid (C3) crystals to a high concentration of BA in the vacuum manifold. Figure 5-5 shows malonic acid (C3) crystals under vacuum before (Figure 5-5a) and after (Figure 5-5b) exposure to ~ 41 Torr of BA. The reaction appears to have converted the surface of the malonic acid (C3) crystals into a viscous material. Note that although suberic acid (C8) did not form a solid salt from aqueous solutions (Figure 5-4b, d) as did the other even carbon diacids, the uptake coefficient was too small to be measured (Table 5-2). When a sample of suberic acid (C8) was exposed to ~ 29 Torr of BA, a similar phase change was observed (Figure 5-5c, d), consistent with the aqueous mixture of amines and diacid remaining liquid. Given that suberic acid (C8) is expected to have the strongest intramolecular dispersion forces and hence the most stable crystal structure of the diacids used in these experiments, the amine may not have enough time to penetrate and disrupt the diacid chains to form the ionic liquid layer under the timescale and amine concentrations of the Knudsen cell experiments. This leads to a small measured uptake coefficient for BA on suberic acid (C8).

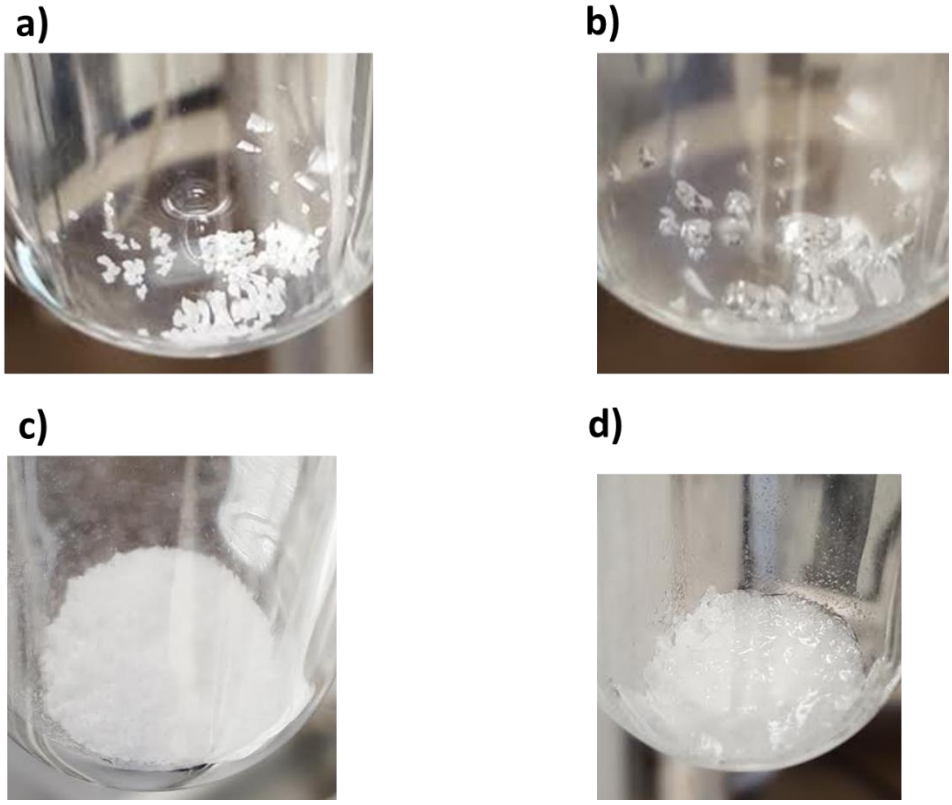

Figure 5-5. Malonic acid (C3) a) before and b) after exposure to 41 Torr pure BA and suberic acid (C8) d) before and d) after exposure to 29 Torr pure BA via vacuum manifold.

As shown in Figure 5-4, mixtures of both 1:1 and 2:1 molar ratios of the C4 and C6 diacids with BA formed solid salts rather than ionic liquids. The observed uptake coefficient of BA on even carbon diacids in Figure 5-1 is far less compared to the odd carbon diacids (Table 5-1). This is expected if the even carbon diacid salts are solids, while the odd carbon diacid salts are ionic liquids. In the case of solids, the initial reaction of the gas with the surface layer disrupts the packing, leading to a highly defective and more porous surface. The gas then continues to penetrate the surface layer slowly and reacts with underlying layers. The gas–solid reaction described earlier was directed towards reactions that converted gas–solid reactants to a

solid product. However, it appears that the products of the reactions of the odd carbon diacids are ionic liquids rather than solid salts. This means that once some number of surface layers have reacted, the surface is no longer a solid, and uptake of the amine is into a liquid layer where diffusion is faster. The measured uptake coefficient will then depend on the true uptake coefficient of the amine onto the liquid, the viscosity of the liquid layer, the dissolution of the underlying solid diacid, and the kinetics of the acid–base reaction in ionic liquid layer.

Uptake measurements were also carried out in the Knudsen cell at higher BA concentrations, $(3 – 5) \times 10^{12}$ molecules cm^{-3}. There is a general trend to higher initial effective uptake coefficients at the higher amine concentrations (Table 5-1). The results were particularly evident for succinic (C4) and glutaric (C5) acids. In these two cases, the uptake profiles also show signs of surface saturation (Figure 5-6, Figure 5-7a). The higher uptake coefficients at higher amine concentrations are unexpected, in that for typical gas–solid reactions, higher concentrations generally lead to smaller measured uptake coefficients as the surface becomes passivated more quickly. It may be that in the case of succinic (C4) and adipic (C6) acids (Table 5-1), which do not form ionic liquids on our time scales, there is a greater disruption of the surface and penetration of the amine into the salt at the higher amine concentrations. This would effectively expose more reactive salt for reaction, leading to higher effective uptake coefficients.

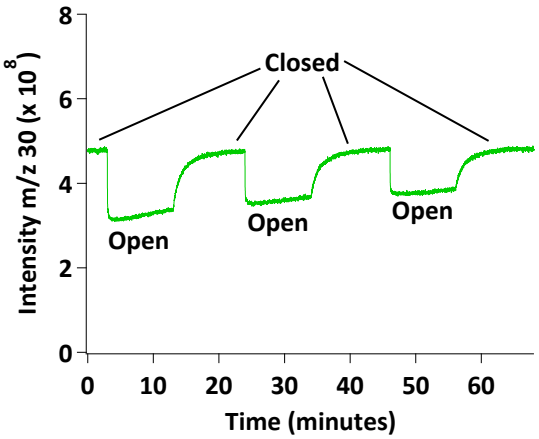

Figure 5-6. Uptake of 5×10^{12} molecules cm^{-3} BA on succinic acid (C4) (A_{surf} ~21 cm^2).

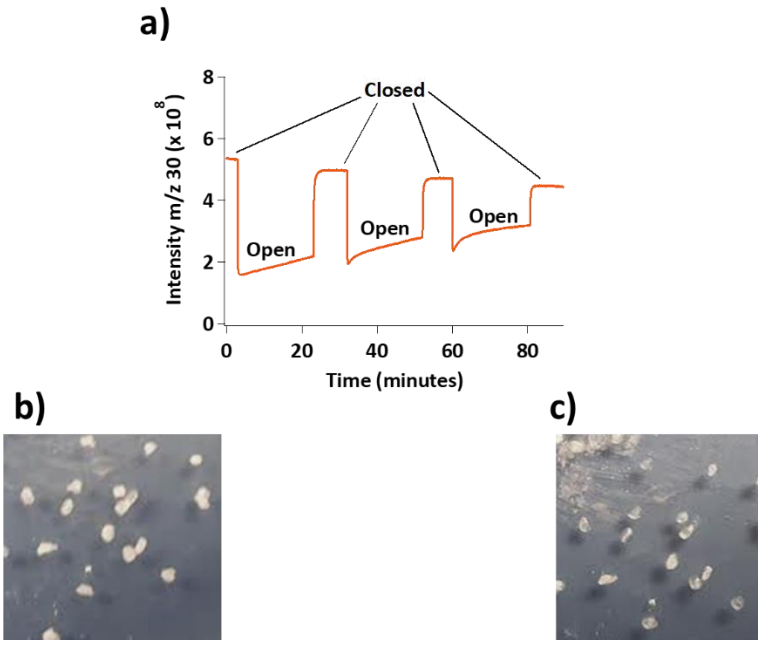

Figure 5-7. a) Uptake profile for 4×10^{12} molecules cm^{-3} BA on glutaric acid (C5) (A_{surf} ~ 2 cm^2). Glutaric acid (C5) b) before and c) after reaction in the Knudsen cell with a total exposure time of 60 minutes.

In addition to surface saturation, there was also a change in the appearance of the glutaric acid (C5) crystals before and after exposure to the amine (Figure 5-7b, c), with the crystal

surface appearing more liquid–like at higher amine concentrations. The higher concentration of amine could be forcing the formation of the surface IL layer in the glutaric acid (C5) reaction at a faster rate than at the lower concentrations. If the rate at which the underlying diacid is dissolving into the liquid layer is not sufficiently fast to replenish the diacid compared to the rate at which the amine molecules are being taken up, surface saturation could become evident.

The kinetic multi–layer model of aerosol surface and bulk chemistry (KM–SUB) was utilized by Dr. Pascale Lakey and Professor Manabu Shiraiwa to gain a molecular level understanding of the BA–diacid system.[210] KM–SUB successfully reproduces the trend in decreasing uptake coefficients with increasing BA concentrations from $(3 – 88) \times 10^{11}$ molecules cm^{-3} as shown in Figure 5-8. The model predicts that as the amine concentration increases, reactive uptake becomes limited by bulk diffusion of the underlying diacid to the surface. The lack of change in uptake coefficients at the low amine concentration imply that rapid replenishment of the underlying diacid allows for continuous uptake into the reactive layer.

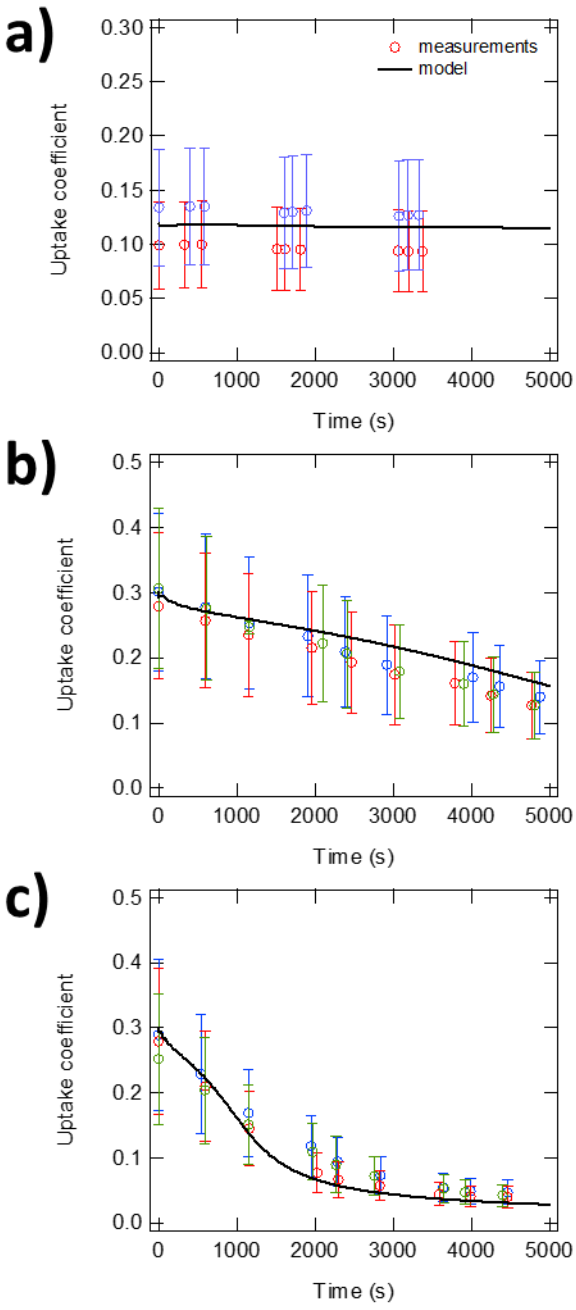

Figure 5-8. Uptake coefficients as a function of time for a) 3×10^{11} molecules cm^{-3}, b) 3.9×10^{12} molecules cm^{-3}, and c) 8.8×10^{12} molecules cm^{-3} BA on glutaric acid (C5) symbols represent experimental values, solid line is the KM–SUB predicted uptake coefficients. The different colors of the symbols represent repeats of the experiments. Model calculations performed by Dr. Pascale Lakey and Professor Manabu Shiraiwa. Adapted from Fairhurst et al.[210]

In addition to providing insights into the reaction on a molecular level, KM–SUB can also predict values that cannot be measured experimentally. Figure 5-9a and b show the temporal evolution of concentrations of glutaric acid (C5) and the products resulting from reaction of BA as predicted by KM–SUB. On the timescale of 5000 seconds, concentrations of glutaric acid (C5) decrease and product concentrations increase significantly. The depth of the product layer is roughly 10 μm. In contrast, Figure 5-9c and d show the evolution of adipic acid (C6) and the products resulting from reaction with BA. Only the first 0.2 μm of adipic acid (C6) is reacted, leading to a small amount of product formed. This is consistent with experimental observations of the uptake coefficient being orders of magnitude lower than that for glutaric acid (C5) (Table 5-1) and that aqueous mixtures of BA with adipic acid (C6) forms a solid salt (Figure 5-4).

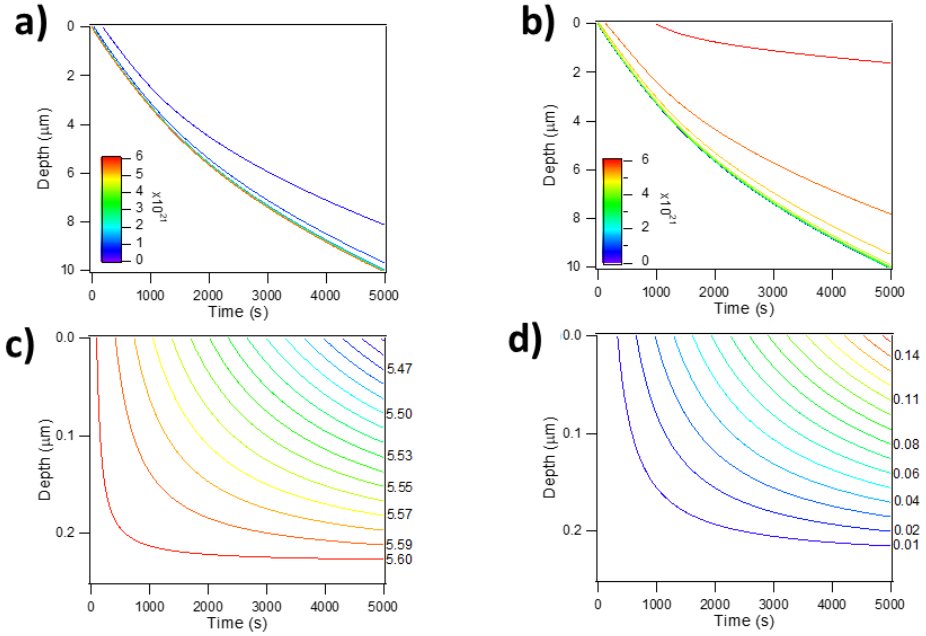

Figure 5-9. Evolution of concentrations of a) glutaric acid (C5) and b) product concentrations after exposure to 8.8×10^{12} molecules cm^{-3} BA (units of contour lines are cm^{-3}). Evolution of concentrations of c) adipic acid (C6) and d) reactant product concentrations after exposure to 4.7×10^{12} molecules cm^{-3} BA (scales of contour lines are 10^{21} cm^{-3}). Model calculations performed by Dr. Pascale Lakey and Professor Manabu Shiraiwa. Figure adapted from Fairhurst et al.[210]

II. Conclusions for BA on Diacids

The uptake of butylamine onto low molecular weight diacids (C3 – C8) depends on the diacid, with the uptake coefficients being larger for odd carbon diacids than for even carbon homologs. Uptake coefficients also decrease with increasing carbon number in each series. Although the uptake coefficient for malonic acid (C3) approaches unity, the other coefficients are smaller. This may have implications for how atmospheric models treat uptake, for example, even for simple acid–base reactions, there is not a "one size fits all" to model the uptake of an amine onto the different diacids, which these reactions have been proposed to play a role in atmospheric particle growth.[26, 211]

The hypothesis that reaction between gaseous BA and solid odd carbon diacids produces ionic liquids in the Knudsen cell is supported by the formation of liquid salts from evaporated 2:1 and 1:1 aqueous mixtures of BA and the diacids (Figure 5-4). It is further supported by the observed liquefaction of the surfaces of solid malonic (C3) (Figure 5-5) and glutaric (C5) (Figure 5-7c) acids when exposed to high concentrations of gaseous BA. The lack of surface saturation may be due to the formation of an ionic liquid layer which dissolves the underlying diacid, thus providing a continuous supply of diacid as the amine is taken up from the gas phase. This picture of the gas–solid interactions developed from the experimental data is supported by quantitative modeling using the KM–SUB model which incorporates diffusion of viscous reactants and products through multiple surface layers. Further work is needed to explore reactions of amines of varying structures and properties on the diacids to determine if size and available sites for hydrogen bond formation, for example, affect uptake.

III. Uptake of Other Amines and Ammonia onto C3 – C7 Diacids

Based on studies with BA on solid diacids, it was shown that reaction of the amine depends on whether the diacid has an even or odd number of carbons. The odd–even alternation was also evident in the propensity of the amine and diacid to form ionic liquids. The next goal of the project was to determine what effect the structure of the amine has on this acid–base reaction.

Figure 5-10 shows typical data for the uptake of amines and ammonia on malonic (C3), succinic (C4) and glutaric (C5) acids at amine concentrations of $(3 – 5) \times 10^{11}$ molecules cm^{-3}. No uptake was observed on a clean, halocarbon wax coated sample holder. Data for adipic (C6)

and pimelic (C7) acids consistently yielded very small decreases in intensities when the lid was open so that values for γ were the same order of magnitude as the error, 2σ, and thus were treated as upper limits for the uptake coefficient. The same is true of TMA uptake on succinic acid (C4). Tables 5-3 to 5-7 summarize the experimental conditions for all base–acid combinations studied here.

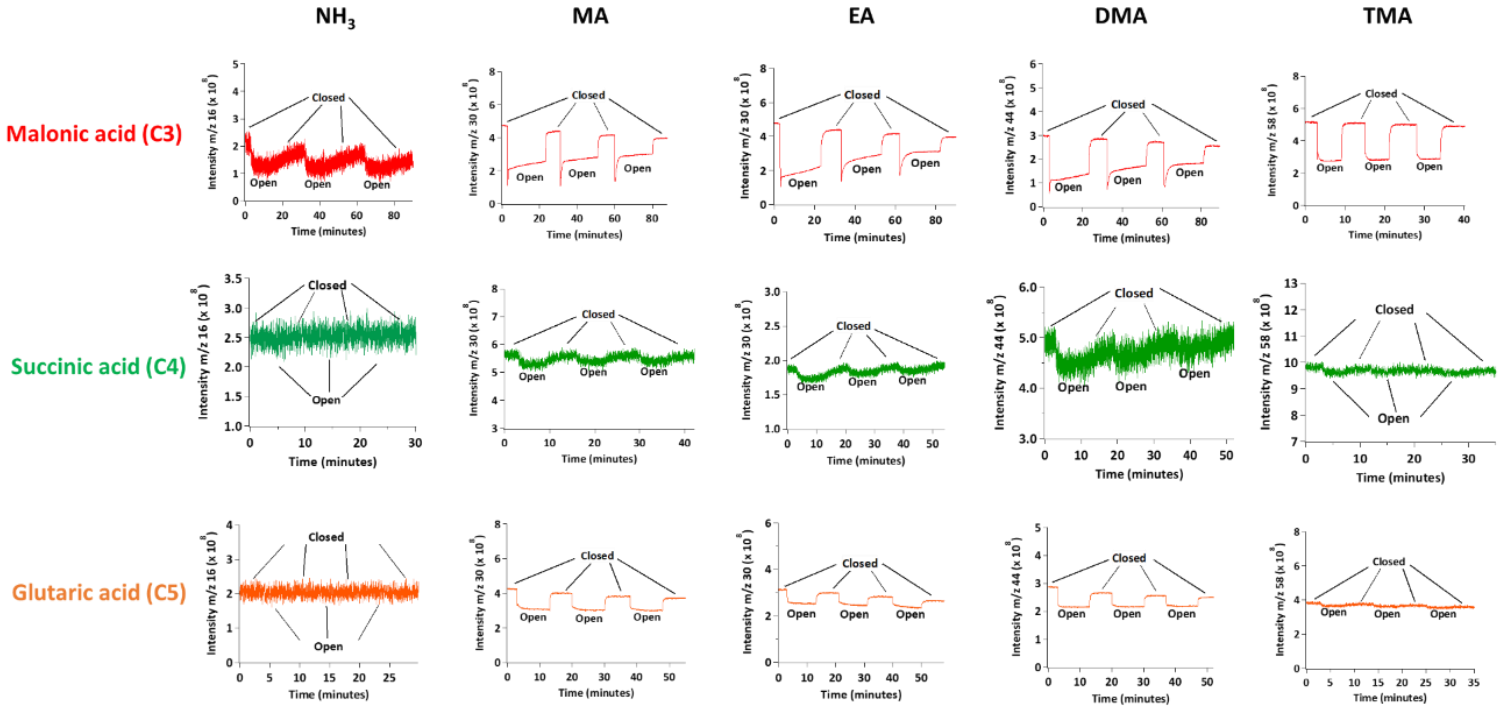

Figure 5-10. Uptake of ammonia (NH_3) and amines at concentrations of $(3 – 5) \times 10^{11}$ molec cm^{-3} on malonic acid (C3), succinic acid (C4) and glutaric acid (C5). The succinic acid surface area was 20 cm^2. For all of the malonic acid runs except NH_3, A_{surf} = 2 cm^2 ; for NH_3, A_{surf} = 9 cm^2. For glutaric acid, A_{surf} = 2 cm^2 for MA, EA and DMA, 14 cm^2 for NH_3 and 16 cm^2 for TMA. Note the expanded scales used to show the succinic acid (C4) data. No uptake was observed on adipic (C6) or pimelic (C7) acids. For all primary and secondary amines on malonic (C3) and glutaric (C5) acids, sensitivity on the lock–in amplifier was 100 mV. For all amines (except for EA) and ammonia on succinic acid (C4) and TMA on glutaric acid (C5) sensitivity on the lock–in amplifier was increased to 3 mV. For EA on succinic acid (C4), the sensitivity was 10 mV.

Table 5-3. Uptake coefficients (γ) for ammonia and amines on malonic acid (C3).

Gas phase species	Surface area ± 2σ [a] (cm^2)	$[Gas]_0 \pm 2\sigma$ [b] (units of 10^{12} molecules cm^{-3})	γ_0 [d] ± 2σ [e]	$\gamma_{0,ss}$ [f] ± 2σ [e]	γ_{ss} [g] ± 2σ [e]
NH_3	9.2 ± 4.6	0.44 ± 0.04 (3)	–	–	$(2.1 \pm 1.2) \times 10^{-3}$
	9.4 ± 4.7	4.0 ± 0.4 (3)	–	–	$(8.8 \pm 2.8) \times 10^{-3}$ [h]
MA	1.7 ± 0.7	0.42 ± 0.07 (4)	0.58 ± 0.21	0.20 ± 0.03	–
	4.3 ± 1.8	0.42 ± 0.09 (4)	0.26 ± 0.04	0.25 ± 0.04	–
	1.6 ± 0.8	4.5 ± 0.4 (4)	0.48 ± 0.10	0.11 ± 0.01	–
	4.1 ± 2.0	4.4 ± 1.4 (3)	0.24 ± 0.10	0.11 ± 0.02	–
EA	1.8 ± 0.7	0.44 ± 0.10 (5)	0.85 ± 0.26	0.39 ± 0.16	–
	4.0 ± 2.0	0.42 ± 0.13 (3)	0.44 ± 0.18		0.38 ± 0.10 [h]
	1.8 ± 0.8	4.7 ± 0.4 (4)	0.99 ± 0.08	0.32 ± 0.09	–
	4.2 ± 1.5	4.5 ± 1.3 (6)	0.55 ± 0.45	0.35 ± 0.05	–
DMA	1.8 ± 0.9	0.42 ± 0.07 (3)	0.75 ± 0.19	0.30 ± 0.03	–
	4.2 ± 2.1	0.40 ± 0.08 (3)	0.43 ± 0.27	0.28 ± 0.05	–
	1.8 ± 0.8	4.2 ± 0.5 (4)	0.78 ± 0.17	0.21 ± 0.04	–
	4.3 ± 2.2	4.5 ± 0.4 (3)	0.48 ± 0.05	0.28 ± 0.04	–
TMA	1.7 ± 0.9	0.37 ± 0.04 (3)	–	–	0.14 ± 0.04
	4.0 ± 2.0	0.38 [c] (3)	–	–	0.13 ± 0.03
	1.7 ± 0.7	3.0 ± 0.6 (4)	–	–	0.13 ± 0.09
	4.1 ± 2.0	2.8 ± 0.4 (3)	–	–	0.15 ± 0.02

[a] Standard deviations represent 2σ for the distribution of crystal sizes in each sample. Orifice areas for all experiments were 0.31 cm^2, except for those with NH_3 which were 0.015 cm^2.
[b] Standard deviations represent 2σ for the variation in amine concentration. Number of experiments given in parentheses. [c] Amine concentration for all samples was the same.
[d] Average of the rapid, initial uptake for the first trial for all samples. [e] Errors are reported as two sample standard deviations of the average of replicate experiments. [f] Uptake coefficients are extrapolated as described in the text for the first trial for all samples. [g] Uptake is constant with time as indicated in Figure 3b. Averages are of repeated trials. [h] Uptake coefficients were steady-state for each trial, however they decreased with each increasing trial, and thus represent an average of the first trial for all samples.

Table 5-4. Uptake coefficients (γ) for ammonia and amines on succinic acid (C4).

Gas phase species	Surface area ± 2σ [a] (cm^2)	$[Gas]_0$ ± 2σ [b] (units of 10^{12} molecules cm^{-3})	γ_{ss} [d] ± 2σ [e]
NH_3	18.9 ± 5.7	0.42 [c] (3)	$\leq 2 \times 10^{-6}$
	19.4 ± 5.8	3.8 ± 0.4 (3)	$\leq 9 \times 10^{-6}$
MA	19.6 ± 5.9	0.41 ± 0.1 (2)	$(6.4 \pm 1.9) \times 10^{-5}$
	19.8 ± 6.0	4.2 ± 1.1 (3)	$(4.0 \pm 0.4) \times 10^{-5}$
EA	18.6 ± 5.6	0.37 ± 0.04 (3)	$(6.7 \pm 2.8) \times 10^{-5}$
	18.9 ± 5.7	3.8 ± 1.0 (3)	$(6.5 \pm 0.7) \times 10^{-5}$
DMA	19.1 ± 5.7	0.43 ± 0.07 (3)	$(1.0 \pm 0.6) \times 10^{-4}$
	19.5 ± 5.9	4.5 ± 0.4 (3)	$(0.45 \pm 0.02) \times 10^{-4}$
TMA	19.4 ± 5.8	0.38 ± 0.04 (3)	$\leq 2 \times 10^{-5}$
	20.1 ± 7.4	4.6 [c] (2)	$\leq 1 \times 10^{-5}$

[a] Standard deviations represent 2σ for the distribution of crystal sizes in each sample. Orifice areas were 0.015 cm^2 for all experiments. [b] Standard deviations represent 2σ for the variation in amine concentration. Number of experiments given in parentheses. [c] Amine concentration for all samples was constant. [d] Uptake coefficients decreased with increasing numbers of trials; these values represent the average of the first trial for all samples. [e] Errors are reported as two sample standard deviations of the average of replicate experiments.

Table 5-5. Uptake coefficients (γ) for ammonia and amines on glutaric acid (C5).

Gas phase species	Surface area ± 2σ [a] (cm^2)	$[Gas]_0 \pm 2\sigma$ [b] (units of 10^{12} molecules cm^{-3})	γ_0 [c] ± 2σ [d]	γ_{ss} [e] ± 2σ [d]
NH_3	14.2 ± 6.6	0.46 ± 0.04 (3)	–	$\leq 3 \times 10^{-5}$
	13.9 ± 6.4	3.9 ± 0.01(3)	–	$\leq 2 \times 10^{-5}$
MA	1.8 ± 0.7	0.45 ± 0.1 (4)	–	0.066 ± 0.025
	4.5 ± 1.8	0.45 ± 0.05 (4)	–	0.046 ± 0.012
	1.9 ± 0.8	4.1 ± 1.1 (4)	0.083 ± 0.025	–
	4.4 ± 2.0	5.1 ± 0.8 (3)	0.085 ± 0.012	–
EA	1.8 ± 0.8	0.42 ± 0.07 (3)	–	0.056 ± 0.030
	4.4 ± 2.0	0.50 ± 0.10 (3)	–	0.056 ± 0.022
	1.9 ± 0.9	4.0 ± 1.0 (4)	0.12 ± 0.03	–
	4.6 ± 2.1	3.9 ± 0.7 (3)	0.10 ± 0.02	–
DMA	1.9 ± 0.9	0.45 ± 0.04 (3)	–	0.038 ± 0.022
	4.5 ± 2.1	0.47 ± 0.04 (3)	–	0.027 ± 0.006
	1.8 ± 0.8	4.3 ± 0.8 (3)	0.10 ± 0.01	–
	4.3 ± 2.0	4.3 ± 0.4 (3)	0.073 ± 0.006	–
TMA	16.6 ± 7.8	0.33 ± 0.09 (3)	–	$(4.2 \pm 1.1) \times 10^{-5}$ [f]
	16.1 ± 7.5	5.1 ± 1.0 (3)	–	$(6.2 \pm 3.1) \times 10^{-5}$ [f]

[a] Standard deviations represent 2σ for the distribution of crystal sizes in each sample. Orifice areas for all experiments were 0.31 cm^2, except for those with NH_3 and TMA which were 0.015 cm^2. [b] Standard deviations represent 2σ for the variation in amine concentration for those runs. Number of experiments are given in parentheses. [c] Uptake coefficients decreased with time, these values represent the average of the initial uptake region for the first trial for all samples. [d] Errors are reported as two sample standard deviations of the average of replicate experiments. [e] Uptake is representative of a steady-state region as indicated in Figure 3b. [f] Uptake coefficients are for a steady state, but decreased with each trial; these values represent the average of the first trial for all samples.

Table 5-6. Uptake coefficients (γ) for ammonia and amines on adipic acid (C6).

Gas phase species	Surface area ± 2σ [a] (cm^2)	$[Gas]_0 \pm 2\sigma$ [b] (units of 10^{12} molecules cm^{-3})	γ_{ss}
NH_3	29.2 ± 18.6	0.48 ± 0.07 (3)	$\leq 6 \times 10^{-6}$
	27.5 ± 17.5	4.0 ± 0.4 (3)	$\leq 3 \times 10^{-6}$
MA	31.3 ± 19.9	0.40 ± 0.1 (3)	$\leq 5 \times 10^{-6}$
	28.7 ± 18.2	4.2 ± 0.6 (3)	$\leq 4 \times 10^{-6}$
EA	28.6 ± 18.1	0.39 ± 0.07 (3)	$\leq 1 \times 10^{-5}$
	28.2 ± 17.9	4.2 ± 1.3 (3)	$\leq 7 \times 10^{-6}$
DMA	28.0 ± 17.8	0.34 ± 0.04 (3)	$\leq 5 \times 10^{-6}$
	27.3 ± 17.3	4.3 ± 0.4 (3)	$\leq 5 \times 10^{-6}$
TMA	30.3 ± 19.3	0.40 ± 0.08 (3)	$\leq 3 \times 10^{-6}$
	30.2 ± 16.6	3.8 ± 1.6 (4)	$\leq 5 \times 10^{-6}$

[a] Standard deviations represent 2σ for the distribution of crystal sizes in each sample. Orifice areas were 0.015 cm^2 for all experiments. [b] Standard deviations represent 2σ for the variation in amine concentration for those runs. Number of experiments given in parentheses.

Table 5-7. Uptake coefficients for ammonia and amines on pimelic acid (C7).

Gas phase species	Surface area ± 2σ [a] (cm^2)	$[Gas]_0 \pm 2\sigma$ [b] (units of 10^{12} molecules cm^{-3})	γ_{ss}
NH_3	9.2 ± 5.0	0.43 ± 0.07 (3)	$\leq 4 \times 10^{-5}$
	9.1 ± 6.1	4.1 ± 0.5 (2)	$\leq 8 \times 10^{-6}$
MA	9.0 ± 4.9	0.41 ± 0.08 (3)	$\leq 2 \times 10^{-5}$
	9.3 ± 5.1	3.7 ± 0.4 (3)	$\leq 2 \times 10^{-5}$
EA	9.1 ± 4.9	0.42 ± 0.13 (3)	$\leq 2 \times 10^{-5}$
	9.2 ± 5.0	4.4 ± 0.8 (3)	$\leq 2 \times 10^{-5}$
DMA	9.1 ± 5.0	0.46 ± 0.07 (3)	$\leq 2 \times 10^{-5}$
	9.2 ± 5.0	4.5 ± 0.4 (3)	$\leq 9 \times 10^{-6}$
TMA	9.1 ± 6.0	0.44 ± 0.05 (2)	$\leq 1 \times 10^{-5}$
	9.2 ± 5.0	4.6 ± 1.0 (3)	$\leq 1 \times 10^{-5}$

[a] Standard deviations represent 2σ for the distribution of crystal sizes in each sample. Orifice areas were 0.015 cm^2 for all experiments. [b] Standard deviations represent 2σ for the variation in amine concentration for those runs. Number of experiments given in parentheses.

Different amine–diacid combinations showed varying time behaviors of the amine uptake. For example, uptake of MA, EA and DMA on malonic acid (C3) showed an initial, very rapid uptake that was not seen for the other diacids (Figure 5-10). This was followed by a slower, declining uptake. In order to quantify both the initial large uptake and that observed at longer times, the data for malonic acid (C3) were analyzed as illustrated schematically in Figure 5-11. Initial uptake coefficients, defined as γ_0, reflect the spike in the uptake at the shortest reaction times; note these may be lower limits as the time resolution of the measurements may not have been sufficiently high to capture the true minimum in I_r. To obtain the steady–state values of the uptake coefficients for malonic acid (C3), the linear portion of the signals that followed the spike were extrapolated back to the time at which the initial spike occurred, t_{spike} (Figure 5-11a), using a linear regression, These values are reported as $\gamma_{0,ss}$. For the rest of the diacids where no initial spike was observed, the steady–state uptake coefficient is defined as γ_{ss} (Figure 5-11b).

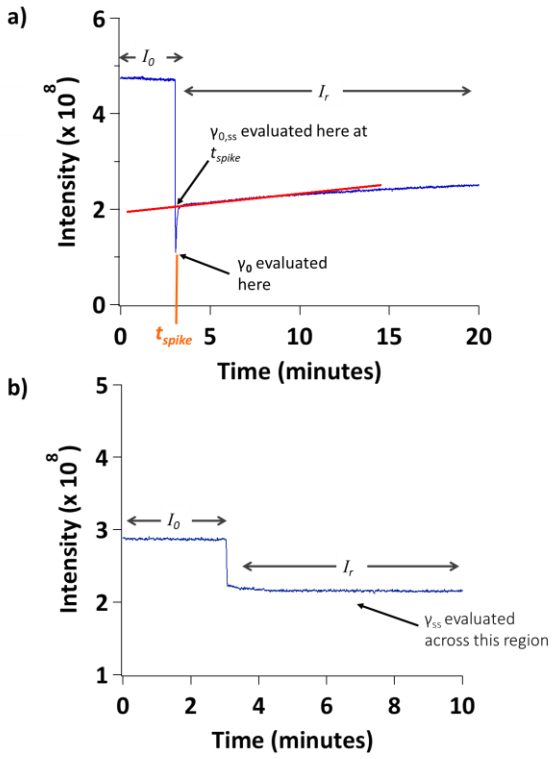

Figure 5-11. Schematic of uptake coefficients derived for a) amines on malonic acid (C3), and b) derivation of steady-state uptake coefficients for all other diacids**.**

Tables 5-3 to 5-7 summarize the measured uptake coefficients for each experimental condition for all base–acid combinations. Note that the uncertainties reported are determined by propagation of errors, and do not include possible systematic errors. As discussed above, the largest potential systematic error is in the available surface area which we estimate to be as much as a factor of two. Thus, uptake coefficients are considered significantly distinctive if they differ by more than a factor of two.

The values of the steady–state uptake coefficients for malonic (C3), succinic (C4) and glutaric (C5) acids that show measurable uptake is independent of the mass of the diacid used,

i.e., of the total surface area, as expected (Tables 5-3 to 5-5). This is not the case for the initial uptake coefficients, γ_0, for malonic acid (C3), where the values were smaller for the larger diacid mass (Table 5-3). Possible reasons for this are discussed below. Uptake coefficients for the most part are relatively insensitive to the amine concentration. The exception is glutaric acid (C5), where there is a trend to higher uptake coefficients at higher gas phase base concentration (Table 5-5).

Figure 5-12 summarizes the uptake coefficients as a function of carbon number for ammonia and each amine. As observed in the earlier studies of BA with diacids, all of the amines studied here exhibit an odd–even carbon trend in the uptake coefficients, with the values decreasing with increasing chain length and uptake coefficients for even carbon diacids are orders of magnitude smaller than those for odd carbon diacids. This behavior likely reflects the crystal structure of the even carbon diacids compared to the odd carbon compounds.[138] Solid diacids self–assemble end–to–end via hydrogen bonds to form infinite chains and adjacent elongated chains aggregate due to hydrophobic interactions between methylene chains. However, there is a difference in inter–chain packing between the even and odd carbon diacids in their crystal structure. Odd carbon diacids have their –COOH groups out of plane with the methylene chains leading to torsional strain on the carbon chains and higher energy conformations. This torsional strain also results in more space between chains. The combination of lower lattice stability and larger inter–chain spacing has been proposed to facilitate the penetration of water in between lattice chains, and thus contribute to a higher aqueous solubility for the odd carbon diacids.[139] A similar phenomenon is expected to allow the gas phase amines to exhibit greater penetration in the odd carbon diacids. In DART–MS (direct analysis in real

time mass spectrometry) studies of amine–reacted diacid particles using a flow reactor, the odd–even alternation was observed in the fraction of amine taken up into the diacid particles.[186] The amount of amine in the diacid particles also decreased with each increasing carbon number.

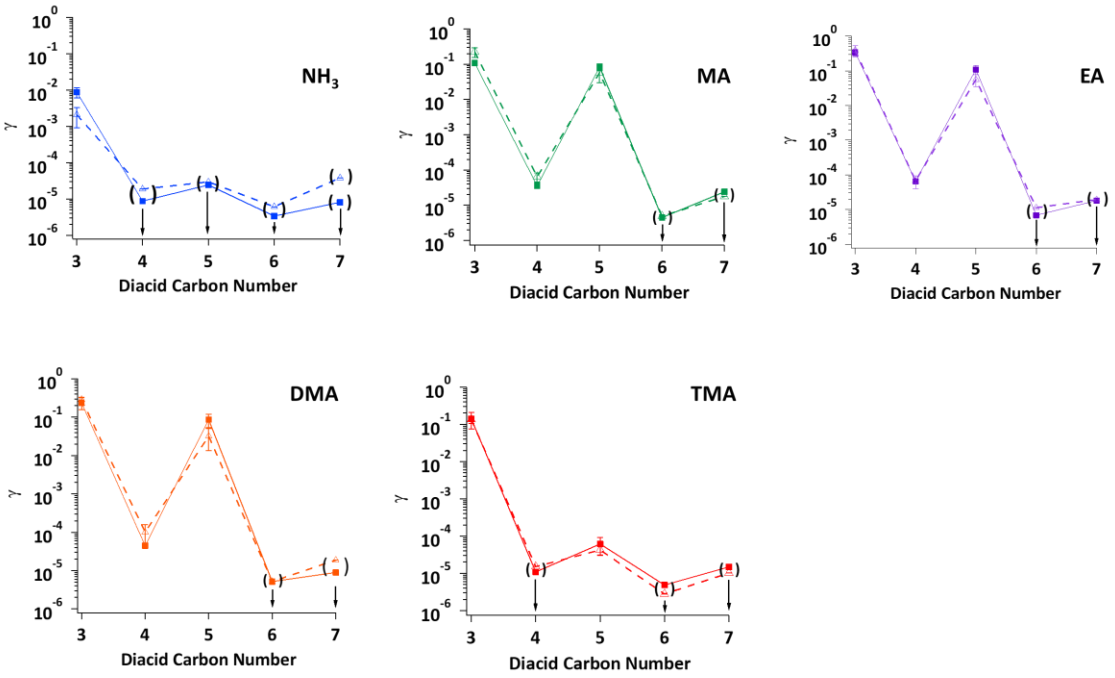

Figure 5-12. Summary of uptake coefficients (γ_{ss}) (± 2σ) for amines and ammonia on C3 – C7 solid diacids. Dashed lines are data at 10^{11} molecules cm^{-3} and solid lines are data at 10^{12} molecules cm^{-3}. Uptake coefficients for MA, EA and DMA on malonic acid (C3) are extrapolated uptake coefficients ($\gamma_{0,ss}$) as reported in Table 1. Values for glutaric acid (C5) at 10^{12} molecules cm^{-3} are γ_0 as reported in Table 5-5. Arrows and parentheses indicate an upper limit.

Malonic acid (C3) is unique in its crystal structure, in that it is the only triclinic structure of the diacids investigated here,[138, 204] has the least crystal symmetry[204] and the weakest hydrophobic interactions compared to the other diacids since there is only a single methylene group interacting between adjacent chains. The orientation of the –COOH groups is different from the rest of the diacid series, in that one acidic group lies roughly in plane with the carbon

chain, while the other is rotated about 90°. This orientation is in contrast to the other odd carbon diacids where there are two regions of symmetry: one along the carbon chain and one within the two –COOH groups.[204] These characteristics suggest that of all the diacids in this study, malonic acid (C3) has the loosest crystal packing, potentially the highest number of crystal defects, and at least one acidic group that might be more readily available for reaction. All these factors may increase its reactivity compared to the larger diacids.

In general, when an ammonia or amine molecule reacts with the diacid surface, the first step involves formation of a mono– ammonium or aminium carboxylate salt (molar ratio 1:1). This is expected to disrupt the crystal surface, making it more porous. This could effectively lead to reaction of many underlying layers of the diacid, not just the surface monolayer. As this occurs, the 1:1 salt can be converted to the dicarboxylate salt (molar ratio 2:1). If these top salt product layers are themselves solid, then surface passivation would be expected to set in as slow diffusion in the solid would limit the depth of penetration and reaction of the amine. This would manifest itself as a decrease in uptake coefficient over timescales that would depend on the magnitude of γ.

The reactions of the *even* carbon diacids fall into this solid product category. For example, as seen in the data for succinic acid (C4) in Figure 5-10, the uptake of MA, EA and DMA is small and all show evidence of surface passivation over the course of the experiments (i.e. initial uptake of the amine onto the diacid surface that decreases slightly within a single measurement and decreases for each subsequent exposure to the amine). Surface saturation times for MA, EA and DMA on succinic acid (C4) were calculated as described in detail

previously.[210] Briefly, the number of diacid molecules in a single unit cell can be calculated using the unit cell dimensions of the diacid. The initial number density of surface sites, S_0, can then be derived using the weighting factor, or the fraction of the surface area that is made up of acidic groups. The first order rate constant (k') for the amine reaction on the surface is derived using kinetic molecular theory, the reactive surface area and S_0. Assuming that the decay in surface sites follows first order kinetics, the decay in reactive sites can be expressed as $S_t = S_0 e^{-k't}$. Thus, the reciprocal of k' will give the $1/e$ lifetime of the reactive sites. The observation of surface saturation in Figure 5-10 for succinic acid (C4) is consistent with a calculated $1/e$ surface saturation time of ~ 5 min, using $\gamma_{ss} = 6.4 \times 10^{-5}$ for MA as an example.

No uptake of NH_3 was observed on succinic acid (C4). While a small change was observed in the TMA signal upon opening the lid (Figure 5-10), I_r was within experimental error of I_0 and as discussed above, only an upper limit for the uptake coefficient was therefore derived. The very small uptake of TMA is likely due to steric factors, where the highly branched amine structure minimizes penetration into the tightly packed first layers of the crystal lattice of the even carbon diacid. The lack of measurable uptake of NH_3 may reflect its lower basicity compared to the amines,[212, 213] which also is responsible for it having the lowest uptake coefficients compared to the amines across the diacid series. Lastly, there was no measurable uptake of NH_3 nor any uptake of the amines on adipic acid (C6) (Table 5-6). This is attributed to the stronger hydrophobic forces between the longer methylene chains of adipic acid (C6), which makes penetration of the amines into the crystal and disruption of the structure energetically less favorable.

In the previous studies of the reactions with BA on the *odd* carbon diacids, uptake of the amine continued at reaction times much longer than expected for the reaction of the gas with the surface layer of the diacids.[210] This was shown to be due to the formation of an ionic liquid (IL) layer that then provided a liquid film into which the gas phase amine and underlying diacid dissolved and reacted continuously.[210] Thus, the system became a multiphase gas–liquid–solid reaction, which did not lead to surface passivation as is usually the case with gas–solid reactions. Formation of ILs for the C3, C5 and C7 diacid reactions was confirmed by mixing aqueous solutions of the acid and base, and evaporating off the water to determine if a solid or liquid salt remained.[210]

In the systems under study here, uptake also continued at much longer reaction times than expected for reaction of just the surface of the odd carbon diacids. Saturation times for malonic (C3) and glutaric (C5) acids were calculated using the same method as described above for succinic acid (C4). For example, for uptake of EA on malonic acid (C3) with $\gamma_{ss} = 0.4$, the expected time to react $1/e$ of the surface molecules at an amine concentration of 4×10^{11} molecules cm^{-3} is of the order of 0.2 seconds, and for glutaric acid (C5) with $\gamma_{ss} = 0.06$, is ~ 0.5 seconds. The data in Figure 2 clearly indicate that uptake continues to occur on much longer timescales. This continuous uptake suggests that more than a monolayer at the surface is available for reaction and that formation of ionic liquids may be occurring similar to the BA reaction.[210] In the case of malonic acid (C3) reacting with the amines, there is a trend to decreasing values of $\gamma_{0,ss}$ with time, which may reflect slower diffusion of the amine through an ever-thickening reacted layer and/or solubility limitations into the developing liquid layer.

Thus, a general scenario for the reaction of the odd diacids is formation of a salt product that is a stable or metastable IL that forms on the surface during reaction. In this case, surface passivation does not shut off the reaction and suggests that these liquid layers on the surface are the cause for continuous uptake observed on odd carbon diacids. The lack of reaction of pimelic acid (C7) may be due to the stronger interactions between the longer methylene chains, making initial disruption of the crystal structure more difficult on the timescale of our experiments.

As shown in Table 5-5, uptake coefficients for MA, EA and DMA on glutaric acid (C5) showed a trend to higher values at higher amine concentrations. This dependence may be due to the kinetic limitations on formation of the IL layer. At the higher amine concentration, the formation of the IL may occur more rapidly than at the smaller concentration, causing more rapid formation of the IL and hence higher initial uptake of the amine into the IL layer.

To probe which amine–diacid combinations form room temperature ionic liquids, aqueous mixtures were prepared and the excess water evaporated off as in earlier studies of the BA reaction.[210] A variety of behaviors were observed in the present study. In some cases, the remaining material was a liquid whose viscosity could be measured, and which remained liquid during storage under nitrogen or ultra–zero air for up to several months. These are considered to be stable, room temperature ionic liquids. In other cases, a liquid was formed for sufficient time to make viscosity measurements, but subsequently formed a slushy material. This suggests that the salt formed initially is a thermodynamically unstable liquid, dubbed here as a metastable ionic liquid (MSIL) which, under the appropriate conditions, converts to a stable higher viscosity salt. In other cases, a solid was formed immediately. The properties of the final solid as visually

observed varied from a hard solid to a softer material. Table 5-8 indicates which products formed a MSIL, and summarizes the results of the viscosity measurements.

Table 5-8. Measured viscosities (μ) and densities (ρ_f) for 2:1 and 1:1 ammonia or amines–diacid mixtures.

	2:1		1:1	
Salt	$\mu \pm 2\sigma$ (Pa·s)	ρ_f (units of 10^3 kg m^{-3})	$\mu \pm 2\sigma$ (Pa·s)	ρ_f (units of 10^3 kg m^{-3})
Malonic (C3) +				
NH_3	[a]	[a]	12.1 ± 3.8 [b]	1.4
MA	0.9 ± 0.4	1.2	[a]	[a]
EA	13.1 ± 1.2 [b]	1.1	10.1 ± 1.4	1.3
DMA	3.5 ± 0.8 [b]	1.2	[a]	[a]
TMA	[a]	[a]	[a]	[a]
Succinic (C4) +				
MA	[a]	[a]	[a]	[a]
EA	[a]	[a]	[a]	[a]
DMA	[a]	[a]	[a]	[a]
TMA	32.3 ± 2.8	1.2	26.3 ± 2.8	1.2
Glutaric (C5) +				
MA	15 ± 4 [b]	1.2	[a]	[a]
EA	8.5 ± 1.6	1.1	[a]	[a]
DMA	[a]	[a]	[a]	[a]
TMA	6.1 ± 0.8	1.1	13.9 ± 2.4	1.1
Adipic (C6) +				
MA	[a]	[a]	[a]	[a]
EA	[a]	[a]	[a]	[a]
DMA	[a]	[a]	[a]	[a]
TMA	[a]	[a]	[a]	[a]
Pimelic (C7) +				
MA	20.5 ± 2 [b]	1.1	[a]	[a]
EA	9.8 ± 1.6 [b]	1.1	18.0 ± 2.2 [b]	1.1
DMA	9.9 ± 1.4	1.1	10.1 ± 1.6	1.1
TMA	13.0 ± 3.4	1.1	9.4 ± 0.6	1.1

[a] Viscosity measurements could not be made. [b] Liquid product is a MSIL that subsequently formed a higher viscosity slushy material over several hours.

Photographs of the hard solid, slushy material, or liquid salts formed from evaporation of amine/ammonia and diacid mixtures are shown in Figure 5-13 (odd carbon diacids) and Figure 5-14 (even carbon diacids). These photographs show that most of the 2:1 mixtures of the odd carbon diacids formed either an IL or MSIL, consistent with continued uptake of most of the amines onto malonic (C3) and glutaric (C5) acids. However, the TMA–malonic acid (C3) and the DMA–glutaric acid (C5) salts were exceptions. In these two cases, the evaporation of the aqueous mixtures formed a slushy material (Figure 5-13) immediately after excess water was removed. Nonetheless, dissolution of both the underlying diacid and the gas phase amine might still be expected to occur in the soft product layer. This is supported by continuous uptake of gas phase TMA on malonic acid (C3), and DMA on glutaric acid (C5) (Figure 5-10). Most amines on pimelic acid (C7) form a stable IL or MSIL (Figure 5-13), however no measurable uptake is observed in the Knudsen cell experiments.

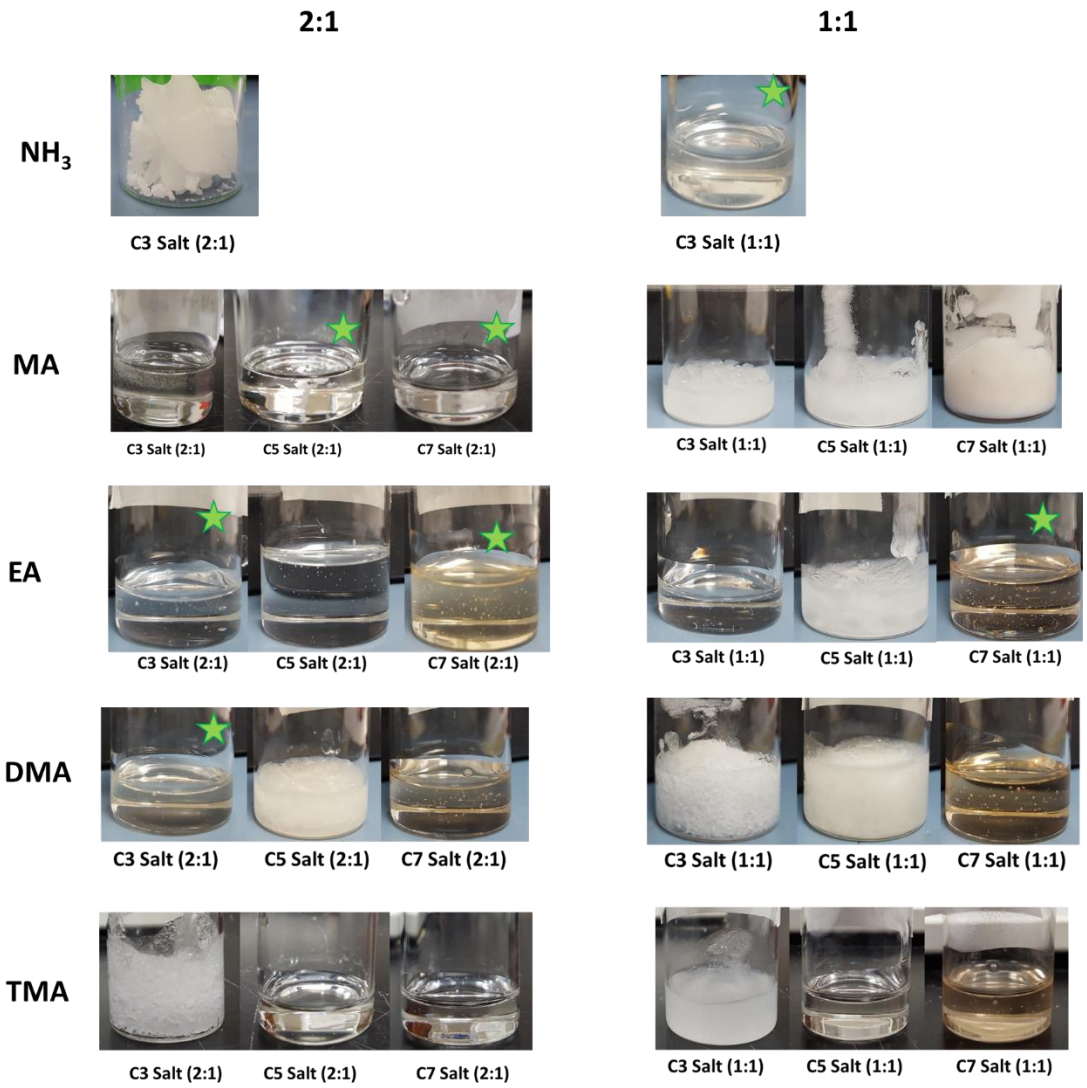

Figure 5-13. Products formed from the evaporation of aqueous 2:1 or 1:1 mixtures of MA, EA, DMA, TMA or NH_3 with odd carbon diacids. Green stars indicate a MSIL that converted to a slushy material.

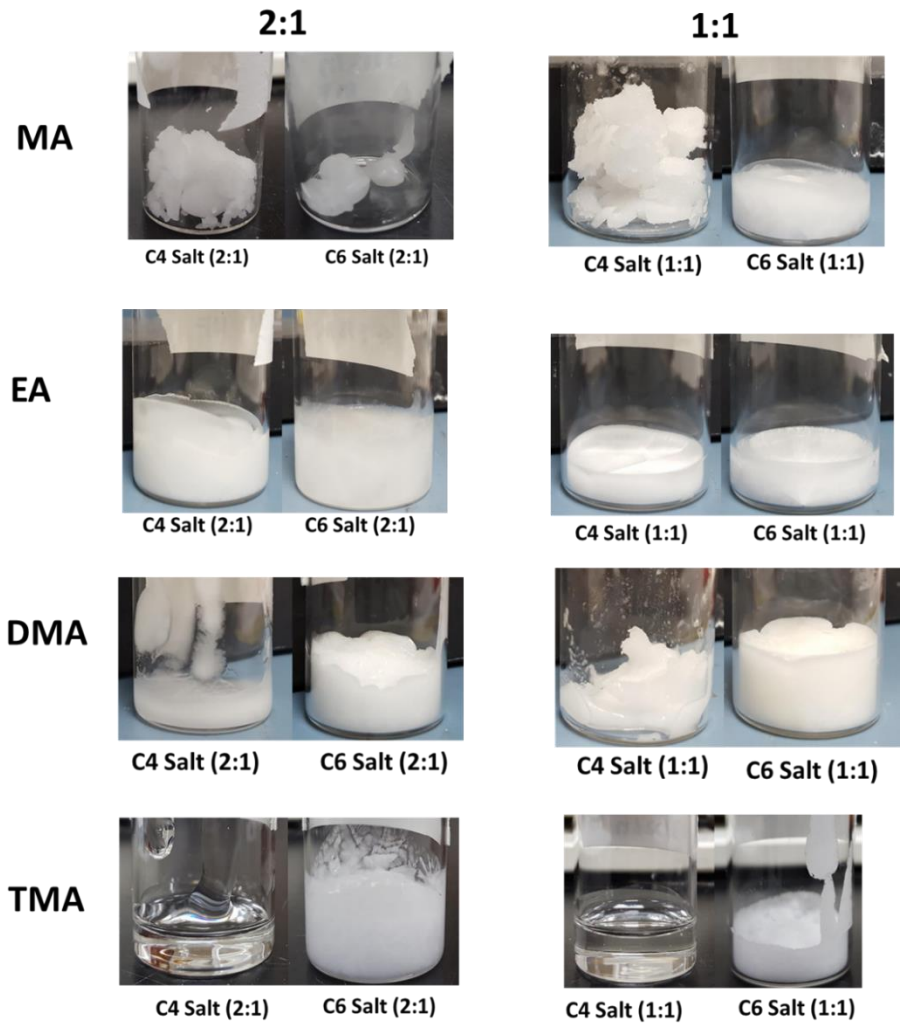

Figure 5-14. Products formed from the evaporation of aqueous 2:1 or 1:1 mixtures of MA, EA, DMA or TMA with even carbon diacids.

Results from the aqueous mixtures of pimelic acid (C7) and Knudsen cell experiments suggest that penetration into the solid and disruption of the crystal structure to form an IL layer is not sufficiently fast on the timescales and small gas phase concentrations of the Knudsen cell experiments to form an IL or MSIL layer, and hence there is no measurable uptake. It should be noted that while the determination of whether various aqueous mixtures form ILs, MSILs or salts provides some insight into the Knudson cell results, there is not a direct correlation in all cases.

This likely reflects very different reaction conditions and timescales for the Knudsen cell experiments compared to evaporation of aqueous mixtures.

The overall trends in uptake shown in Figure 5-10 and Figure 5-12 and summarized in Tables 5-3 to 5-7 indicate the following. First, the uptake coefficients for all amines on malonic acid (C3) are large ($\gamma > 0.1$) and reflect the unique crystal structure of malonic acid (C3) discussed above. Of all the amines, EA and DMA have the largest uptake coefficients. Their larger values compared to MA may be due to their higher gas phase basicity[212, 213] and larger dispersion forces, while steric factors come into play with TMA. Second, the higher uptake on odd carbon diacids seen earlier for BA[210] continues to hold for the series of amines studied here. Finally, the even carbon diacids have uptake coefficients that are orders of magnitude smaller than for the odd carbon compounds, and only succinic acid (C4) gave measurable uptake for MA, EA and DMA. Lower uptake onto even carbon diacids is consistent with their more stable crystal structure and the fact that they tend to form hard solid salts rather than ILs (Figure 5-14). The exception is the TMA–succinic acid (C4) reaction for which there was no measurable uptake but the aqueous mixtures did form a viscous IL (Table 5-8). Steric factors are likely to play a role in the penetration of TMA into the crystal, limiting the extent of reaction and formation of a liquid layer at the concentrations and timescales of the Knudsen cell experiments.

Ammonia has a much smaller uptake coefficient on malonic acid (C3) compared to the amines, and shows no evidence of observable uptake on any of the other diacids. The reaction of NH_3 with malonic acid (C3) shows signs of surface saturation (Table 5-3), consistent with the formation of a hard solid from its 2:1 aqueous mixture (Figure 5-13). This one reaction of

malonic acid (C3) therefore falls into the same category of succinic acid (C4), i.e. a gas–solid reaction without formation of a quasi-liquid layer.

Unique to malonic acid (C3) is a large initial uptake for most amines when the lid is first opened (Figure 5-10). This is indicative of the presence of highly reactive sites such as the steps and edges of a crystal.[214] Once those have reacted, the molecules in the more stable crystal structure dominate, resulting in a slower gas uptake. Such behavior was previously observed for example, in the reaction of gas phase HNO_3 with solid NaCl.[176-178, 202, 215] In the case of malonic acid (C3), the more easily accessible acidic group may provide the highly reactive sites, in addition to any steps/edges present on the crystals. The large initial uptake was not present with TMA in the current study, or in studies with BA on malonic acid (C3).[210] It could be that MA, EA and DMA are small enough to access these highly reactive sites more readily than BA or TMA.

It is, however, unusual that this initial "uptake spike" occurs repeatedly when the lid is opened and closed a number of times on one sample. In the case of HNO_3–NaCl, the spikes only occur at the first exposures since the highly reactive sites are removed by reaction.[176, 178, 202] The repetition of the spikes within one experiment seen here for malonic acid (C3) (Figure 5-10) suggests that if it is due to some highly reactive sites, they must be regenerated relatively rapidly. Since these reactions form ILs and/or MSILs as the reaction proceeds (Table 5-8), it is possible that once the lid is closed, the ionic liquid layer may coalesce into small regions, exposing new reactive sites so that when the lid is subsequently opened, another rapid, initial uptake of the amine occurs. A similar reorganization of the sodium nitrate surface layer resulting from the

reaction of NaCl with gas phase nitric acid or NO_2 was observed; in that case, exposure to water vapor induced recrystallization to generate a fresh NaCl surface.[215, 216] Reactions of SO_2 with $CaCO_3$ in the presence of water vapor were also observed to form islands and microcrystallite layers of $CaSO_3$ which subsequently exposed fresh $CaCO_3$ sites for further reaction.[217] The reactions of MA, EA and DMA with malonic acid (C3) reported here are, however, unique in that water vapor is not required for this hypothesized reorganization.

IV. Conclusions

Successful studies on using a Knudsen cell coupled to a QMS have shown that in the reaction of amines with solid diacids, uptake coefficients exhibit an odd–even trend. Comparing uptake coefficients for flow reactor studies to Knudsen cell experiments, all uptake coefficients for diacids in the flow reactor experiments were ~ 10^{-2} whether odd or even carbon diacids. The signficiant different in uptake coefficients measured with the Knudsen cell indicate that uptake coefficients obtained from flow reactor studies may reflect saturation of the surface due to limitations in the time resolution and therefore, missing the crucial, initial uptake of the amine onto the diacids.

In the case of ammonia, uptake was only visible on malonic acid (C3) and was lower than all the amines. This is thought to be due to the lower gas phase basicity of ammonia. Uptake coefficients for odd carbon diacids are orders of magnitude larger than their even carbon homologs. The difference in uptake is thought to stem from the differences in crystal structure between odd and even carbon diacids. Odd carbon crystal lattices have torsional strain causing them to be higher in energy and have more spacing between adjacent chains. This is thought to

help facilitate the penetration of amines in the crystal lattice and in addition, these reactions tend to form ionic liquids.

The formation of ionic liquids (ILs) on the surface of odd carbon diacids was confirmed using aqueous mixtures of the amine and diacid. BA formed stable ILs, while MA, EA, DMA, and TMA either formed ILs or thermodynamically unstable ILs defined as a metastable IL. This may lie in the similar chain length of BA to the diacids causing them to have similar electrostatic interactions, which may help facilitate the formation of stable ILs. This may also explain why BA had higher measured uptake coefficients compared to the other amines in this study.

These Knudsen cell studies show that not only does the structure of the solid substrate (diacid) play a role in reaction and uptake, but the structure of the gas phase species governs uptake behavior and reaction as well. These data suggest that the factors affecting gas–solid uptake are varied and numerous. Although solid diacid salts are not typically found in the atmosphere, it is possible that ionic liquids may be formed via reactions of amines with the acidic components of semi–solid SOA. This illustrates the importance of having a molecular level understanding in order to translate the results of laboratory studies into atmospheric models and ultimately into control strategies.

CONCLUSIONS AND ATMOSPHERIC IMPLICATIONS

Atmospheric particles adversely affect climate and health, thus an understanding of their formation and growth mechanisms in the atmosphere is necessary. Part of the lack of a complete understanding of these mechanisms is due to the complex chemistry occurring in the atmosphere. Experiments were conducted to study the uptake of gas phase species of differing polarities onto low viscosity liquid substrates and laboratory generated SOA. The effect on polarity and viscosity of the substrate was analyzed to determine if the chemical properties of the gas and condensed phases affect the uptake mechanism of the gas onto the substrate. Studies of the uptake of isobutyl nitrate (IBN) on squalane was rapid, which may due to the low viscosity of squalane. At the time of the first IR scan, evaporation of IBN may already be present, indicating a rapid establishment of equilibrium between the two species. In the uptake on IBN on Fomblin ®, a higher concentration of IBN was needed in order to see uptake which is presumed to be due to the increased number of polar groups on Fomblin ® compared to squalane. The uptake of IBN on SOA generated from the ozonolysis of α–pinene was significantly different from squalane in that diffusion into and out of SOA was much slower. This is due to the large number of oxygenated products resulting from the oxidation of α–pinene, as well as the much higher viscosity of SOA compared to squalane.

The reaction of amines with solid dicarboxylic acids (diacids) was studied using two different approaches: a flow reactor or Knudsen cell coupled to a quadrupole mass spectrometer. In the first approach, uptake coefficients for *n*–butylamine (BA) on solid C2 – C5 diacids were on the order of $10^{-3} – 10^{-2}$. Knudsen cell studies resulted in uptake coefficients ranging from 10^{-1}

to upper limits of 10^{-6}, which differed based on the number of carbons in the diacid. The time constant used in the flow reactor experiments may have been too slow to capture the initial uptake region of the gas phase amine reacting with the diacid. This is evident in the uptake coefficients for all diacids having similar orders of magnitude as well as surface saturation observed for some diacids.

Uptake coefficients for BA measured using the Knudsen cell were dependent on whether the diacid had an even or odd number of carbons in the backbone. Odd carbon diacids had uptake coefficients that were several orders of magnitude higher than the even carbon diacids, with the uptake coefficients decreasing with increasing carbon number in a given series. This higher uptake in odd carbon diacids may be due to the differences in packing in the crystal structure of the diacids. It was also shown that evaporation of aqueous mixtures of BA with odd carbon diacids formed stable ionic liquids in which underlying diacid can dissolve into this liquid layer and provide a replenishment of unreacted diacid. Subsequent studies on various primary amines, as well as dimethylamine (DMA), trimethylamine (TMA), and ammonia showed that not only does the structure of the diacid affect uptake, but the structure of the amine does as well.

Results from these studies show that reaction and uptake behavior differs when the phase of the substrate is solid or liquid. The largest uptake coefficients for the amine–diacid system were on the order of magnitude of 10^{-1} for BA on the odd carbon diacids, while for the other amines, the larger uptake coefficients were around 10^{-2}. This work shows that for a simple acid–base reaction, it may be invalid to assume uptake coefficients as unity. Additionally, there should not be a "one size fits all" parameter in atmospheric models for a given type of reaction,

as seen in these laboratory studies, the uptake coefficients differed based on the gas phase amine. These data will help atmospheric models more accurately predict ambient particle concentrations based on a better understanding of the amine–diacid system, since amines are prevalent in the atmosphere and diacids have been found in particles in various environments. On a larger scale, the expansion of this work to measure uptake coefficients for a variety of different chemical reactions will help build a database of values to help modelers incorporate these uptake coefficients into the atmospheric models. The synergy between experimental studies and atmospheric models will help bring a better understanding of the complex chemistry occurring in the atmosphere.

REFERENCES

1. Mannucci, P. M.; Harari, S.; Martinelli, I.; Franchini, M., Effects on health of air pollution: a narrative review. *Intern. Emerg. Med.* **2015,** *10* (6), 657-662.
2. Heal, M. R.; Kumar, P.; Harrison, R. M., Particles, air quality, policy and health. *Chem. Soc. Rev.* **2012,** *41* (19), 6606-6630.
3. Finlayson-Pitts, B. J.; Pitts Jr, J. N., *Chemistry of the Upper and Lower Atmosphere: Theory, Experiments, and Applications*. Academic press: 2000.
4. Poschl, U., Atmospheric aerosols: Composition, transformation, climate and health effects. *Angew. Chem., Int. Ed.* **2005,** *44* (46), 7520-7540.
5. Pope, C. A.; Dockery, D. W., Health effects of fine particulate air pollution: Lines that connect. *J. Air Waste Manage. Assoc.* **2006,** *56* (6), 709-742.
6. Dockery , D. W.; Pope , C. A.; Xu , X.; Spengler , J. D.; Ware , J. H.; Fay , M. E.; Ferris , B. G. J.; Speizer , F. E., An association between air pollution and mortality in six U.S. cities. *New England Journal of Medicine* **1993,** *329* (24), 1753-1759.
7. Hopke, P. K., New directions: Reactive particles as a source of human health effects. *Atmos. Environ.* **2008,** *42* (13), 3192-3194.
8. Gurjar, B. R.; Jain, A.; Sharma, A.; Agarwal, A.; Gupta, P.; Nagpure, A. S.; Lelieveld, J., Human health risks in megacities due to air pollution. *Atmos. Environ.* **2010,** *44* (36), 4606-4613.
9. Mauderly, J. L.; Chow, J. C., Health effects of organic aerosols. *Inhal. Toxicol.* **2008,** *20* (3), 257-288.
10. Wyzga, R. E.; Rohr, A. C., Long-term particulate matter exposure: Attributing health effects to individual PM components. *J. Air Waste Manage. Assoc.* **2015,** *65* (5), 523-543.
11. Lakey, P. S. J.; Berkemeier, T.; Tong, H. J.; Arangio, A. M.; Lucas, K.; Poschl, U.; Shiraiwa, M., Chemical exposure-response relationship between air pollutants and reactive oxygen species in the human respiratory tract. *Sci. Rep.* **2016,** *6*, 32916.
12. Poschl, U.; Shiraiwa, M., Multiphase chemistry at the atmosphere-biosphere interface influencing climate and public health in the anthropocene. *Chem. Rev.* **2015,** *115* (10), 4440-4475.
13. Halonen, J. I.; Lanki, T.; Yli-Tuomi, T.; Tiittanen, P.; Kulmala, M.; Pekkanen, J., Particulate air pollution and acute cardiorespiratory hospital admissions and mortality among the elderly. *Epidemiology* **2009,** *20* (1), 143-153.
14. Tie, X. X.; Wu, D.; Brasseur, G., Lung cancer mortality and exposure to atmospheric aerosol particles in Guangzhou, China. *Atmos. Environ.* **2009,** *43* (14), 2375-2377.
15. Lelieveld, J.; Evans, J. S.; Fnais, M.; Giannadaki, D.; Pozzer, A., The contribution of outdoor air pollution sources to premature mortality on a global scale. *Nature* **2015,** *525* (7569), 367-371.
16. Pryor, W. A.; Squadrito, G. L.; Friedman, M., The cascade mechanism to explain ozone toxicity - the role of lipid ozonation products. *Free Radicals Biol. Med.* **1995,** *19* (6), 935-941.
17. Enami, S.; Hoffmann, M. R.; Colussi, A. J., Acidity enhances the formation of a persistent ozonide at aqueous ascorbate/ozone gas interfaces. *Proc. Natl. Acad. Sci. U.S.A.* **2008,** *105* (21), 7365-7369.

18. Kim, H. I.; Kim, H. J.; Shin, Y. S.; Beegle, L. W.; Jang, S. S.; Neidholdt, E. L.; Goddard, W. A.; Heath, J. R.; Kanik, I.; Beauchamp, J. L., Interfacial reactions of ozone with surfactant protein B in a model lung surfactant system. *J. Am. Chem. Soc.* **2010,** *132* (7), 2254-2263.
19. Stocker, T.; Qin, D.; Plattner, G.; Tignor, M.; Allen, S.; Boschung, J.; Nauels, A.; Xia, Y.; Bex, B.; Midgley, B. *IPCC, 2013: Climate change 2013: The physical science basis. Contribution of working group I to the fifth assessment report of the intergovernmental panel on climate change*; 2013.
20. Farmer, D. K.; Cappa, C. D.; Kreidenweis, S. M., Atmospheric processes and their controlling influence on cloud condensation nuclei activity. *Chem. Rev.* **2015,** *115* (10), 4199-4217.
21. McNeill, V. F.; Sareen, N.; Schwier, A. N., Surface-active organics in atmospheric aerosols. In *Atmospheric and Aerosol Chemistry*, McNeill, V. F.; Ariya, P. A., Eds. Springer Berlin Heidelberg: Berlin, Heidelberg, 2014; pp 201-259.
22. Andreae, M. O.; Rosenfeld, D., Aerosol-cloud-precipitation interactions. Part 1. The nature and sources of cloud-active aerosols. *Earth-Sci. Rev.* **2008,** *89* (1-2), 13-41.
23. Sun, J. M.; Ariya, P. A., Atmospheric organic and bio-aerosols as cloud condensation nuclei (CCN): A review. *Atmos. Environ.* **2006,** *40* (5), 795-820.
24. Ervens, B., Modeling the Processing of Aerosol and Trace Gases in Clouds and Fogs. *Chemical Reviews* **2015,** *115* (10), 4157-4198.
25. von Schneidemesser, E.; Monks, P. S.; Allan, J. D.; Bruhwiler, L.; Forster, P.; Fowler, D.; Lauer, A.; Morgan, W. T.; Paasonen, P.; Righi, M.; Sindelarova, K.; Sutton, M. A., Chemistry and the linkages between air quality and climate change. *Chem. Rev.* **2015,** *115* (10), 3856-3897.
26. Riipinen, I.; Yli-Juuti, T.; Pierce, J. R.; Petaja, T.; Worsnop, D. R.; Kulmala, M.; Donahue, N. M., The contribution of organics to atmospheric nanoparticle growth. *Nat. Geosci.* **2012,** *5* (7), 453-458.
27. Hallquist, M.; Wenger, J. C.; Baltensperger, U.; Rudich, Y.; Simpson, D.; Claeys, M.; Dommen, J.; Donahue, N. M.; George, C.; Goldstein, A. H.; Hamilton, J. F.; Herrmann, H.; Hoffmann, T.; Iinuma, Y.; Jang, M.; Jenkin, M. E.; Jimenez, J. L.; Kiendler-Scharr, A.; Maenhaut, W.; McFiggans, G.; Mentel, T. F.; Monod, A.; Prevot, A. S. H.; Seinfeld, J. H.; Surratt, J. D.; Szmigielski, R.; Wildt, J., The formation, properties and impact of secondary organic aerosol: current and emerging issues. *Atmos. Chem. Phys.* **2009,** *9* (14), 5155-5236.
28. Ziemann, P. J.; Atkinson, R., Kinetics, products, and mechanisms of secondary organic aerosol formation. *Chem. Soc. Rev.* **2012,** *41* (19), 6582-6605.
29. Seinfeld, J. H.; Pankow, J. F., Organic atmospheric particulate material. *Annu. Rev. Phys. Chem.* **2003,** *54*, 121-140.
30. Kroll, J. H.; Seinfeld, J. H., Chemistry of secondary organic aerosol: Formation and evolution of low-volatility organics in the atmosphere. *Atmos. Environ.* **2008,** *42* (16), 3593-3624.
31. Zhang, R. Y.; Khalizov, A.; Wang, L.; Hu, M.; Xu, W., Nucleation and growth of nanoparticles in the atmosphere. *Chem. Rev.* **2012,** *112* (3), 1957-2011.
32. Vehkamaki, H.; Riipinen, I., Thermodynamics and kinetics of atmospheric aerosol particle formation and growth. *Chem. Soc. Rev.* **2012,** *41* (15), 5160-5173.
33. Kulmala, M.; Kerminen, V. M., On the formation and growth of atmospheric nanoparticles. *Atmos. Res.* **2008,** *90* (2-4), 132-150.

34. Kulmala, M.; Petaja, T.; Ehn, M.; Thornton, J.; Sipila, M.; Worsnop, D. R.; Kerminen, V. M., Chemistry of atmospheric nucleation: On the recent advances on precursor characterization and atmospheric cluster composition in connection with atmospheric new particle formation. *Annu. Rev. Phys. Chem.* **2014,** *65*, 21-37.
35. Hegg, D. A.; Baker, M. B., Nucleation in the atmosphere. *Rep Prog Phys* **2009,** *72* (5), 1-21.
36. Donahue, N. M.; Ortega, I. K.; Chuang, W.; Riipinen, I.; Riccobono, F.; Schobesberger, S.; Dommen, J.; Baltensperger, U.; Kulmala, M.; Worsnop, D. R.; Vehkamaki, H., How do organic vapors contribute to new-particle formation? *Faraday Discuss.* **2013,** *165*, 91-104.
37. Koop, T.; Bookhold, J.; Shiraiwa, M.; Poschl, U., Glass transition and phase state of organic compounds: dependency on molecular properties and implications for secondary organic aerosols in the atmosphere. *Phys. Chem. Chem. Phys.* **2011,** *13* (43), 19238-19255.
38. Shiraiwa, M.; Seinfeld, J. H., Equilibration timescale of atmospheric secondary organic aerosol partitioning. *Geophys. Res. Lett.* **2012,** *39*, L24801.
39. Shiraiwa, M.; Ammann, M.; Koop, T.; Poschl, U., Gas uptake and chemical aging of semisolid organic aerosol particles. *Proc. Natl. Acad. Sci. U.S.A.* **2011,** *108* (27), 11003-11008.
40. Odum, J. R.; Hoffmann, T.; Bowman, F.; Collins, D.; Flagan, R. C.; Seinfeld, J. H., Gas/particle partitioning and secondary organic aerosol yields. *Environ. Sci. Technol.* **1996,** *30* (8), 2580-2585.
41. Donahue, N. M.; Epstein, S. A.; Pandis, S. N.; Robinson, A. L., A two-dimensional volatility basis set: 1. organic-aerosol mixing thermodynamics. *Atmos. Chem. Phys.* **2011,** *11* (7), 3303-3318.
42. Donahue, N. M.; Robinson, A. L.; Stanier, C. O.; Pandis, S. N., Coupled partitioning, dilution, and chemical aging of semivolatile organics. *Environ. Sci. Technol.* **2006,** *40* (8), 2635-2643.
43. Pankow, J. F., An absorption-model of gas-particle partitioning of organic-compounds in the atmosphere. *Atmos. Environ.* **1994,** *28* (2), 185-188.
44. Pankow, J. F., An absorption-model of the gas aerosol partitioning involved in the formation of secondary organic aerosol. *Atmos. Environ.* **1994,** *28* (2), 189-193.
45. Pankow, J. F., Phase considerations in the gas/particle partitioning of organic amines in the atmosphere. *Atmos. Environ.* **2015,** *122*, 448-453.
46. Perraud, V.; Bruns, E. A.; Ezell, M. J.; Johnson, S. N.; Yu, Y.; Alexander, M. L.; Zelenyuk, A.; Imre, D.; Chang, W. L.; Dabdub, D.; Pankow, J. F.; Finlayson-Pitts, B. J., Nonequilibrium atmospheric secondary organic aerosol formation and growth. *Proc. Natl. Acad. Sci. U.S.A.* **2012,** *109* (8), 2836-2841.
47. Odum, J. R.; Jungkamp, T. P. W.; Griffin, R. J.; Forstner, H. J. L.; Flagan, R. C.; Seinfeld, J. H., Aromatics, reformulated gasoline, and atmospheric organic aerosol formation. *Environ. Sci. Technol.* **1997,** *31* (7), 1890-1897.
48. Odum, J. R.; Jungkamp, T. P. W.; Griffin, R. J.; Flagan, R. C.; Seinfeld, J. H., The atmospheric aerosol-forming potential of whole gasoline vapor. *Science* **1997,** *276* (5309), 96-99.
49. Pandis, S. N.; Paulson, S. E.; Seinfeld, J. H.; Flagan, R. C., Aerosol formation in the photooxidation of isoprene and b-pinene. *Atmos. Environ., Part A* **1991,** *25* (5-6), 997-1008.
50. Zhang, S. H.; Shaw, M.; Seinfeld, J. H.; Flagan, R. C., Photochemical aerosol formation from a-pinene and b-pinene. *J. Geophys. Res.: Atmos.* **1992,** *97* (D18), 20717-20729.

51. Hoffmann, T.; Odum, J. R.; Bowman, F.; Collins, D.; Klockow, D.; Flagan, R. C.; Seinfeld, J. H., Formation of organic aerosols from the oxidation of biogenic hydrocarbons. *J. Atmos. Chem.* **1997,** *26* (2), 189-222.
52. Griffin, R. J.; Cocker, D. R.; Flagan, R. C.; Seinfeld, J. H., Organic aerosol formation from the oxidation of biogenic hydrocarbons. *J. Geophys. Res.: Atmos.* **1999,** *104* (D3), 3555-3567.
53. Abramson, E.; Imre, D.; Beranek, J.; Wilson, J.; Zelenyuk, A., Experimental determination of chemical diffusion within secondary organic aerosol particles. *Phys. Chem. Chem. Phys.* **2013,** *15* (8), 2983-2991.
54. Cappa, C. D.; Wilson, K. R., Evolution of organic aerosol mass spectra upon heating: implications for OA phase and partitioning behavior. *Atmos. Chem. Phys.* **2011,** *11* (5), 1895-1911.
55. Kidd, C.; Perraud, V.; Finlayson-Pitts, B. J., New insights into secondary organic aerosol from the ozonolysis of a-pinene from combined infrared spectroscopy and mass spectrometry measurements. *Phys. Chem. Chem. Phys.* **2014,** *16* (41), 22706-22716.
56. Kidd, C.; Perraud, V.; Wingen, L. M.; Finlayson-Pitts, B. J., Integrating phase and composition of secondary organic aerosol from the ozonolysis of a-pinene. *Proc. Natl. Acad. Sci. U.S.A.* **2014,** *111* (21), 7552-7557.
57. Shrivastava, M.; Zelenyuk, A.; Imre, D.; Easter, R.; Beranek, J.; Zaveri, R. A.; Fast, J., Implications of low volatility SOA and gas-phase fragmentation reactions on SOA loadings and their spatial and temporal evolution in the atmosphere. *J. Geophys. Res.: Atmos.* **2013,** *118* (8), 3328-3342.
58. Vaden, T. D.; Imre, D.; Beranek, J.; Shrivastava, M.; Zelenyuk, A., Evaporation kinetics and phase of laboratory and ambient secondary organic aerosol. *Proc. Natl. Acad. Sci. U.S.A.* **2011,** *108* (6), 2190-2195.
59. Zelenyuk, A.; Imre, D.; Beranek, J.; Abramson, E.; Wilson, J.; Shrivastava, M., Synergy between secondary organic aerosols and long-range transport of polycyclic aromatic hydrocarbons. *Environ. Sci. Technol.* **2012,** *46* (22), 12459-12466.
60. Saukko, E.; Kuuluvainen, H.; Virtanen, A., A method to resolve the phase state of aerosol particles. *Atmos. Meas. Tech.* **2012,** *5* (1), 259-265.
61. Virtanen, A.; Joutsensaari, J.; Koop, T.; Kannosto, J.; Yli-Pirila, P.; Leskinen, J.; Makela, J. M.; Holopainen, J. K.; Poschl, U.; Kulmala, M.; Worsnop, D. R.; Laaksonen, A., An amorphous solid state of biogenic secondary organic aerosol particles. *Nature* **2010,** *467* (7317), 824-827.
62. Renbaum-Wolff, L.; Grayson, J. W.; Bateman, A. P.; Kuwata, M.; Sellier, M.; Murray, B. J.; Shilling, J. E.; Martin, S. T.; Bertram, A. K., Viscosity of a-pinene secondary organic material and implications for particle growth and reactivity. *Proc. Natl. Acad. Sci. U.S.A.* **2013,** *110* (20), 8014-8019.
63. Li, Y. J.; Liu, P. F.; Gong, Z. H.; Wang, Y.; Bateman, A. P.; Bergoend, C.; Bertram, A. K.; Martin, S. T., Chemical reactivity and liquid/nonliquid states of secondary organic material. *Environ. Sci. Technol.* **2015,** *49* (22), 13264-13274.
64. O'Brien, R. E.; Neu, A.; Epstein, S. A.; MacMillan, A. C.; Wang, B. B.; Kelly, S. T.; Nizkorodov, S. A.; Laskin, A.; Moffet, R. C.; Gilles, M. K., Physical properties of ambient and laboratory-generated secondary organic aerosol. *Geophys. Res. Lett.* **2014,** *41* (12), 4347-4353.

65. Seinfeld, J. H.; Pandis, S. N., *Atmospheric Chemistry and Physics: From Air Pollution to Climate Change*. John Wiley & Sons: 1998.
66. Berndt, T.; Stratmann, F.; Sipila, M.; Vanhanen, J.; Petaja, T.; Mikkila, J.; Gruner, A.; Spindler, G.; Mauldin, R. L.; Curtius, J.; Kulmala, M.; Heintzenberg, J., Laboratory study on new particle formation from the reaction OH + SO_2: influence of experimental conditions, H_2O vapour, NH_3 and the amine *tert*-butylamine on the overall process. *Atmos. Chem. Phys.* **2010,** *10* (15), 7101-7116.
67. Schobesberger, S.; Franchin, A.; Bianchi, F.; Rondo, L.; Duplissy, J.; Kurten, A.; Ortega, I. K.; Metzger, A.; Schnitzhofer, R.; Almeida, J.; Amorim, A.; Dommen, J.; Dunne, E. M.; Ehn, M.; Gagne, S.; Ickes, L.; Junninen, H.; Hansel, A.; Kerminen, V. M.; Kirkby, J.; Kupc, A.; Laaksonen, A.; Lehtipalo, K.; Mathot, S.; Onnela, A.; Petaja, T.; Riccobono, F.; Santos, F. D.; Sipila, M.; Tome, A.; Tsagkogeorgas, G.; Viisanen, Y.; Wagner, P. E.; Wimmer, D.; Curtius, J.; Donahue, N. M.; Baltensperger, U.; Kulmala, M.; Worsnop, D. R., On the composition of ammonia-sulfuric-acid ion clusters during aerosol particle formation. *Atmos. Chem. Phys.* **2015,** *15* (1), 55-78.
68. McMurry, P. H.; Takano, H.; Anderson, G. R., Study of the ammonia (gas) sulfuric-acid (aerosol) reaction-rate. *Environ. Sci. Technol.* **1983,** *17* (6), 347-352.
69. Robbins, R. C.; Cadle, R. D., Kinetics of the reaction between gaseous ammonia and sulfuric acid droplets in an aerosol. *J. Phys. Chem.* **1958,** *62* (4), 469-471.
70. Huntzicker, J. J.; Cary, R. A.; Ling, C. S., Neutralization of sulfuric-acid aerosol by ammonia. *Environ. Sci. Technol.* **1980,** *14* (7), 819-824.
71. Jen, C. N.; McMurry, P. H.; Hanson, D. R., Stabilization of sulfuric acid dimers by ammonia, methylamine, dimethylamine, and trimethylamine. *J. Geophys. Res.: Atmos.* **2014,** *119* (12), 7502-7514.
72. Zollner, J. H.; Glasoe, W. A.; Panta, B.; Carlson, K. K.; McMurry, P. H.; Hanson, D. R., Sulfuric acid nucleation: power dependencies, variation with relative humidity, and effect of bases. *Atmos. Chem. Phys.* **2012,** *12* (10), 4399-4411.
73. Wang, L.; Lal, V.; Khalizov, A. F.; Zhang, R. Y., Heterogeneous chemistry of alkylamines with sulfuric acid: Implications for atmospheric formation of alkylaminium sulfates. *Environ. Sci. Technol.* **2010,** *44* (7), 2461-2465.
74. Almeida, J.; Schobesberger, S.; Kurten, A.; Ortega, I. K.; Kupiainen-Maatta, O.; Praplan, A. P.; Adamov, A.; Amorim, A.; Bianchi, F.; Breitenlechner, M.; David, A.; Dommen, J.; Donahue, N. M.; Downard, A.; Dunne, E.; Duplissy, J.; Ehrhart, S.; Flagan, R. C.; Franchin, A.; Guida, R.; Hakala, J.; Hansel, A.; Heinritzi, M.; Henschel, H.; Jokinen, T.; Junninen, H.; Kajos, M.; Kangasluoma, J.; Keskinen, H.; Kupc, A.; Kurten, T.; Kvashin, A. N.; Laaksonen, A.; Lehtipalo, K.; Leiminger, M.; Leppa, J.; Loukonen, V.; Makhmutov, V.; Mathot, S.; McGrath, M. J.; Nieminen, T.; Olenius, T.; Onnela, A.; Petaja, T.; Riccobono, F.; Riipinen, I.; Rissanen, M.; Rondo, L.; Ruuskanen, T.; Santos, F. D.; Sarnela, N.; Schallhart, S.; Schnitzhofer, R.; Seinfeld, J. H.; Simon, M.; Sipila, M.; Stozhkov, Y.; Stratmann, F.; Tome, A.; Trostl, J.; Tsagkogeorgas, G.; Vaattovaara, P.; Viisanen, Y.; Virtanen, A.; Vrtala, A.; Wagner, P. E.; Weingartner, E.; Wex, H.; Williamson, C.; Wimmer, D.; Ye, P. L.; Yli-Juuti, T.; Carslaw, K. S.; Kulmala, M.; Curtius, J.; Baltensperger, U.; Worsnop, D. R.; Vehkamaki, H.; Kirkby, J., Molecular understanding of sulphuric acid-amine particle nucleation in the atmosphere. *Nature* **2013,** *502* (7471), 359-369.

75. Berndt, T.; Sipila, M.; Stratmann, F.; Petaja, T.; Vanhanen, J.; Mikkila, J.; Patokoski, J.; Taipale, R.; Mauldin, R. L.; Kulmala, M., Enhancement of atmospheric H_2SO_4/H_2O nucleation: organic oxidation products versus amines. *Atmos. Chem. Phys.* **2014,** *14* (2), 751-764.
76. Erupe, M. E.; Viggiano, A. A.; Lee, S. H., The effect of trimethylamine on atmospheric nucleation involving H_2SO_4. *Atmos. Chem. Phys.* **2011,** *11* (10), 4767-4775.
77. Chen, H. H.; Finlayson-Pitts, B. J., New particle formation from methanesulfonic acid and amines/ammonia as a function of temperature. *Environ. Sci. Technol.* **2017,** *51* (1), 243-252.
78. Chen, H. H.; Varner, M. E.; Gerber, R. B.; Finlayson-Pitts, B. J., Reactions of methanesulfonic acid with amines and ammonia as a source of new particles in air. *J. Phys. Chem. B* **2016,** *120* (8), 1526-1536.
79. Chen, H. H.; Ezell, M. J.; Arquero, K. D.; Varner, M. E.; Dawson, M. L.; Gerber, R. B.; Finlayson-Pitts, B. J., New particle formation and growth from methanesulfonic acid, trimethylamine and water. *Phys. Chem. Chem. Phys.* **2015,** *17* (20), 13699-13709.
80. Dawson, M. L.; Varner, M. E.; Perraud, V.; Ezell, M. J.; Gerber, R. B.; Finlayson-Pitts, B. J., Simplified mechanism for new particle formation from methanesulfonic acid, amines, and water via experiments and ab initio calculations. *Proc. Natl. Acad. Sci. U.S.A.* **2012,** *109* (46), 18719-18724.
81. Bzdek, B. R.; Ridge, D. P.; Johnston, M. V., Reactivity of methanesulfonic acid salt clusters relevant to marine air. *J. Geophys. Res.: Atmos.* **2011,** *116*, D03301.
82. Arquero, K. D.; Gerber, R. B.; Finlayson-Pitts, B. J., The role of oxalic acid in new particle formation from methanesulfonic acid, methylamine, and water. *Environ. Sci. Technol.* **2017,** *51* (4), 2124-2130.
83. Xu, J.; Finlayson-Pitts, B. J.; Gerber, R. B., Proton transfer in mixed clusters of methanesulfonic acid, methylamine, and oxalic acid: Implications for atmospheric particle formation. *J. Phys. Chem. A* **2017,** *121* (12), 2377-2385.
84. Ge, X. L.; Wexler, A. S.; Clegg, S. L., Atmospheric amines - Part I. A review. *Atmos. Environ.* **2011,** *45* (3), 524-546.
85. Dawson, M. L.; Perraud, V.; Gomez, A.; Arquero, K. D.; Ezell, M. J.; Finlayson-Pitts, B. J., Measurement of gas-phase ammonia and amines in air by collection onto an ion exchange resin and analysis by ion chromatography. *Atmos. Meas. Tech.* **2014,** *7* (8), 2733-2744.
86. You, Y.; Kanawade, V. P.; de Gouw, J. A.; Guenther, A. B.; Madronich, S.; Sierra-Hernandez, M. R.; Lawler, M.; Smith, J. N.; Takahama, S.; Ruggeri, G.; Koss, A.; Olson, K.; Baumann, K.; Weber, R. J.; Nenes, A.; Guo, H.; Edgerton, E. S.; Porcelli, L.; Brune, W. H.; Goldstein, A. H.; Lee, S. H., Atmospheric amines and ammonia measured with a chemical ionization mass spectrometer (CIMS). *Atmos. Chem. Phys.* **2014,** *14* (22), 12181-12194.
87. Schade, G. W.; Crutzen, P. J., Emission of aliphatic-amines from animal husbandry and their reactions - Potential source of N_2O and HCN. *J. Atmos. Chem.* **1995,** *22* (3), 319-346.
88. Gibb, S. W.; Mantoura, R. F. C.; Liss, P. S., Ocean-atmosphere exchange and atmospheric speciation of ammonia and methylamines in the region of the NW Arabian Sea. *Global Biogeochem. Cycles* **1999,** *13* (1), 161-177.
89. Chang, I. H.; Lee, C. G.; Lee, D. S., Development of an automated method for simultaneous determination of low molecular weight aliphatic amines and ammonia in ambient air by diffusion scrubber coupled to ion chromatography. *Anal. Chem.* **2003,** *75* (22), 6141-6146.

90. VandenBoer, T. C.; Petroff, A.; Markovic, M. Z.; Murphy, J. G., Size distribution of alkyl amines in continental particulate matter and their online detection in the gas and particle phase. *Atmos. Chem. Phys.* **2011,** *11* (9), 4319-4332.
91. Chan, L. P.; Chan, C. K., Displacement of Ammonium from Aerosol Particles by Uptake of Triethylamine. *Aerosol Sci. Technol.* **2012,** *46* (2), 236-247.
92. Kurten, T.; Loukonen, V.; Vehkamaki, H.; Kulmala, M., Amines are likely to enhance neutral and ion-induced sulfuric acid-water nucleation in the atmosphere more effectively than ammonia. *Atmos. Chem. Phys.* **2008,** *8* (14), 4095-4103.
93. Murphy, S. M.; Sorooshian, A.; Kroll, J. H.; Ng, N. L.; Chhabra, P.; Tong, C.; Surratt, J. D.; Knipping, E.; Flagan, R. C.; Seinfeld, J. H., Secondary aerosol formation from atmospheric reactions of aliphatic amines. *Atmos. Chem. Phys.* **2007,** *7* (9), 2313-2337.
94. Price, D. J.; Kacarab, M.; Cocker, D. R.; Purvis-Roberts, K. L.; Silva, P. J., Effects of temperature on the formation of secondary organic aerosol from amine precursors. *Aerosol Sci. Technol.* **2016,** *50* (11), 1216-1226.
95. Ge, Y. L.; Liu, Y. C.; Chu, B. W.; He, H.; Chen, T. Z.; Wang, S. X.; Wei, W.; Cheng, S. Y., Ozonolysis of trimethylamine exchanged with typical ammonium salts in the particle phase. *Environ. Sci. Technol.* **2016,** *50* (20), 11076-11084.
96. Angelino, S.; Suess, D. T.; Prather, K. A., Formation of aerosol particles from reactions of secondary and tertiary alkylamines: Characterization by aerosol time-of-flight mass spectrometry. *Environ. Sci. Technol.* **2001,** *35* (15), 3130-3138.
97. Price, D. J.; Clark, C. H.; Tang, X. C.; Cocker, D. R.; Purvis-Roberts, K. L.; Silva, P. J., Proposed chemical mechanisms leading to secondary organic aerosol in the reactions of aliphatic amines with hydroxyl and nitrate radicals. *Atmos. Environ.* **2014,** *96*, 135-144.
98. Tang, X.; Price, D.; Praske, E.; Lee, S. A.; Shattuck, M. A.; Purvis-Roberts, K.; Silva, P. J.; Asa-Awuku, A.; Cocker, D. R., NO_3 radical, OH radical and O_3-initiated secondary aerosol formation from aliphatic amines. *Atmos. Environ.* **2013,** *72*, 105-112.
99. Malloy, Q. G. J.; Qi, L.; Warren, B.; Cocker, D. R.; Erupe, M. E.; Silva, P. J., Secondary organic aerosol formation from primary aliphatic amines with NO_3 radical. *Atmos. Chem. Phys.* **2009,** *9* (6), 2051-2060.
100. Atkinson, R.; Perry, R.; Pitts Jr, J., Rate constants for the reaction of the OH radical with CH_3SH and CH_3NH_2 over the temperature range 299–426 K. *J. Chem. Phys.* **1977,** *66* (4), 1578-1581.
101. Atkinson, R.; Perry, R.; Pitts Jr, J., Rate constants for the reactions of the OH radical with $(CH_3)_2NH$, $(CH_3)_3N$, and $C_2H_5NH_2$ over the temperature range 298–426 K. *J. Chem. Phys.* **1978,** *68* (4), 1850-1853.
102. Atkinson, R.; Pitts Jr, J., Kinetics of the reactions of $O(^3P)$ atoms with the amines CH_3NH_2, $C_2H_5NH_2$, $(CH_3)_2NH$, and $(CH_3)_3N$ over the temperature range 298–440° K. *J. Chem. Phys.* **1978,** *68* (3), 911-915.
103. Pitts Jr, J. N.; Grosjean, D.; Van Cauwenberghe, K.; Schmid, J. P.; Fitz, D. R., Photooxidation of aliphatic amines under simulated atmospheric conditions: formation of nitrosamines, nitramines, amides, and photochemical oxidant. *Environ. Sci. Technol.* **1978,** *12* (8), 946-953.
104. Harris, G. W.; Atkinson, R.; Pitts, J. N., Kinetics of the reactions of the OH radical with hydrazine and methylhydrazine. *J. Phys. Chem.* **1979,** *83* (20), 2557-2559.

105. Carter, W. P. L.; Tuazon, E. C.; Winer, A. M.; Pitts, J. N., Gas-phase reactions of N,N-dimethylhydrazine with ozone and NO_x in simulated atmospheres - facile formation of N-nitrosodimethylamine. *ACS Sym. Ser.* **1981,** *174*, 117-131.
106. Tuazon, E. C.; Carter, W. P. L.; Atkinson, R.; Winer, A. M.; Pitts, J. N., Atmospheric reactions of N-nitrosodimethylamine and dimethylnitramine. *Environ. Sci. Technol.* **1984,** *18* (1), 49-54.
107. Atkinson, R.; Tuazon, E. C.; Wallington, T. J.; Aschmann, S. M.; Arey, J.; Winer, A. M.; Pitts, J. N., Atmospheric chemistry of aniline, N,N-dimethylaniline, pyridine, 1,3,5-triazine, and nitrobenzene. *Environ. Sci. Technol.* **1987,** *21* (1), 64-72.
108. Babar, Z. B.; Park, J.-H.; Lim, H.-J., Influence of NH_3 on secondary organic aerosols from the ozonolysis and photooxidation of α-pinene in a flow reactor. *Atmos. Environ.* **2017,** *164*, 71-84.
109. Na, K.; Song, C.; Switzer, C.; Cocker, D. R., Effect of ammonia on secondary organic aerosol formation from a-pinene ozonolysis in dry and humid conditions. *Environ. Sci. Technol.* **2007,** *41* (17), 6096-6102.
110. Bell, D. M.; Imre, D.; Martin, S. T.; Zelenyuk, A., The properties and behavior of a-pinene secondary organic aerosol particles exposed to ammonia under dry conditions. *Phys. Chem. Chem. Phys.* **2017,** *19* (9), 6497-6507.
111. Hinks, M. L.; Brady, M. V.; Lignell, H.; Song, M. J.; Grayson, J. W.; Bertram, A. K.; Lin, P.; Laskin, A.; Laskin, J.; Nizkorodov, S. A., Effect of viscosity on photodegradation rates in complex secondary organic aerosol materials. *Phys. Chem. Chem. Phys.* **2016,** *18* (13), 8785-8793.
112. Updyke, K. M.; Nguyen, T. B.; Nizkorodov, S. A., Formation of brown carbon via reactions of ammonia with secondary organic aerosols from biogenic and anthropogenic precursors. *Atmos. Environ.* **2012,** *63*, 22-31.
113. Chu, B. W.; Zhang, X.; Liu, Y. C.; He, H.; Sun, Y.; Jiang, J. K.; Li, J. H.; Hao, J. M., Synergetic formation of secondary inorganic and organic aerosol: effect of SO_2 and NH_3 on particle formation and growth. *Atmos. Chem. Phys.* **2016,** *16* (22), 14219-14230.
114. Liu, Y.; Liggio, J.; Staebler, R.; Li, S. M., Reactive uptake of ammonia to secondary organic aerosols: kinetics of organonitrogen formation. *Atmos. Chem. Phys.* **2015,** *15* (23), 13569-13584.
115. Kuwata, M.; Martin, S. T., Phase of atmospheric secondary organic material affects its reactivity. *Proc. Natl. Acad. Sci. U.S.A.* **2012,** *109* (43), 17354-17359.
116. Lee, H. J.; Aiona, P. K.; Laskin, A.; Laskin, J.; Nizkorodov, S. A., Effect of solar radiation on the optical properties and molecular composition of laboratory proxies of atmospheric brown carbon. *Environ. Sci. Technol.* **2014,** *48* (17), 10217-10226.
117. Bones, D. L.; Henricksen, D. K.; Mang, S. A.; Gonsior, M.; Bateman, A. P.; Nguyen, T. B.; Cooper, W. J.; Nizkorodov, S. A., Appearance of strong absorbers and fluorophores in limonene-O_3 secondary organic aerosol due to NH_4^+-mediated chemical aging over long time scales. *J. Geophys. Res.: Atmos.* **2010,** *115*, D05203.
118. Yang, H.; Xu, J. H.; Wu, W. S.; Wan, C. H.; Yu, J. Z., Chemical characterization of water-soluble organic aerosols at Jeju Island collected during ACE-Asia. *Environ. Chem.* **2004,** *1* (1), 13-17.

119. Liu, S.; Day, D. A.; Shields, J. E.; Russell, L. M., Ozone-driven daytime formation of secondary organic aerosol containing carboxylic acid groups and alkane groups. *Atmos. Chem. Phys.* **2011,** *11* (16), 8321-8341.
120. Jung, J. S.; Kawamura, K., Enhanced concentrations of citric acid in spring aerosols collected at the Gosan background site in East Asia. *Atmos. Environ.* **2011,** *45* (30), 5266-5272.
121. Ivleva, N. P.; McKeon, U.; Niessner, R.; Poschl, U., Raman microspectroscopic analysis of size-resolved atmospheric aerosol particle samples collected with an ELPI: Soot, humic-like substances, and inorganic compounds. *Aerosol Sci. Technol.* **2007,** *41* (7), 655-671.
122. Salma, I.; Meszaros, T.; Maenhaut, W.; Vass, E.; Majer, Z., Chirality and the origin of atmospheric humic-like substances. *Atmos. Chem. Phys.* **2010,** *10* (3), 1315-1327.
123. Liu, Y. C.; Ma, Q. X.; He, H., Heterogeneous uptake of amines by citric acid and humic acid. *Environ. Sci. Technol.* **2012,** *46* (20), 11112-11118.
124. Kawamura, K.; Ikushima, K., Seasonal-changes in the distribution of dicarboxylic-acids in the urban atmosphere. *Environ. Sci. Technol.* **1993,** *27* (10), 2227-2235.
125. Kawamura, K.; Imai, Y.; Barrie, L. A., Photochemical production and loss of organic acids in high Arctic aerosols during long-range transport and polar sunrise ozone depletion events. *Atmos. Environ.* **2005,** *39* (4), 599-614.
126. Fraser, M. P.; Cass, G. R.; Simoneit, B. R. T., Air quality model evaluation data for organics. 6. C3-24 organic acids. *Environ. Sci. Technol.* **2003,** *37* (3), 446-453.
127. Yue, Z. W.; Fraser, M. P., Polar organic compounds measured in fine particulate matter during TexAQS 2000. *Atmos. Environ.* **2004,** *38* (20), 3253-3261.
128. Limbeck, A.; Kraxner, Y.; Puxbaum, H., Gas to particle distribution of low molecular weight dicarboxylic acids at two different sites in central Europe (Austria). *J. Aerosol Sci.* **2005,** *36* (8), 991-1005.
129. Limbeck, A.; Puxbaum, H.; Otter, L.; Scholes, M. C., Semivolatile behavior of dicarboxylic acids and other polar organic species at a rural background site (Nylsvley, RSA). *Atmos. Environ.* **2001,** *35* (10), 1853-1862.
130. Satsumabayashi, H.; Kurita, H.; Yokouchi, Y.; Ueda, H., Photochemical formation of particulate dicarboxylic-acids under long-range transport in Central Japan. *Atmos. Environ., Part A* **1990,** *24* (6), 1443-1450.
131. Saarikoski, S.; Carbone, S.; Decesari, S.; Giulianelli, L.; Angelini, F.; Canagaratna, M.; Ng, N. L.; Trimborn, A.; Facchini, M. C.; Fuzzi, S.; Hillamo, R.; Worsnop, D., Chemical characterization of springtime submicrometer aerosol in Po Valley, Italy. *Atmos. Chem. Phys.* **2012,** *12* (18), 8401-8421.
132. Smith, J. N.; Barsanti, K. C.; Friedli, H. R.; Ehn, M.; Kulmala, M.; Collins, D. R.; Scheckman, J. H.; Williams, B. J.; McMurry, P. H., Observations of aminium salts in atmospheric nanoparticles and possible climatic implications. *Proc. Natl. Acad. Sci. U.S.A.* **2010,** *107* (15), 6634-6639.
133. Schlag, P.; Rubach, F.; Mentel, T.; Reimer, D.; Canonaco, F.; Henzing, J.; Moerman, M.; Otjes, R.; Prévôt, A.; Rohrer, F., Ambient and laboratory observations of organic ammonium salts in PM 1. *Faraday Discuss.* **2017**, DOI: 10.1039/c7fd00027h.
134. Makela, J. M.; Yli-Koivisto, S.; Hiltunen, V.; Seidl, W.; Swietlicki, E.; Teinila, K.; Sillanpaa, M.; Koponen, I. K.; Paatero, J.; Rosman, K.; Hameri, K., Chemical composition of aerosol during particle formation events in boreal forest. *Tellus B.* **2001,** *53* (4), 380-393.

135. Cappa, C. D.; Lovejoy, E. R.; Ravishankara, A. R., Determination of evaporation rates and vapor pressures of very low volatility compounds: A study of the C4-C10 and C12 dicarboxylic acids. *J. Phys. Chem. A* **2007,** *111* (16), 3099-3109.
136. Bilde, M.; Barsanti, K.; Booth, M.; Cappa, C. D.; Donahue, N. M.; Emanuelsson, E. U.; McFiggans, G.; Krieger, U. K.; Marcolli, C.; Tropping, D.; Ziemann, P.; Barley, M.; Clegg, S.; Dennis-Smither, B.; Hallquist, M.; Hallquist, A. M.; Khlystov, A.; Kulmala, M.; Mogensen, D.; Percival, C. J.; Pope, F.; Reid, J. P.; da Silva, M. A. V. R.; Rosenoern, T.; Salo, K.; Soonsin, V. P.; Yli-Juuti, T.; Prisle, N. L.; Pagels, J.; Rarey, J.; Zardini, A. A.; Riipinen, I., Saturation vapor pressures and transition enthalpies of low-volatility organic molecules of atmospheric relevance: from dicarboxylic acids to complex mixtures. *Chem. Rev.* **2015,** *115* (10), 4115-4156.
137. Bilde, M.; Svenningsson, B.; Monster, J.; Rosenorn, T., Even-odd alternation of evaporation rates and vapor pressures of C3-C9 dicarboxylic acid aerosols. *Environ. Sci. Technol.* **2003,** *37* (7), 1371-1378.
138. Thalladi, V. R.; Nusse, M.; Boese, R., The melting point alternation in a,w-alkanedicarboxylic acids. *J. Am. Chem. Soc.* **2000,** *122* (38), 9227-9236.
139. Zhang, H.; Xie, C.; Liu, Z. K.; Gong, J. B.; Bao, Y.; Zhang, M. J.; Hao, H. X.; Hou, B. H.; Yin, Q. X., Identification and molecular understanding of the odd-even effect of dicarboxylic acids aqueous solubility. *Ind. Eng. Chem. Res.* **2013,** *52* (51), 18458-18465.
140. Zhang, H.; Yin, Q. X.; Liu, Z. K.; Gong, J. B.; Bao, Y.; Zhang, M. J.; Hao, H. X.; Hou, B. H.; Xie, C., An odd-even effect on solubility of dicarboxylic acids in organic solvents. *J. Chem. Thermodyn.* **2014,** *77*, 91-97.
141. Dzepina, K.; Volkamer, R. M.; Madronich, S.; Tulet, P.; Ulbrich, I. M.; Zhang, Q.; Cappa, C. D.; Ziemann, P. J.; Jimenez, J. L., Evaluation of recently-proposed secondary organic aerosol models for a case study in Mexico City. *Atmos. Chem. Phys.* **2009,** *9* (15), 5681-5709.
142. Heald, C. L.; Jacob, D. J.; Park, R. J.; Russell, L. M.; Huebert, B. J.; Seinfeld, J. H.; Liao, H.; Weber, R. J., A large organic aerosol source in the free troposphere missing from current models. *Geophys. Res. Lett.* **2005,** *32* (18), L18809.
143. Volkamer, R.; Jimenez, J. L.; San Martini, F.; Dzepina, K.; Zhang, Q.; Salcedo, D.; Molina, L. T.; Worsnop, D. R.; Molina, M. J., Secondary organic aerosol formation from anthropogenic air pollution: Rapid and higher than expected. *Geophys. Res. Lett.* **2006,** *33* (17), L17811.
144. Matsui, H.; Koike, M.; Takegawa, N.; Kondo, Y.; Griffin, R. J.; Miyazaki, Y.; Yokouchi, Y.; Ohara, T., Secondary organic aerosol formation in urban air: Temporal variations and possible contributions from unidentified hydrocarbons. *J. Geophys. Res.: Atmos.* **2009,** *114*, D04201.
145. Wiegel, A. A.; Wilson, K. R.; Hinsberg, W. D.; Houle, F. A., Stochastic methods for aerosol chemistry: a compact molecular description of functionalization and fragmentation in the heterogeneous oxidation of squalane aerosol by OH radicals. *Phys. Chem. Chem. Phys.* **2015,** *17* (6), 4398-4411.
146. Cappa, C. D.; Che, D. L.; Kessler, S. H.; Kroll, J. H.; Wilson, K. R., Variations in organic aerosol optical and hygroscopic properties upon heterogeneous OH oxidation. *J. Geophys. Res.: Atmos.* **2011,** *116*, D15204.
147. Katrib, Y.; Biskos, G.; Buseck, P. R.; Davidovits, P.; Jayne, J. T.; Mochida, M.; Wise, M. E.; Worsnop, D. R.; Martin, S. T., Ozonolysis of mixed oleic-acid/stearic-acid particles: Reaction kinetics and chemical morphology. *J. Phys. Chem. A* **2005,** *109* (48), 10910-10919.

148. Mendez, M.; Visez, N.; Gosselin, S.; Crenn, V.; Riffault, V.; Petitprez, D., Reactive and nonreactive ozone uptake during aging of oleic acid particles. *J. Phys. Chem. A* **2014,** *118* (40), 9471-9481.
149. Kolb, C. E.; Cox, R. A.; Abbatt, J. P. D.; Ammann, M.; Davis, E. J.; Donaldson, D. J.; Garrett, B. C.; George, C.; Griffiths, P. T.; Hanson, D. R.; Kulmala, M.; McFiggans, G.; Poschl, U.; Riipinen, I.; Rossi, M. J.; Rudich, Y.; Wagner, P. E.; Winkler, P. M.; Worsnop, D. R.; O' Dowd, C. D., An overview of current issues in the uptake of atmospheric trace gases by aerosols and clouds. *Atmos. Chem. Phys.* **2010,** *10* (21), 10561-10605.
150. Abbatt, J. P. D.; Lee, A. K. Y.; Thornton, J. A., Quantifying trace gas uptake to tropospheric aerosol: recent advances and remaining challenges. *Chem. Soc. Rev.* **2012,** *41* (19), 6555-6581.
151. Zhang, Q.; Alfarra, M. R.; Worsnop, D. R.; Allan, J. D.; Coe, H.; Canagaratna, M. R.; Jimenez, J. L., Deconvolution and quantification of hydrocarbon-like and oxygenated organic aerosols based on aerosol mass spectrometry. *Environ. Sci. Technol.* **2005,** *39* (13), 4938-4952.
152. Lal, K.; Tripathi, N.; Dubey, G. P., Densities, viscosities, and refractive indices of binary liquid mixtures of hexane, decane, hexadecane, and squalane with benzene at 298.15 K. *J Chem. Eng. Data* **2000,** *45* (5), 961-964.
153. Togashi, T.; Kanai, T.; Sekikawa, T.; Watanabe, S.; Chen, C. T.; Zhang, C. Q.; Xu, Z. Y.; Wang, J. Y., Generation of vacuum-ultraviolet light by an optically contacted, prism-coupled $KBe_2BO_3F_2$ crystal. *Opt. Lett.* **2003,** *28* (4), 254-256.
154. Talukdar, R. K.; Herndon, S. C.; Burkholder, J. B.; Roberts, J. M.; Ravishankara, A. R., Atmospheric fate of several alkyl nitrates .1. Rate coefficients of the reactions alkyl nitrates with isotopically labelled hydroxyl radicals. *J. Chem. Soc., Faraday Trans.* **1997,** *93* (16), 2787-2796.
155. Roberts, J. M., The atmospheric chemistry of organic nitrates. *Atmos. Environ., Part A* **1990,** *24* (2), 243-287.
156. Ma, S. X.; Rindelaub, J. D.; McAvey, K. M.; Gagare, P. D.; Nault, B. A.; Ramachandran, P. V.; Shepson, P. B., a-Pinene nitrates: synthesis, yields and atmospheric chemistry. *Atmos. Chem. Phys.* **2011,** *11* (13), 6337-6347.
157. Lockwood, A. L.; Shepson, P. B.; Fiddler, M. N.; Alaghmand, M., Isoprene nitrates: preparation, separation, identification, yields, and atmospheric chemistry. *Atmos. Chem. Phys.* **2010,** *10* (13), 6169-6178.
158. Perring, A. E.; Bertram, T. H.; Wooldridge, P. J.; Fried, A.; Heikes, B. G.; Dibb, J.; Crounse, J. D.; Wennberg, P. O.; Blake, N. J.; Blake, D. R.; Brune, W. H.; Singh, H. B.; Cohen, R. C., Airborne observations of total $RONO_2$: new constraints on the yield and lifetime of isoprene nitrates. *Atmos. Chem. Phys.* **2009,** *9* (4), 1451-1463.
159. Clemitshaw, K. C.; Williams, J.; Rattigan, O. V.; Shallcross, D. E.; Law, K. S.; Cox, R. A., Gas-phase ultraviolet absorption cross-sections and atmospheric lifetimes of several C2-C5 alkyl nitrates. *J. Photochem. Photobiol. A-Chem.* **1997,** *102* (2-3), 117-126.
160. Shepson, P. B.; Mackay, E.; Muthuramu, K., Henry's law constants and removal processes for several atmospheric b-hydroxy alkyl nitrates. *Environ. Sci. Technol.* **1996,** *30* (12), 3618-3623.
161. Higgins, C. M.; Evans, L. A.; Lloyd-Jones, G. C.; Shallcross, D. E.; Tew, D. P.; Orr-Ewing, A. J., Quantum yields for photochemical production of NO_2 from organic nitrates at tropospherically relevant wavelengths. *J. Phys. Chem. A* **2014,** *118* (15), 2756-2764.

162. Tuazon, E. C.; Atkinson, R., A Product Study of the Gas-Phase Reaction of Methacrolein with the OH Radical in the Presence of Nox. *Int. J. Chem. Kinet.* **1990,** *22* (6), 591-602.
163. Carter, W. P. L.; Atkinson, R., Development and evaluation of a detailed mechanism for the atmospheric reactions of isoprene and NOx. *Int. J. Chem. Kinet.* **1996,** *28* (7), 497-530.
164. Singh, H. B.; Ohara, D.; Herlth, D.; Sachse, W.; Blake, D. R.; Bradshaw, J. D.; Kanakidou, M.; Crutzen, P. J., Acetone in the atmosphere - distribution, sources, and sinks. *J. Geophys. Res.: Atmos.* **1994,** *99* (D1), 1805-1819.
165. Arnold, F.; Schneider, J.; Gollinger, K.; Schlager, H.; Schulte, P.; Hagen, D. E.; Whitefield, P. D.; vanVelthoven, P., Observation of upper tropospheric sulfur dioxide and acetone pollution: Potential implications for hydroxyl radical and aerosol formation. *Geophys. Res. Lett.* **1997,** *24* (1), 57-60.
166. Singh, H. B.; Kanakidou, M.; Crutzen, P. J.; Jacob, D. J., High-concentrations and photochemical fate of oxygenated hydrocarbons in the global troposphere. *Nature* **1995,** *378* (6552), 50-54.
167. Chebbi, A.; Carlier, P., Carboxylic acids in the troposphere, occurrence, sources, and sinks: A review. *Atmos. Environ.* **1996,** *30* (24), 4233-4249.
168. Kawamura, K.; Ng, L. L.; Kaplan, I. R., Determination of organic acids (C1-C10) in the atmosphere, motor exhausts, and engine oils. *Environ. Sci. Technol.* **1985,** *19* (11), 1082-1086.
169. Kumar, N.; Kulshrestha, U. C.; Khare, P.; Saxena, A.; Kumari, K. M.; Srivastava, S. S., Measurements of formic and acetic acid levels in the vapour phase at Dayalbagh, Agra, India. *Atmos. Environ.* **1996,** *30* (20), 3545-3550.
170. Nolte, C. G.; Solomon, P. A.; Fall, T.; Salmon, L. G.; Cass, G. R., Seasonal and spatial characteristics of formic and acetic acids concentrations in the southern California atmosphere. *Environ. Sci. Technol.* **1997,** *31* (9), 2547-2553.
171. Norton, R. B., Measurements of gas-phase formic and acetic-acids at the Mauna-Loa, Observatory, Hawaii during the Mauna-Loa Observatory photochemistry experiment 1988. *J. Geophys. Res.: Atmos.* **1992,** *97* (D10), 10389-10393.
172. Harrick, N. J., *Internal Reflection Spectroscopy*. Harrick Scientific Corporation: 1967.
173. Ezell, M. J.; Johnson, S. N.; Yu, Y.; Perraud, V.; Bruns, E. A.; Alexander, M. L.; Zelenyuk, A.; Dabdub, D.; Finlayson-Pitts, B. J., A new aerosol flow system for photochemical and thermal studies of tropospheric aerosols. *Aerosol Sci. Technol.* **2010,** *44* (5), 329-338.
174. Kalsi, P., *Spectroscopy of Organic Compounds*. New Age International: 2007.
175. Lide, D. R., *CRC Handbook of Chemistry and Physics*. CRC press: 2004; Vol. 85.
176. Beichert, P.; Finlayson-Pitts, B. J., Knudsen cell studies of the uptake of gaseous HNO_3 and other oxides of nitrogen on solid NaCl: The role of surface-adsorbed water. *J. Phys. Chem.* **1996,** *100* (37), 15218-15228.
177. Fenter, F. F.; Caloz, F.; Rossi, M. J., Kinetics of nitric-acid uptake by salt. *J. Phys. Chem.* **1994,** *98* (39), 9801-9810.
178. Hoffman, R. C.; Kaleuati, M. A.; Finlayson-Pitts, B. J., Knudsen cell studies of the reaction of gaseous HNO_3 with NaCl using less than a single layer of particles at 298 K: A modified mechanism. *J. Phys. Chem. A* **2003,** *107* (39), 7818-7826.
179. Leu, M. T.; Timonen, R. S.; Keyser, L. F.; Yung, Y. L., Heterogeneous Reactions of $HNO_{3(G)}+NaCl_{(S)} \rightarrow HCl_{(G)}+NaNO_{3(S)}$ and $N_2O_{5(G)}+NaCl_{(S)} \rightarrow ClNO_{2(G)}+NaNO_{3(S)}$. *J. Phys. Chem.* **1995,** *99* (35), 13203-13212.

180. Caloz, F.; Fenter, F. F.; Tabor, K. D.; Rossi, M. J., Paper I: Design and construction of a Knudsen-cell reactor for the study of heterogeneous reactions over the temperature range 130-750 K: Performances and limitations. *Rev. Sci. Instrum.* **1997,** *68* (8), 3172-3179.
181. Golden, D. M.; Spokes, G. N.; Benson, S. W., Very low-pressure pyrolysis (VLPP) - Versatile kinetic tool. *Angew. Chem., Int. Ed. Engl.* **1973,** *12* (7), 534-546.
182. Winterbottom, W.; Hirth, J., Diffusional contribution to the total flow from a Knudsen cell. *J. Chem. Phys.* **1962,** *37* (4), 784-793.
183. Taylor, J. R., *An Introduction to Error Analysis : the Study of Uncertainties in Physical Measurements*. 2nd ed.; University Science Books: Sausalito, Calif., 1997; p xvii, 327 p.
184. Lavi, A.; Segre, E.; Gomez-Hernandez, M.; Zhang, R. Y.; Rudich, Y., Volatility of atmospherically relevant alkylaminium carboxylate salts. *J. Phys. Chem. A* **2015,** *119* (19), 4336-4346.
185. Franzini, J. B.; Finnemore, E. J.; Daugherty, R. L., *Fluid Mechanics with Engineering Applications*. 9th ed.; McGraw-Hill: New York, 1997; p xxi, 807 p.
186. Zhao, Y.; Fairhurst, M. C.; Wingen, L. M.; Perraud, V.; Ezell, M. J.; Finlayson-Pitts, B. J., New insights into atmospherically relevant reaction systems using direct analysis in real-time mass spectrometry (DART-MS). *Atmos. Meas. Tech.* **2017,** *10* (4), 1373-1386.
187. Socrates, G., Infrared and Raman Characteristic Group Frequencies: Tables and Charts. *Wiley, Chichester* **2001**.
188. McLaughlin, R. P.; Bird, B.; Reid, P. J., Vibrational analysis of isopropyl nitrate and isobutyl nitrate. *Spectrochim Acta A* **2002,** *58* (12), 2571-2580.
189. Treves, K.; Shragina, L.; Rudich, Y., Henry's law constants of some b-, g-, and d-hydroxy alkyl nitrates of atmospheric interest. *Environ. Sci. Technol.* **2000,** *34* (7), 1197-1203.
190. Kish, J. D.; Leng, C. B.; Kelley, J.; Hiltner, J.; Zhang, Y. H.; Liu, Y., An improved approach for measuring Henry's law coefficients of atmospheric organics. *Atmos. Environ.* **2013,** *79*, 561-565.
191. Zhao, J.; Levitt, N. P.; Zhang, R. Y.; Chen, J. M., Heterogeneous reactions of methylglyoxal in acidic media: Implications for secondary organic aerosol formation. *Environ. Sci. Technol.* **2006,** *40* (24), 7682-7687.
192. Ip, H. S. S.; Huang, X. H. H.; Yu, J. Z., Effective Henry's law constants of glyoxal, glyoxylic acid, and glycolic acid. *Geophys. Res. Lett.* **2009,** *36*, L01802.
193. Pankow, J. F.; Asher, W. E., SIMPOL.1: a simple group contribution method for predicting vapor pressures and enthalpies of vaporization of multifunctional organic compounds. *Atmos. Chem. Phys.* **2008,** *8* (10), 2773-2796.
194. Grayson, J. W.; Zhang, Y.; Mutzel, A.; Renbaum-Wolff, L.; Boge, O.; Kamal, S.; Herrmann, H.; Martin, S. T.; Bertram, A. K., Effect of varying experimental conditions on the viscosity of alpha-pinene derived secondary organic material. *Atmos. Chem. Phys.* **2016,** *16* (10), 6027-6040.
195. Moller, B.; Rarey, J.; Ramjugernath, D., Estimation of the vapour pressure of non-electrolyte organic compounds via group contributions and group interactions. *J Mol. Liq.* **2008,** *143* (1), 52-63.
196. Nannoolal, Y.; Rarey, J.; Ramjugernath, D., Estimation of pure component properties - Part 3. Estimation of the vapor pressure of non-electrolyte organic compounds via group contributions and group interactions. *Fluid Phase Equilibr.* **2008,** *269* (1-2), 117-133.

197. Ruehl, C. R.; Wilson, K. R., Surface organic monolayers control the hygroscopic growth of submicrometer particles at high relative humidity. *J. Phys. Chem. A* **2014,** *118* (22), 3952-3966.
198. De Haan, D. O.; Finlayson-Pitts, B. J., Knudsen cell studies of the reaction of gaseous nitric acid with synthetic sea salt at 298 K. *J. Phys. Chem. A* **1997,** *101* (51), 9993-9999.
199. Gebel, M. E.; Finlayson-Pitts, B. J., Uptake and reaction of $ClONO_2$ on NaCl and synthetic sea salt. *J. Phys. Chem. A* **2001,** *105* (21), 5178-5187.
200. Gebel, M. E.; Finlayson-Pitts, B. J.; Ganske, J. A., The uptake of SO_2 on synthetic sea salt and some of its components. *Geophys. Res. Lett.* **2000,** *27* (6), 887-890.
201. Hoffman, R. C.; Gebel, M. E.; Fox, B. S.; Finlayson-Pitts, B. J., Knudsen cell studies of the reactions of N_2O_5 and $ClONO_2$ with NaCl: development and application of a model for estimating available surface areas and corrected uptake coefficients. *Phys. Chem. Chem. Phys.* **2003,** *5* (9), 1780-1789.
202. Davies, J. A.; Cox, R. A., Kinetics of the heterogeneous reaction of HNO_3 with NaCl: Effect of water vapor. *J. Phys. Chem. A* **1998,** *102* (39), 7631-7642.
203. Laux, J. M.; Hemminger, J. C.; Finlayson-Pitts, B. J., X-Ray photoelectron spectroscopic studies of the heterogenous reaction of gaseous nitric-acid with sodium-chloride - kinetics and contribution to the chemistry of the marine troposphere. *Geophys. Res. Lett.* **1994,** *21* (15), 1623-1626.
204. Goedkoop, J. A.; Macgillavry, C. H., The crystal structure of malonic acid. *Acta Crystallogr.* **1957,** *10* (2), 125-127.
205. Morrison, J. D.; Robertson, J. M., The crystal and molecular structure of certain dicarboxylic acids .4. b-succinic acid. *J. Chem. Soc.* **1949**, 980-986.
206. Liu, Y.; Han, C.; Liu, C.; Ma, J.; Ma, Q.; He, H., Differences in the reactivity of ammonium salts with methylamine. *Atmos. Chem. Phys.* **2012,** *12* (11), 4855-4865.
207. Bzdek, B. R.; Ridge, D. P.; Johnston, M. V., Size-dependent reactions of ammonium bisulfate clusters with dimethylamine. *J. Phys. Chem. A* **2010,** *114* (43), 11638-11644.
208. Govinda, V.; Venkatesu, P.; Bahadur, I., Molecular interactions between ammonium-based ionic liquids and molecular solvents: current progress and challenges. *Phys. Chem. Chem. Phys.* **2016,** *18* (12), 8278-8326.
209. Greaves, T. L.; Weerawardena, A.; Fong, C.; Krodkiewska, I.; Drummond, C. J., Protic ionic liquids: Solvents with tunable phase behavior and physicochemical properties. *J. Phys. Chem. B* **2006,** *110* (45), 22479-22487.
210. Fairhurst, M. C.; Ezell, M. J.; Kidd, C.; Lakey, P. S. J.; Shiraiwa, M.; Finlayson-Pitts, B. J., Kinetics, mechanisms and ionic liquids in the uptake of *n*-butylamine onto low molecular weight dicarboxylic acids. *Phys. Chem. Chem. Phys.* **2017,** *19* (6), 4827-4839.
211. Yli-Juuti, T.; Barsanti, K.; Hildebrandt Ruiz, L.; Kieloaho, A. J.; Makkonen, U.; Petaja, T.; Ruuskanen, T.; Kulmala, M.; Riipinen, I., Model for acid-base chemistry in nanoparticle growth (MABNAG). *Atmos. Chem. Phys.* **2013,** *13* (24), 12507-12524.
212. Merrill, G. N.; Fletcher, G. D., The prediction of gas-phase and aqueous basicities for alkyl amines. *J. Mol. Struct.: THEOCHEM* **2008,** *849*, 84-97.
213. Brauman, J. I.; Riveros, J. M.; Blair, L. K., Gas-phase basicities of amines. *J. Am. Chem. Soc.* **1971,** *93* (16), 3914-3916.

214. Qiu, C.; Wang, L.; Lal, V.; Khalizov, A. F.; Zhang, R. Y., Heterogeneous reactions of alkylamines with ammonium sulfate and ammonium bisulfate. *Environ. Sci. Technol.* **2011,** *45* (11), 4748-4755.
215. Allen, H. C.; Laux, J. M.; Vogt, R.; Finlayson-Pitts, B. J.; Hemminger, J. C., Water-induced reorganization of ultrathin nitrate films on NaCl: Implications for the tropospheric chemistry of sea salt particles. *J. Phys. Chem.* **1996,** *100* (16), 6371-6375.
216. Vogt, R.; Finlayson-Pitts, B. J., A diffuse-reflectance infrared fourier-transform spectroscopic (DRIFTS) study of the surface-reaction of NaCl with gaseous NO_2 and HNO_3. *J. Phys. Chem.* **1994,** *98* (14), 3747-3755.
217. Al-Hosney, H. A.; Carlos-Cuellar, S.; Baltrusaitis, J.; Grassian, V. H., Heterogeneous uptake and reactivity of formic acid on calcium carbonate particles: a Knudsen cell reactor, FTIR and SEM study. *Phys. Chem. Chem. Phys.* **2005,** *7* (20), 3587-3595.